Spatiotemporal Structure of the Groundwater-River Interaction at Mountain-Plain Transitional Landscapes

A Dissertation Submitted to
the Graduate School of Life and Environmental Sciences,
the University of Tsukuba
in Partial Fulfillment of the Requirements
for the Degree of Doctor of Philosophy in Science
(Doctoral Program in Geoenvironmental Sciences)

Yaping LIU

Abstract

River is not only an important recharge source but also an important discharge path of groundwater in nearly all the river catchment. The mountain-plain transitional landscape is especially important as groundwater recharge zone. The unique characteristic in geographical/geological settings usually makes the groundwater-river interaction complicated in the mountain-plain transitional landscape. Therefore, making clear the unique feature of groundwater-river interaction in the mountain-plain transitional landscape is very significant.

The principal objectives of the present study are (1) to reveal the spatial and temporal characteristics of groundwater recharge and discharge, with a special emphasis on the river seepage and its potential influencing factors; (2) to improve the methodology for such purposes. Both tracer approach and numerical simulation approach were applied to two study areas (Nasunogahara area and Ashikaga area, Tochigi Prefecture, central Japan) with different geographical/geological features.

The main conclusions from the present study are summarized as follows:

1. The main recharge sources to plain aquifers are precipitation, river water, paddy field water and mountain block recharged groundwater. Precipitation is the most dominant recharge source especially at areas far from river channel. River seepage is also an important recharge mechanism especially at areas close to river channel, while its contribution is variable depending on the distance from the channel and geographical/geological settings. River acts as not only a recharge source but also as a discharge path in lower elevation zones as well as springs and pumping wells. Such groundwater-river interaction moderately changes seasonally although it is relatively more intensive in wet season.
2. In the Nasunogahara area, the spatial characteristic of the river seepage is symmetric with respect to the channel. The extent of river-recharge dominated area reaches to 2.5 km from the channel in the upstream and 1.5 km in the downstream. The seepage of the Sabi River, an intermittent river, is larger than two permanent rivers (i.e., Naka River and Houki River).

However, the spatiotemporal variation of seepage from the Sabi River is especially large. Eighty percent of seepage from the Sabi River occurs in the upstream area and the monthly seepage in wet season is 4 times greater than in dry season.

3. In the Ashikaga area, the spatial characteristic of river seepage is asymmetric with respect to the channel. The extent of river recharge dominated area extends up to 4 km from the channel in the south side of the midstream reach, while it is less than 1 km in the north side. However, even near the river channel, mountain block recharge tends to suppress the river seepage toward the mountain side. The contribution ratio of river water increases from dry season to wet season.
4. Factors affecting the groundwater-river interaction in the mountain-plain transitional landscapes are large-scale topographic settings (i.e., slope direction versus river flow direction), location (i.e., fan apex/middle/rim zones) and geology (i.e., fault, syncline/anticline structures).
5. The contribution of paddy field water to groundwater recharge is remarkable in paddy field-dominated area. However, the mean contribution ratio of paddy field water over the whole area is relatively small in comparison to that of precipitation and river water. Limited distribution of paddy field and the short irrigation period are main reasons restricting the recharge from paddy field.
6. The numerical simulation approach with stable isotopes supplies more reliable results than the tracer approach does. This approach is especially useful for areas with sparse hydrometric data. Although the uncertain inputs and the sub-grid-scale heterogeneity may induce errors especially for computing the contribution ratio of paddy field water at point scale, combined use of tracer and numerical simulation is capable of improving reliability of the results and mitigating limitations in the numerical simulation approach.

Key words: Groundwater-river interaction, tracer, numerical simulation, groundwater recharge, groundwater discharge, mountain-plain transitional landscape.

Contents

List of Tables

List of Figures

List of Symbols

Symbol	Definition	Unit
C	simulated concentration of each recharge source	ML^{-3}
C^k	dissolved concentration of species k	ML^{-3}
C^k_s	the concentration of the source or sink flux for species k	ML^{-3}
D_{ij}	hydrodynamic dispersion coefficient tensor	L^2T^{-1}
h	the potentiometric head	L
K_x	horizontal hydraulic conductivity along x axis	LT^{-1}
K_y	horizontal hydraulic conductivity along y axis	LT^{-1}
K_z	vertical hydraulic conductivity	LT^{-1}
p	probability of obtaining a test statistic	-
q_s	the volumetric flow rate per unit volume of aquifer representing fluid sources (positive) and sinks (negative)	T^{-1}
R	mean contribution ratio of recharge sources to groundwater	%
r	correlation coefficient for linear regression	-
r^2	determination coefficient for linear regression	-
RMS	root mean squared error	-
S_s	specific storage	-
S_y	specific yield	L^{-1}
Sens	sensitivity	-
t	time	T
V_i	the seepage or linear pore water velocity. It related to the specific discharge or Darcy flux through the relationship of $V_i=q_i/\theta$;	LT^{-1}
W	a volumetric source/sink term	L^3T^{-1}

x_i	the distance along the respective Cartesian coordinate axis	L
$\sum R_n$	the chemical reaction term	$ML^{-3}T^{-1}$
γ	the 1st tracer used in EMMA	-
$\bar{\gamma}$	mean concentration/composition of tracer γ	-
δ	stable isotope ratios of oxygen (^{18}O) or hydrogen (D) in water	‰
$\delta^{18}O$	stable isotope ratios of oxygen in water	‰
δD	stable isotope ratios of hydrogen in water	‰
θ	porosity of the subsurface medium	-
λ	the 2nd tracer used in EMMA	-
$\bar{\lambda}$	mean concentration/ composition of tracer λ	-
σ_R	standard deviation of contribution ratio estimation for each recharge source (the populations in the EMMA is not correlated)	-
$\sigma_R^{'}$	standard deviation of contribution ratio estimation for each recharge source (the populations in the EMMA is correlated)	-
$\sigma^2_{\bar{\gamma}}$	variances of $\bar{\gamma}$ for recharge sources and mixture	-
$\sigma^2_{\bar{\lambda}}$	variances of $\bar{\lambda}$ for recharge sources and mixture	
$\sigma_{\bar{\gamma},\bar{\lambda}}$	covariance between $\bar{\gamma}$ and $\bar{\lambda}$ for recharge sources and mixture	-

Chapter 1
Introduction

1.1 Background

Groundwater and surface water are not isolated components of the hydrologic cycle. The interactions between them are widely existed in many forms from both aspects of quantity and quality. However, in many countries, groundwater and surface water resources have often been managed independently. Understanding of the processes and dynamics of groundwater and surface water interaction is thus very urgent not only for effective management of water quantity and quality, but also for the management and preservation of groundwater dependent ecosystems and riparian habitat (Fleckenstein et al., 2010; Sophocleous, 2002). River is a very common existing type of surface water. The interaction between groundwater and river occurs in nearly all the river catchments. Based on the exchange scale of groundwater system and river system, the interaction between groundwater and river can generally be classified as: (1) large scale (or basin scale) interactions and (2) small scale (or channel scale, or hyporheic zone scale) interactions (Harvey et al., 1996).

The groundwater-river interaction studies conducted in the mountain-plain transitional landscape are mainly focus on either valley scale or small scale. For large scale studies conducted in the landscape, limited researches restricted to assess the water balance (Weingartner et al. 2007), to estimate groundwater recharge (Smerdon et al., 2009) and to study the variations of groundwater-river interaction states along a river (Banks et al., 2011). The detailed spatiotemporal variations of groundwater and river in the mountain-plain transitional landscape remain unclear.

The method of using environmental tracers such as chemical ions (Harvey et al., 1996), oxygen and hydrogen stable isotopes (Hunt et al., 2005; Lambs, 2004) and electric conductivity (Vogt et al., 2010) is convenient, inexpensive and effective. As this method is usually based on several

assumptions and is mainly applied for qualitatively analysis, the numerical method is thus developed and improved for quantitatively elucidating the dynamics of groundwater-river interactions (Cho et al., 2010; Jones et al., 2006; Kim et al., 2008; Sarwar and Eggers, 2006). Since model usually associated with uncertainty in the measured and interpolated hydraulic parameters, environmental tracer and chemical data were introduced to be as additional calibration targets to improve the model output (Carroll et al., 2008; Dahan et al., 2004; Eastoe et al., 2010). However, using stable isotopes as one simulation term to calibrate numerical simulation results is limited. These studies were mainly restricted to steady-state condition (eg. Stichler et al., 2008), simple model (eg. Yamanaka and Wakui, 2009) or in a coastal wetland system (eg. Reynolds and Marimuthu, 2006).

1.2 Objectives

This study aims (1) to reveal the spatial distribution and temporal dynamics of groundwater recharge and discharge in mountain-plain transitional landscapes, with a special emphasis on the dynamics of river seepage and its potential influencing factors; (2) to improve the methodology by applying isotope tracers to numerical model for addressing the first objective. For achieving the objectives, two mountain-plain transitional areas (Nasunogahara area and Ashikaga area) with different geographical/geological features were investigated. Moreover, the tracer approach except for the numerical simulation was also applied for validating the improved numerical simulation method.

1.3 Outline of the present study

Chapter 2 reviewed recent studies about groundwater-river interactions around the world. This chapter also reviewed methods for revealing the interaction between groundwater and river. Chapter 3 descripted the study areas and the research states of the study areas. The results and discussions were presented in Chapter 4 to Chapter 7. Chapter 4 and Chapter 5 elucidated the

results of tracer approach and numerical simulation for the Nasunogahara area. The tracer approach and numerical simulation results for Ashikaga area are shown in Chapter 6 and Chapter 7. Chapter 8 generally discussed the results for two study areas and the advantage and disadvantage of two approaches. Finally, conclusions were given in Chapter 9. The flow chart of this study was shown in Fig. 1.1.

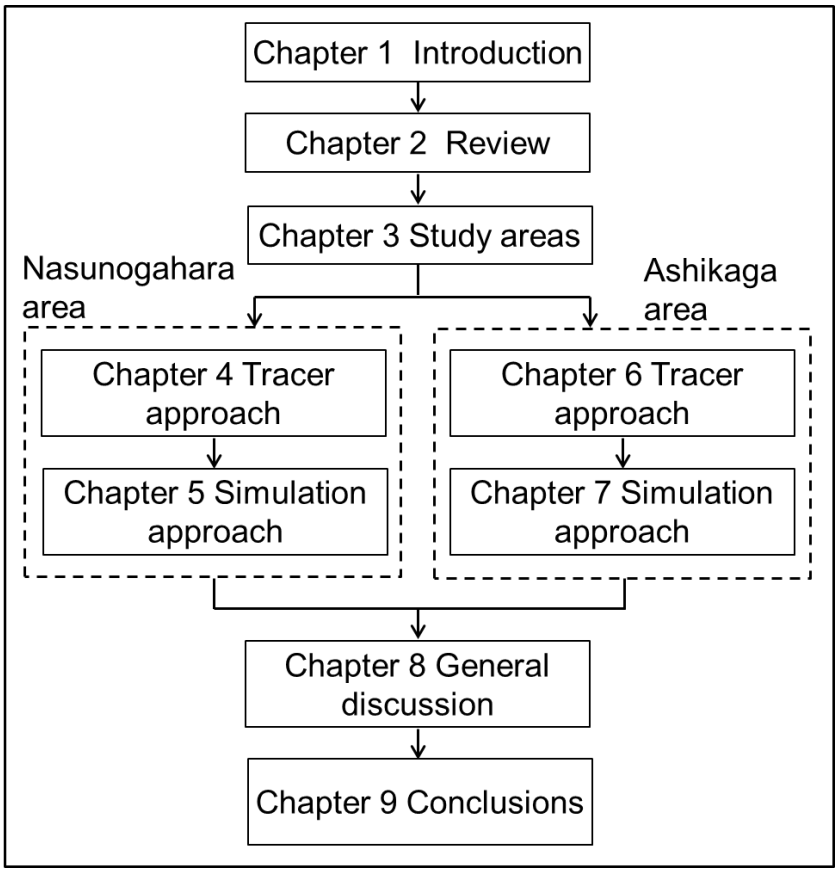

Figure 1.1 The flow chart of this study.

Chapter 2
Review of literatures

2.1 General review of the groundwater-river interaction

Groundwater and surface water are two interconnected components of one single resource and the connections between them are not only from quantity aspect but also from quality aspect (Winter et al., 1998). As one kind of very common existing groundwater-surface water interaction types, the interaction between groundwater and river widely exists in various forms. River infiltration constitutes an import recharge source of groundwater aquifer in many river basins and even channel infiltration could constitute a substantial component of the vertical recharge of groundwater (eg. Ponce et al., 1999). Conversely, groundwater drains into river as a base flow or a source of river. In qualitative aspects, river water is possibly degraded by discharge of saline or other low-quality groundwater and vice versa (Winter et al., 1998). In addition, human activities could modify the interaction between groundwater and river. For example, pumping groundwater close to river may induce additional seepage from river to groundwater and change the hydraulic condition of a river from gaining to losing (Sanz et al., 2009). Meanwhile, this induced flow could potentially lead to streamflow depletion and made the groundwater more vulnerable to river water pollution (Hancock, 2002). Overexploitation of water resources in the upstream and midstream of a river would cause groundwater level decline and quality pollution in the downstream (Xi et al., 2010). Understanding of the basic principles of interactions between groundwater and river is thus very necessary for effective management of water resources and preservation of groundwater dependent ecosystems and riparian habitat (Fleckenstein et al., 2010; Sophocleous, 2002).

According to the scale of exchange flows between channels and groundwater system, the interaction between groundwater and channels can generally to be classified as: (1) large scale (or

basin scale) interactions and (2) small scale (or channel scale, or hyporheic zone scale) interactions (Harvey et al., 1996).

2.1.1 Small scale interactions

The small scale interactions, also called hyporheic zone scale interactions or channel scale interactions, mainly refer to water exchange near channels. The exchange extent is various from centimeters to tens of meters depending on bed geometry and hydraulic-potential strengths (Woessner, 2000). River water levels and topography are the main causes of the exchange between groundwater and river water through the river bank (Lambs, 2004). The asymmetrical distribution of channel and floodplain sediment deposits controls different groundwater-river interaction in two sides of rivers (O'Driscoll et al., 2010). The flux of groundwater entering the alluvium from the sides and beneath is also a key factor controlling exchange flow between aquifers and rivers (Storey et al., 2003). Wroblicky et al. (1998) investigated the interaction between river and groundwater flow systems along two rivers with distinctly different alluvial sediments and bedrock lithology. The results indicated that the lateral hyporheic zone varies with the hydraulic conductivity of aquifer and streambed sediments and the size of the hyporheic zone lateral to the stream decreased during high flow conditions. Also, many other studies focused on the small scale interactions between groundwater and river. For example, Constantz (2008) was interested in streambed water exchange. Derx et al. (2010) focused on the influence of fluctuations of river water levels on the river-aquifer mixing zone, which pointed out that the mixing zone extent is not only caused by dispersion but also by advection. Harvey and Sibray (2001) evaluated the impacts of irrigation canal leakage on local groundwater system in a wetland.

2.1.2 Large scale interactions

The large scale interactions, also called basin scale interactions between channels and groundwater, refer to the exchange range in scale from hundreds of meters, in which transport occurs on a timescale of years. The interaction of groundwater with river in a large scale is controlled by (1) the distribution, magnitude and heterogeneity properties of hydraulic

conductivities of both the channel and the associated aquifers; (2) the relation of stream stage to the adjacent groundwater gradients; and (3) the geometry and position of the stream channel within the fluvial plain (Harvey et al., 1996; O'Driscoll et al., 2010; Storey et al., 2003; Woessner, 2000). The aquifer heterogeneity can have significant impacts on the spatial distribution of river seepage in an intermediate-scale (10^2 m), but the net annual seepage was not very sensitive to the aquifer heterogeneity (Fleckenstein et al., 2006). In addition, the geological structures, such as faults and folds are potentially impact the exchange between groundwater and channels through controlling local groundwater flow systems (eg. Ben-Itzhak and Gvirtzman, 2005; Yuan et al., 2011).

Understanding the process dynamics of groundwater-river interaction in various landscapes are the interests of many researchers around the world. For instance, Ponce et al. (1999) estimated the amount of groundwater recharger by channel leakage in a river basin of Mexico. Girard et al. (2003) investigated interactions between a river and groundwater and analyzed the influence of a new constructed dam on the interactions in a floodplain in the Brazilian Pantanal. Krause et al. (2007) analyzed the impacts of groundwater-river interaction on the groundwater recharge dynamics and riparian water balance in a floodplain catchment of Germany. The extent of groundwater and river interaction in an alluvial plain of India was identified by Kumar et al. (2009). Sanz et al. (2011) modeled groundwater-river interaction under the influence of groundwater abstraction in a river basin, Spain.

2.1.3 Methods for addressing groundwater-river interaction

New methods and models to improve understanding of processes and dynamics of groundwater-surface water interactions were reviewed by Fleckenstein et al. (2010). It pointed out that environmental tracers, geophysical and statistical technique, and numerical models et al. had been widely used to improve understanding of process and dynamics of groundwater-surface water interactions. In this study, we mainly reviewed the development and application of

environmental tracer approaches and numerical simulation approaches for revealing the groundwater-river interaction. The details see section 2.3 and 2.4.

2.2 Groundwater-river interaction in the mountain-plain transitional landscape

In the mountain-plain transitional area, the interaction between groundwater and river is particularly complicated due to the unique geography and hydrogeology. As shown in the conceptual diagram of mountain front recharge (Fig. 2.1), the subsurface component of mountain front recharge was called mountain block recharge which refers to the water flow through the mountain block (i.e., bed rocks) to the adjacent basin aquifers. It should be noted that the groundwater flow through very shallow aquifers of mountain slopes to aquifers of the adjacent plain, which was usually recharged by precipitation in the nearby hills, belongs to aquifer lateral recharge but not mountain block recharge. The occurrence of mountain block recharge usually makes the groundwater-river interaction more complicated. For example, a normal fault can act as a conduit for transferring precipitation in mountain areas to a plain (Yuan et al. 2011). The geological folding diverts groundwater along syncline axes from mountain aquifers towards rift valley aquifers (Ben-Itzhak and Gvirtzman, 2005). The mountain-plain transitional landscape has been reported as an important recharge zone in arid and semiarid regions (Wilson and Guan, 2004). Even under humid climates, deep groundwater in plain aquifers is recharged along plain margins adjacent to mountains (Mikita et al. 2011; Yamanaka et al. 2011a). Therefore, making clear the general characteristics of groundwater-river interactions in the mountain-plain transitional landscape could also improve the understanding of groundwater recharge mechanism in the landscape.

The previous studies conducted in the mountain-plain transitional landscapes are mainly focused on either valley scale or small scale studies, which are briefly descripted as follows. Harvey and Bencala (1993) studied the effect of streambed topography on surface-subsurface

water exchange in mountain catchments. Niswonger et al. (2005) simulated the distribution and quantity of streamflow and seepage losses along a mountain front stream. Westbrook et al. (2006) focused on the influence of beaver dams and overbank floods on the groundwater-river interaction of a mountain riparian area. Covino and McGlynn (2007) took interests in the impacts of stream gains and losses on watershed hydrology and stream water chemistry in a mountain to valley transition landscape. Winter et al. (2008) evaluated the effect of terrace geology on the groundwater-river interaction on a mountainside near a lake. Gauthier (2009) simulated the influence of the heterogeneity on the groundwater-river interaction in a valley scale.

For large scale studies, Weingartner et al. (2007) assessed the water balance in a highland-lowland-system. Smerdon et al., (2009) estimated groundwater recharge in a mountainous-to-valley landscape. Banks et al. (2011) focused on the changes of groundwater-river interactions along river reaches in an entire river catchment. However, the detailed spatiotemporal characteristics of groundwater-river interactions in the large scale of mountain-plain transitional landscape are still not very clear.

2.3 Environmental tracer approaches

Environmental tracer approaches are inexpensive and effective for investigating the interaction between groundwater and river. Chemical ions and stable isotopes are widely existed environmental tracers and they are easy to obtain and analyze. Numerous researches devoted to improve the understanding of groundwater-river interaction with the help of hydrochemistry and stable isotope tracers. Harvey et al. (1996) evaluated the reliability of the stream tracer approach to characterize channel-subsurface water exchange by comparing the results from hydrometric approach and stream tracer approach. Lambs (2004) investigated the interaction between groundwater and river at river banks and the confluence of rivers using conductivity and stable isotopes and pointed that stable isotopes, such as ^{18}O, are useful tools that allow water movement to be traced. Harvey and Sibray (2001) used water chemistry and environmental isotopes

delineated the extent of river leakage. Hunt et al. (2005) investigated river-well interaction using stable isotope tracers. Song et al. (2006) revealed the interaction condition between river and groundwater in a river basin by using stable isotopes and chloride ion. Kumar et al., (2009) pointed out that combination of an empirical and statistical relationship between different ionic species and sampling locations can provide greater confidence in identifying the extent of groundwater-river interaction and exchange processes. Except for chemical ions and isotopes, electrical conductivity (EC; Vogt et al., 2010), heat (Westhoff et al., 2010), and electrical resistivity (Ward et al., 2010) have also been used to trace groundwater-river interaction. However, the natural tracer approach usually based on several assumptions and applied for qualitatively analysis. For detailed process and dynamics of exchange between groundwater and river, we have to seek help from numerical models. The environmental tracer method was usually used as a prior condition to opt for expensive and time consuming methods such as numerical simulation.

2.4 Numerical simulation approaches

Numerical simulation approaches are quantitative to compute the complex interaction process between groundwater and river and have been widely used. The leakage between aquifers and rivers was firstly studied using an idealized 1-dimensioanl model in 1980s (Rushton and Tomlinson, 1979) and then additional routines and modules were added to the codes to better represent groundwater and river water exchange process (Prudic, 1989). With the development and improvement of groundwater flow and transport simulation model, such as MODFLOW (a modular three-dimensional finite-difference ground-water flow model; Harbaugh and McDonald, 1996a, 1996b) and FEFLOW (a finite element subsurface flow system; Diersch, 1979), more complex model of surface water has been linked to existed groundwater model to simulate groundwater and river interaction. For example, BRANCH, a one-dimensional open-channel model has been linked to MODFLOW (Swain and Wexler, 1992) and was used to investigate the impacts of climate change on groundwater levels (Scibek et al., 2007). A semi-distributed

agricultural watershed model SWAT was linked to MODFLOW and was used to investigate irrigation effects on streamflow and groundwater levels in a river watershed (Sophocleous and Perkins, 2000). This method was further modified by Kim et al. (2008) to simulate the spatiotemporal distribution of groundwater recharge rates and groundwater evapotranspiration and the interaction between groundwater and channels. Facchi et al. (2004) coupled SVAT, a model code for simulating the main hydrological processes in the vadose zone, with MODFLOW for water resources simulation in irrigated alluvial plains. For modeling catchment delineation and water balance within wetlands and floodplains, the deterministic distributed hydrological model WASIM-ETH was linked to MODFLOW and developed an integrated water balance and nutrient dynamics model IWAN (Krause and Bronstert, 2005; Krause et al., 2007). Sarwar and Eggers (2006) used a simple water balance approach to estimate net recharge to the aquifer and then set the net recharge as an input to groundwater water model FEFLOW for the water balance calculation and simulation. Rodriguez et al. (2008) conservatively coupled HEC-RAS (Hydrologic Engineering Centers-River Analysis System) program with MODFLOW to simulate the groundwater discharge to the surface water in a drainage basin. For simulating groundwater and pesticide movement in the saturated zone, Dynamic Agriculture Non-point Source Assessment Tool was linked to MODFLOW and MT3D (a modular three-dimensional transport model) (Cho et al., 2010).

In addition, integrated hydrology models were also developed and improved for better simulating the groundwater-surface water interaction. For instance, the Integrated Groundwater and Surface water Model (LaBolle et al., 2003), the MIKE SHE integrated catchment modeling (Refsgaard and Storm, 1995) and the Integrated Hydrology Model (VanderKwaak, 1999; VanderKwaak and Loague, 2001)) were developed and applied to investigate groundwater-surface water interaction (eg. Jones et al., 2006, 2008; Henriksen et al., 2008). In this study, a Streamflow-Routing Package (Prudic, 1989) linked with MODFLOW-2000 (Harbaugh et al., 2000) was used to simulate the hydraulic interaction between groundwater and river.

Since numerical models usually associated with uncertainty in the measured and interpolated hydraulic parameters, thus additional targets other than hydraulic head were introduced to calibrate and improve the model output. For instance, Izbicki et al. (2004) compared the groundwater flow model with the distribution of delta-deuterium data and groundwater ages interpreted on the basis of tritium and carbon-14 data. Dahan et al. (2004) parallel applied multi-variable mixing cell model, which represent the hydrochemical approach, and numerical model, and then used the hydrochemical approach results to calibrate and validate hydrogeologic groundwater modeling. ^{14}C activities and the positions of certain flow zones defined by the hydrochemical data were used as additional targets to calibrate groundwater flow model by Sanford et al. (2004). Reynolds and Marimuthu (2006) used deuterium composition and flow path analysis as additional calibration targets to calibrate groundwater flow simulation in a coastal wetland system. Lautz and Siegel (2006) calibrated modeling of surface and groundwater mixing in the hyporheic zone through comparing the simulation result of hydraulic head and Na:Ca ratio. Stichler et al. (2008) used oxygen-18 and deuterium tracers as calibration terms of a steady state flow and transport simulation to define the capture zone of a drinking water supply near a dredge lake. Carroll et al. (2008) compared of groundwater fluxes computed with MODFLOW and a steady state mixing model using deuterium. Eastoe et al. (2010) characterized the interaction of a river with an alluvial basin aquifer based on results of two methods: tracer method (stable isotopes and electric conductivity) and water budgets of modeling method.

Previous studies either use independent qualitatively analyzed results from hydrochemistry and isotope analysis to calibration model or focused mainly on application of radioisotopes (^{14}C) (eg. Sanford et al., 2004) and major ions concentrations (eg. Lautz and Siegel, 2006) as simulation terms to improve model output. It is limited that using stable isotopes as one simulation term to calibrate numerical simulation results. These studies were mainly restricted to steady-state condition (eg. Stichler et al., 2008), simple model (eg. Yamanaka and Wakui, 2009), or in a coastal wetlands system (eg. Reynolds and Marimuthu, 2006).

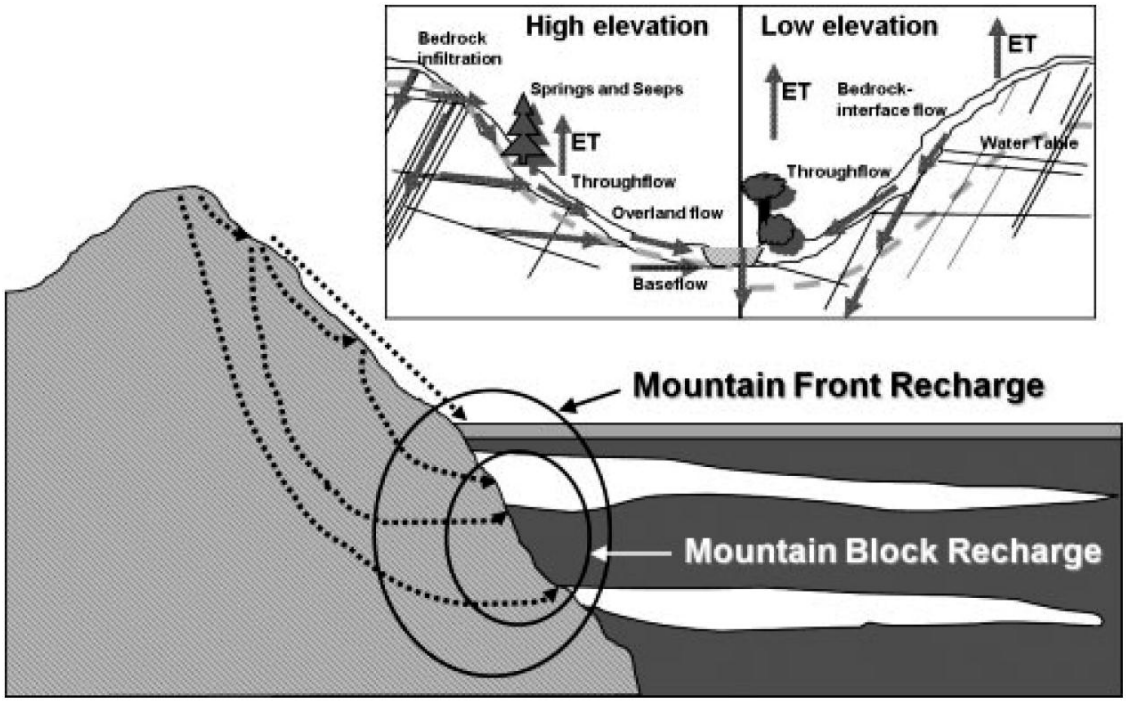

Figure 2.1 Conceptual diagram for mountain front recharge and mountain block recharge. Insert diagram depicts upland subcatchment routing of precipitation that may include discharge of groundwater to streamflow and subsequent streamflow loss to groundwater recharge via channel seepage (from Aishlin and McNamara, 2011).

Chapter 3
Study areas

For revealing the general characteristics of groundwater-river interactions in the mountain-plain transitional landscape, Nasunogahara area and Ashikaga area in Tochigi Prefecture of Japan with different physical geographic characteristics and human geographic characteristics were selected as the study areas (Fig. 3.1a). The two study areas are both approximately 400 km^2, and belong to humid temperate zone with broad variations in temperature. The detailed geographical, climate, geology, land use and water use in two study areas are described as follows.

3.1 Nasunogahara area

3.1.1 General description of the Nasunogahara area

a) Geographical location

The Nasunogahara area (139°53′-140°7.5′ E and 36°47′-37°3′ N), which located at the northern part of Tochigi Prefecture, is a compound alluvial fan formed by the Naka River, the Houki River, the Sabi River and the Kuma River (Fig. 3.1b). Its elevation ranged from 100 to 600 m above mean sea level (a.m.s.l.). The Nasunogahara area is bounded by the Houki River on the west and south, the Naka River on the northeast and east, and the Shimotsuke Mountains on the northwest.

b) Climate

The study area belongs to a humid temperate zone with broad variations in temperature. As shown in Fig. 3.2, the highest monthly mean temperature occurs in August (23.5°C) and the lowest occurs in January (0.6 °C) according to climatic normals (1981 to 2010) calculated from observed data of Japan Meteorological Agency (http://www.jma.go.jp/jma/index.html). Annual mean precipitation is 1533 mm and approximately 83% of the annual precipitation occurs during the

wet season from April to October. The largest monthly mean precipitation of 247.7 mm falls in August and the lowest monthly mean precipitation of 31.5 mm falls in January. The monthly mean temperature is the second highest and monthly mean precipitation is the second largest in July. They are 22.2°C and 238.4 mm, respectively.

During 2004 to 2006, the temperature varied from 0.2 to 24.6°C and the annual mean temperature was 12.4°C, which was close to long-term annual mean temperature (11.7°C). The annual mean precipitation was 1553 mm, which was also close to long-term annual mean precipitation. The highest monthly mean temperature occurred in August (24.1°C) but the monthly mean precipitation was only 149 mm in this month. However, the largest monthly mean precipitation (338.3 mm) occurred in July and the second highest monthly mean temperature (23°C) also occurred in this month. The lowest monthly mean precipitation (20 mm) and the lowest monthly mean temperature (0.6°C) occurred in January. The precipitation and temperature data were from the Kuroiso Station (36°58.9' N, 140°01.1' E and 343 m a.m.s.l.).

c) Land use

Land use map shows that forest, agricultural area, and residual and industrial area are three major land use and land cover types in the Nasunogahara area (Fig. 3.3). Rice is the major farm crop. Approximately 40 percent of land is used as paddy field in the Nasunogahara area, but most of the paddy field distributed in the downstream of the study area and along rivers. The irrigation period for paddy field is usually begins in April and ends in early August.

d) Water use

In the upstream of the Nasunogahara area, river water was extracted and transported by canals to supply urban water use and irrigate paddy field. In the midstream and downstream areas, the source of water consumption gradually changed from river water to groundwater. The groundwater within the study area is abstracted for local consumption and none of wells are metered. However, no large water consumption wells were found for industry and agriculture in

this area. Therefore, the groundwater abstraction is expected to be very small and has not a large impact on groundwater system in the Nasunogahara area.

e) Geology and hydrogeology

The Nasunogahara area is covered by recent alluvial sediments (sand and pebble) and volcanic soil (loam) (Fig. 3.4a). The thickness of the unconfined aquifer varies from upstream to downstream of the study area (Fig. 3.4b). The northwestern part of the study area is bounded by an impermeable fault which behaves as an aquiclude. The impermeable fault separates the alluvial aquifers from mountain aquifers/mountain blocks. The alluvial aquifers are mainly composed of gravel and sand, and aquitard consists of pumice and clay (Fig. 3.4c). The bottom of the shallow alluvial aquifers is defined by tuff and clay.

Many springs with large discharge occur in the downstream of the Nasunogahara area. Due to high permeability of the river beds, the midstream reach of the Sabi River dries up and only has water in rain days of the wet season. In the downstream, the Sabi River receives groundwater discharge and becomes a permanent river reach again. The Houki River, a branch of the Sabi River, is also an intermittent river. The river bed and river banks of the Houki River were covered by concrete and the stable isotopic analysis showed that the influence of the Houki River on groundwater was limited (Wakui and Yamanaka, 2006). Thus, the seepage of the Houki River is expected to be limited for the whole study area and was not considered in this study.

3.1.2 Research states about the Nasunogahara area

As one of the greatest alluvial fan and one important rice paddy agriculture and livestock production area in Japan, the Nasunogahara area attracts many researchers' interests. Early field work found that the distribution of the groundwater table almost parallel with ground surface in the midstream of the Nasunogahara area (Sasaki et al., 1958). After that, the spatial distribution of the temperature, pH and EC of groundwater in the midstream of the Nasunogahara area were investigated by Yamamoto and Terada (1980). The seasonal variation of groundwater table in the midstream and downstream of the study area was first descripted by Momikura (1986). The first

detailed spatial and seasonal variation of groundwater hydrochemistry was investigated by Hiyama and Suzuki (1991), which divided the Nasunogahara area into 5 regions based on the water quality of shallow groundwater (Fig. 3.5).

Isotopes were first applied in this area after 1970s. Sai and Oba (1978) clarified the groundwater flow system in the western part of the Nasunogahara area. Wakui and Yamanaka (2006) estimated the contribution ratios of three mainly recharge sources (precipitation, river and paddy field water) to groundwater at wells in the midstream of the Nasunogahara area based on oxygen and deuterium stable isotopes analysis.

The model was used in this region began at 1980s. Fujinawa (1981) used a Galerkin-finite element simulation model to simulate the groundwater flow. After that, Elhassan et al. (2001, 2003 and 2006) calculated the annual dynamics of different recharge sources and discharge sources by combining a modified tank model with a two-dimensional groundwater flow model. Somura et al. (2008) added groundwater quality simulation part to this model and then simulated the NO^3-N load in the Nasunogahara area. For addressing the groundwater-river interaction, a compartmental mixing cell model with isotope tracer calibration term was applied to reveal the temporal changes of river seepage, precipitation infiltration and paddy field water infiltration along rivers (Wakui, 2007; Yamanaka and Wakui, 2009).

However, the detailed spatial and temporal distribution of the groundwater recharge and discharge in this study area is still need to make clear with the help of 3-dimensional groundwater flow and transport model.

3.2 Ashikaga area

3.2.1 General description of the Ashikaga area

a) Geographical location

The Ashikaga area (36°15.3’-36°27’ N, 139°19’-139°33’E, Fig. 3.1c) with elevation of 14 to 681 m a.m.s.l. is situated at the northern margin of the Kanto Plain, which is the largest plain in

Japan. The area is bounded on the north by the Ashio Mountains. The Watarase River, which has a total length of 106.7 km, originates in Mt. Sukai (elevation, 2,144 m a.m.s.l.) in the Ashio Mountains and runs across the central part of the study area. The river flows to the southwest and then turns southeast along the margin of the plain. The study area is located in the middle reaches of this river. There are several tributaries to the Watarase within the study area that originate in low mountains with elevations that range from 223 to 681 m a.m.s.l.

b) Climate

The study area is located in a humid temperate zone that shows broad variations in temperature. Summer in the region is characterized by warm and humid conditions, while winter is cold and relatively arid. Based on observed data collected by the Japan Meteorological Agency (http://www.jma.go.jp/jma/index.html) from 1981-2010, the monthly mean air temperature ranges from 2.8°C (January) to 25.7°C (August), and the annual precipitation is approximately 1200 mm (Fig. 3.6). About 75% of the annual precipitation occurs during the rainy season from May to October. The precipitation data were collected from Ashikaga Station (36°18.1' N, 139°28.4' E and 28 m a.m.s.l.), while the temperature data were from Sano Station (36°21.8' N, 139°34.2'E and 68 m a.m.s.l.).

During the study period (September 2010 to October 2011), the monthly mean air temperature was 15.5°C, which was a bit higher than the long-term annual mean air temperature. The annual mean precipitation was approximately 1574 mm, which was also larger than the long-term annual mean precipitation. Typically, the precipitations were approximately 100 or up to 200 mm larger than long-term mean values in May, July and September. The highest monthly air temperature and largest monthly precipitation occurred in July 2010, which were 26.7°C and 349 mm, respectively.

c) Land use

Forest is the dominant land cover for the mountains, while residential areas are mainly located in the lowlands along the Watarase River (Fig. 3.7). Rice paddy fields are also distributed along the

Watarase River and its tributaries, but their total area accounts for only 10% of the entire study area. In additional, irrigation period occurs during rainy seasons from June to September.

d) Water use

No facilities consuming large amounts of water were found in the study area, except for seven water purification plants (AT1 - AT7 in Fig. 6.1) with 17 municipal wells. These plants are distributed along the Watarase River and supply tap water to local residents. The municipal water supply system in Ashikaga City is solely dependent on groundwater. In addition to tap water, many residents also utilize water drawn from private wells on their own land for domestic purposes. Because these wells are private, hydrometric measurements are not available. It should also be noted that the drainage system in the study area is well developed; therefore, domestic wastewater can be rapidly drained to rivers and away from the study area without re-entering local groundwater systems. Accordingly, the seepage of domestic wastewater to groundwater in the study area was not considered in this study.

e) Geology and hydrogeology

As shown on the surficial geology map (Fig. 3.8), the mountains in the study area are characterized by a series of distinct NE-SW trending anticline and syncline tectonic movements. The lithology of the mountains consists mostly of chert, sandstone with interbedded slate or mudstone, and some limestone. Plains and valleys in the region are overlain by recent alluvial sediments (sand and gravel) and volcanic soil (loam). The geologic cross section (Fig. 3.8b) shows that the thickness of the aquifer increases from 55 to more than 150 m from northwest to southeast in the plain. The aquifer is mainly composed of gravel and sand, and the aquitard consists of red and blue clay. The bedrock is composed of chert.

3.2.2 Research states about the Ashikaga area

The previous studies about the related studies in the Ashikaga area are very few and only sparse observation data were found from Groundwater Level Chronology and Water Information System (http://www1.river.go.jp/) of Japan. The groundwater table and subsidence have been

observed slightly decreased from 1979 to 1991 with long-time pumping (Fig. 3.9). Therefore, it is urgent to make clear two questions: 1) how does the river influence local groundwater system, and 2) does the long-time pumping intense the river seepage?

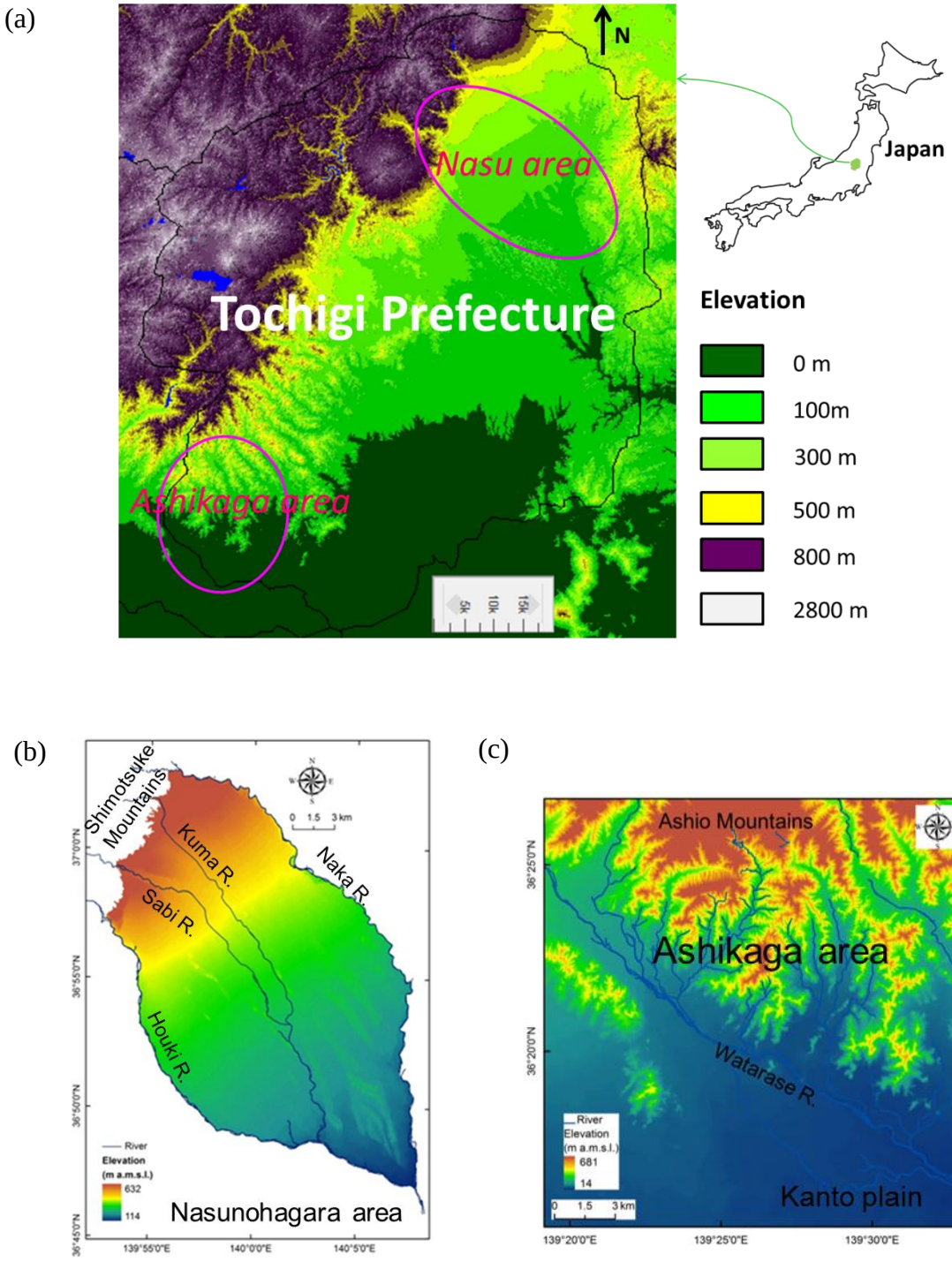

Figure 3.1 The location of the study areas. (a) Tochigi Prefecture, (b) Nasunogahara area and (c) Ashikaga area.

(a)

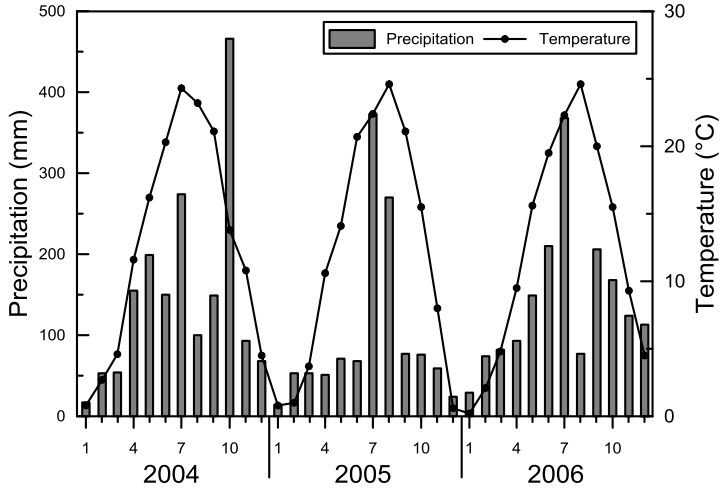

(b)

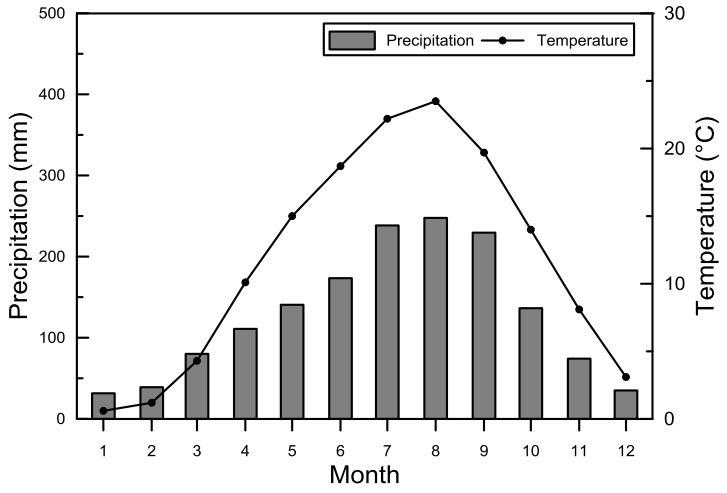

Figure 3.2 Inter-monthly variations of (a) air temperature and precipitation during the study period from 2004 to 2006 and (b) 30 years long mean values (1981-2010) in the Nasunogahara area.

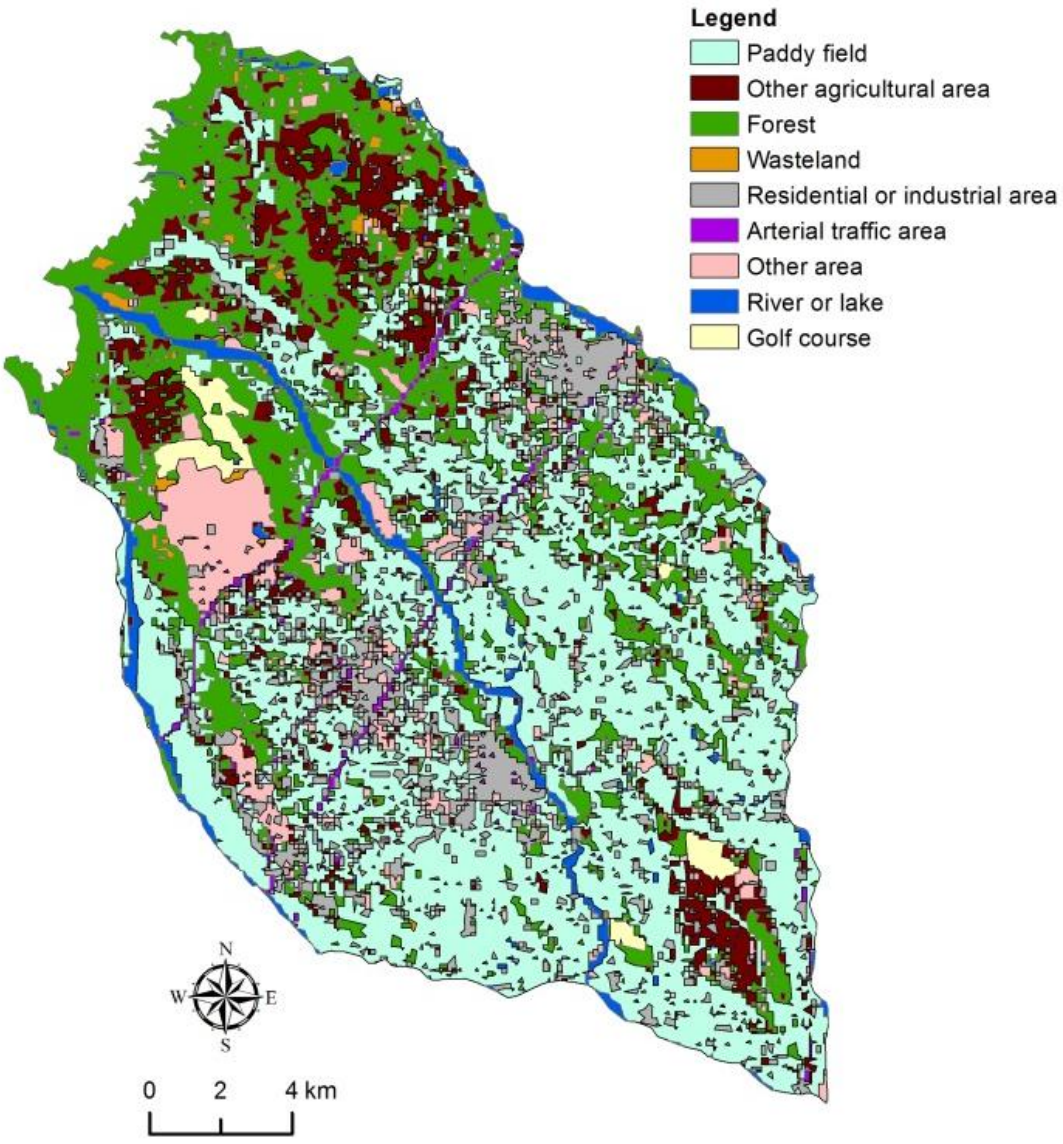

Figure 3.3 Land use map of the Nasunogahara area..

(a)

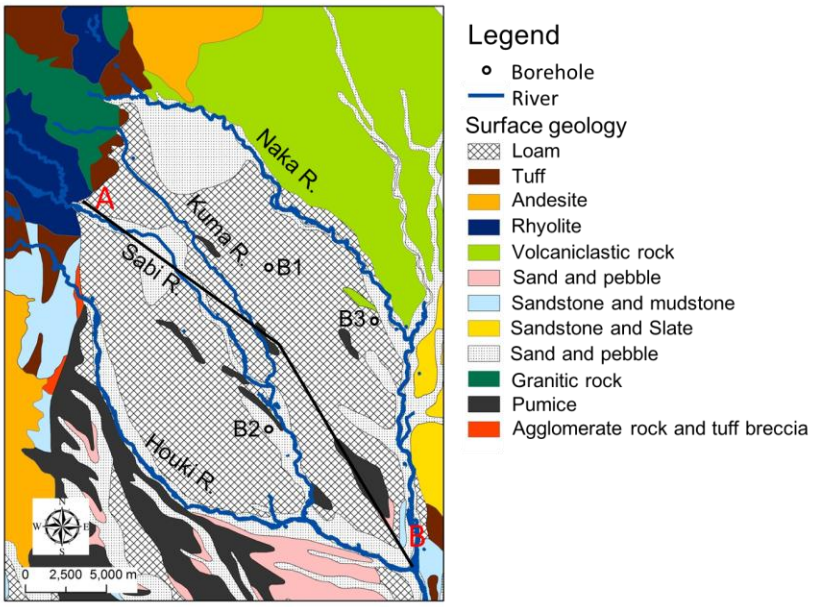

(b)

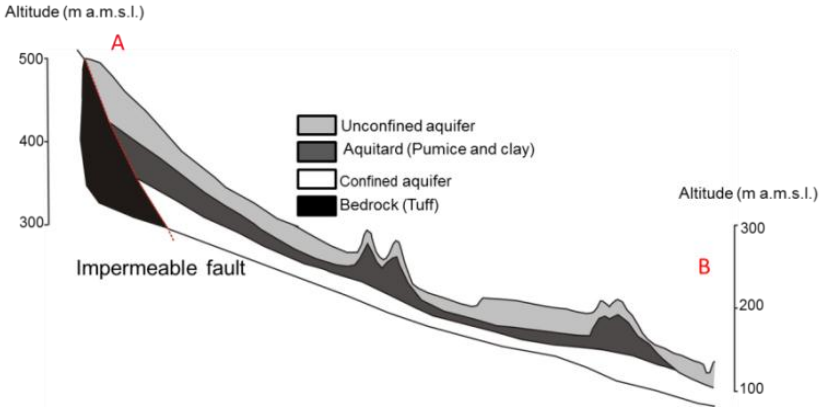

(c)

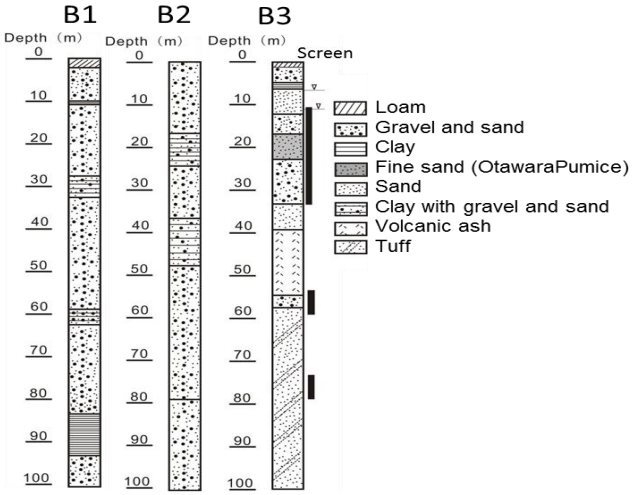

Figure 3.4 Surficial geology map (a) of the Nasunogahara area (National Land Survey Division, Land and Water Bureau, Japan; http://tochi.mlit.go.jp/tockok/) with (b) cross-section A-B showing the location of the impermeable fault and the distribution of unconfined aquifer and (c) lithological diagram of boreholes.

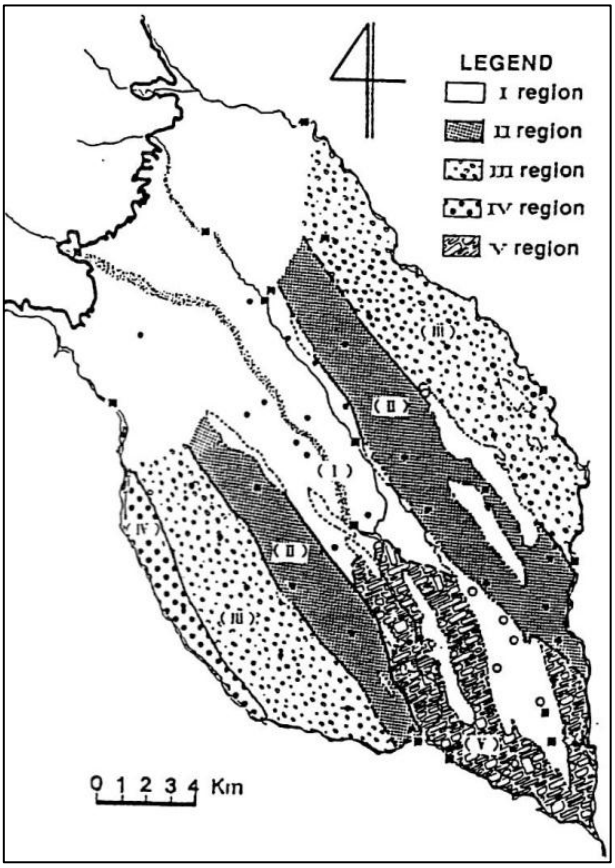

Figure 3.5 Regional classification of the Nasunogahara area based on water quality (from Hiyama and Suzuki, 1991).

(a)

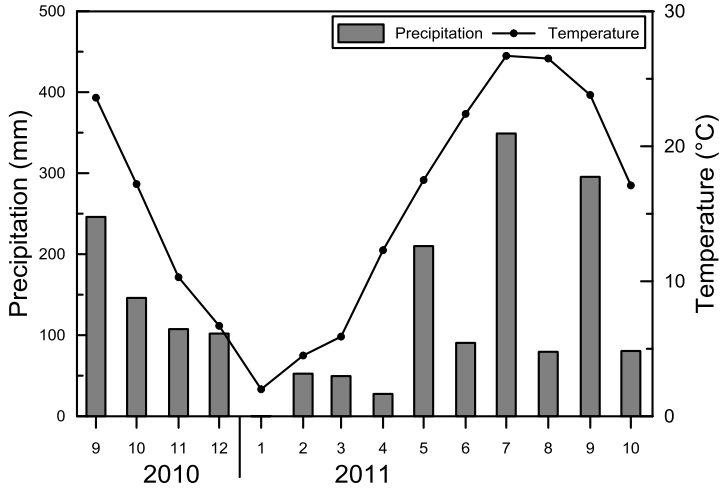

(b)

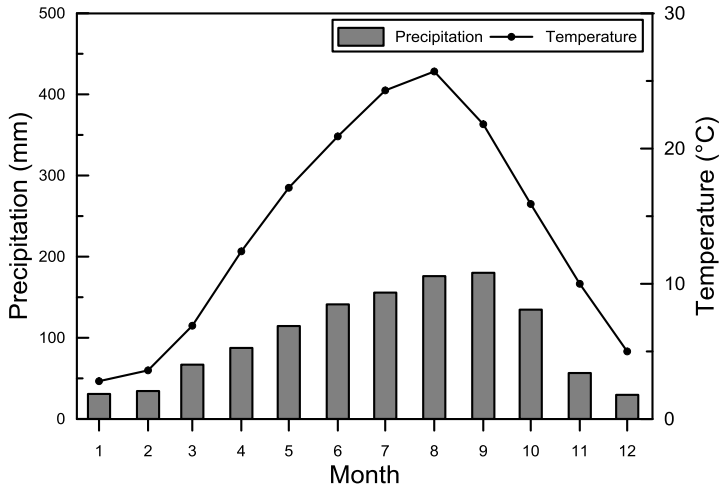

Figure 3.6 Inter-monthly variations of (a) air temperature and precipitation from September 2010 to October 2011 and (b) 30 years long mean values (1981-2010) in the Ashikaga area.

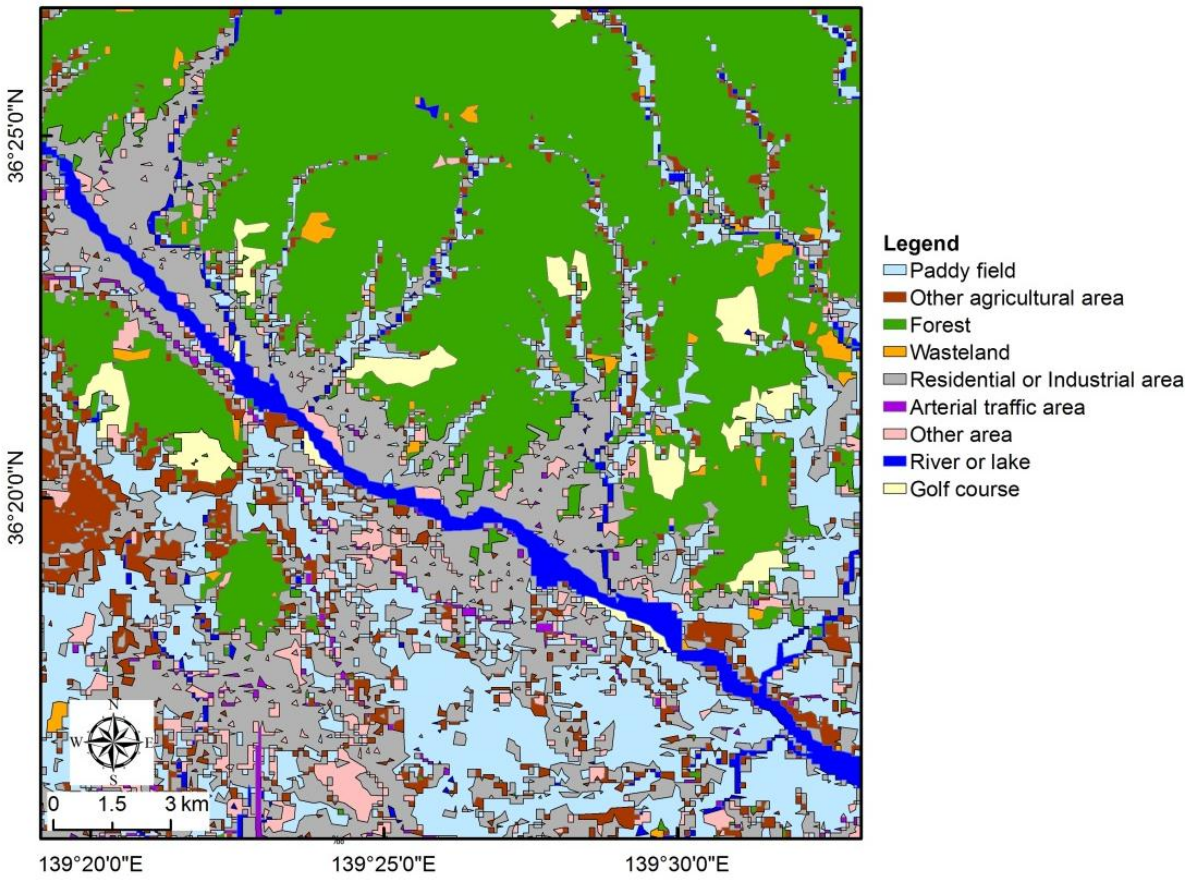

Figure 3.7 Land use map of the Ashikaga area.

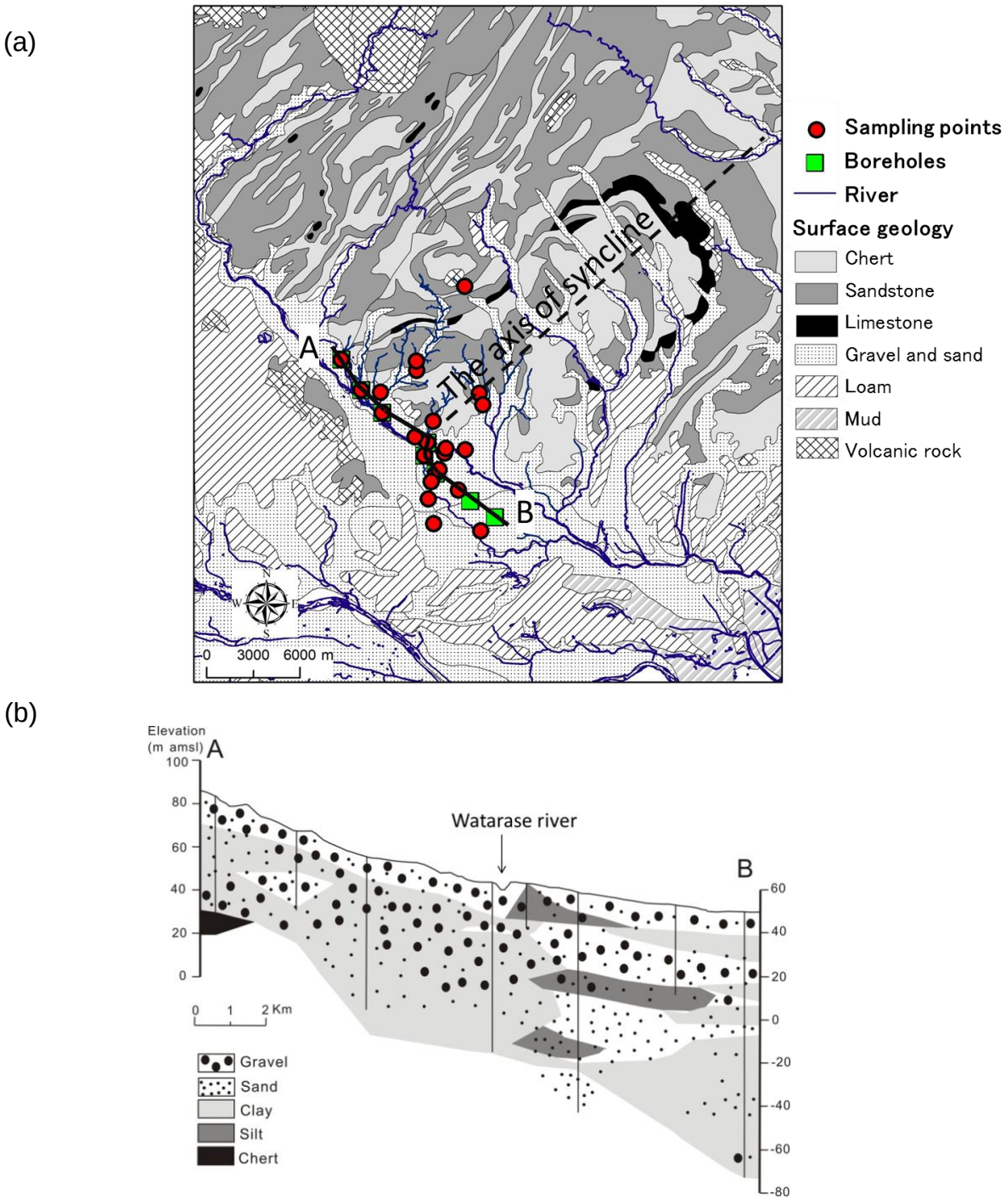

Figure 3.8 Surficial geology map (a) of the Ashikaga area (National Land Survey Division, Land and Water Bureau, Japan; http://tochi.mlit.go.jp/tockok/) with (b) cross-section A-B showing lithology of aquifers (drawn based on borehole logs).

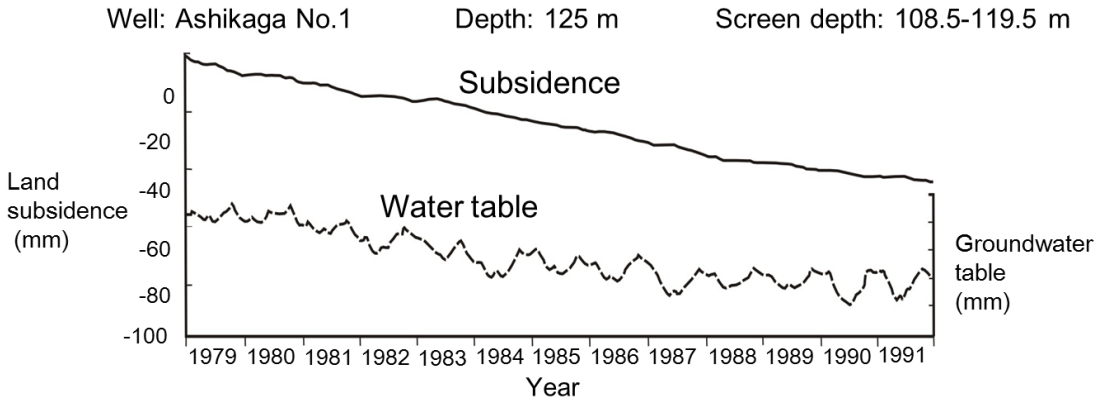

Figure 3.9 Diagram of land subsidence and annual changes of groundwater table in the Ashikaga area (from report of groundwater map, Ibaraki and Tochigi Prefectures, 1:200,000, 1995).

Chapter 4
Tracer approach for the Nasunogahara area

4.1 Introduction

The detailed hydrochemical and isotopic characteristics in the Nasunogahara area were done by Wakui and Yamanaka (2006). The precipitation, river and paddy field water were identified to be three main recharge sources of local groundwater system in the Nasunogahara area. A spatial distribution of contribution ratios of groundwater recharge sources in the midstream of the study area was obtained based on end-member mixing analysis (EMMA) approach. However, the error of EMMA caused by the uncertain concentrations of end-members and the resultant mixtures was not discussed in the previous study. Therefore, the specific objective of this chapter is to re-estimate the contribution ratios of recharge sources considering the potential error of EMMA. Furthermore, the potential influence factors of river seepage were further discussed.

4.2 Material and methods

4.2.1 Data sets

The data sets used in this study were from Wakui and Yamanka (2006). Field works were conducted monthly from February 2004 to February 2005 for sampling well waters (Fig. 4.1), river waters, and paddy field waters. Meanwhile, the precipitation samples were collected monthly from March 2004 to February 2005. All the samples were collected for the oxygen-18 and deuterium compositions analysis. Meanwhile, the groundwater depths were measured for all the sampling wells during fieldwork period. The compositions of ^{18}O and D were expressed by $\delta^{18}O$ and δD, respectively relative to Vienna Standard Mean Ocean Water. The measurement accuracy was $\pm 0.1\%$ for $\delta^{18}O$ and $\pm 1\%$ for δD.

4.2.2 End-member mixing analysis

End-member mixing analysis based on the mass balance of tracers has conventionally been used for hydrograph separation (Burns et al., 2001; Doctor et al., 2006). EMMA can also be used to evaluate the contribution ratio of each recharge source of groundwater (Wakui and Yamanaka, 2006; Nakaya et al., 2007; Qin et al., 2011). This technique assumes the following (Barthold et al., 2011): (1) groundwater is a mixture of source substances with a fixed composition; (2) the mixing process is linear and completely dependent on hydrodynamic mixing; (3) the substances used as tracers are conservative; and (4) the source substances have extreme concentrations.

The respective contributions of source A, B and C components to groundwater M can be calculated by using the three following mass balance equations:

$$R_A + R_B + R_c = 1 \tag{4-1}$$

$$\bar{\gamma}_M = \bar{\gamma}_A R_A + \bar{\gamma}_B R_B + \bar{\gamma}_C R_C \tag{4-2}$$

$$\bar{\lambda}_M = \bar{\lambda}_A R_A + \bar{\lambda}_B R_B + \bar{\lambda}_C R_C \tag{4-3}$$

where R is the mean contribution ratio of each recharge source, $\bar{\gamma}$ and $\bar{\lambda}$ are the mean concentration/ composition of tracer γ and tracer λ respectively, and subscripts *A*, *B*, and *C* refers to three potential recharge sources. If the concentrations of two tracers are known, the R for each potential source could be estimated using the following equations:

$$R_A = \frac{(\bar{\gamma}_M - \bar{\gamma}_C)(\bar{\lambda}_B - \bar{\lambda}_C) - (\bar{\lambda}_M - \bar{\lambda}_C)(\bar{\gamma}_B - \bar{\gamma}_C)}{(\bar{\gamma}_A - \bar{\gamma}_C)(\bar{\lambda}_B - \bar{\lambda}_C) - (\bar{\lambda}_A - \bar{\lambda}_C)(\bar{\gamma}_B - \bar{\gamma}_C)} \tag{4-4}$$

$$R_B = \frac{(\bar{\gamma}_M - \bar{\gamma}_C)(\bar{\lambda}_A - \bar{\lambda}_C) - (\bar{\lambda}_M - \bar{\lambda}_C)(\bar{\gamma}_A - \bar{\gamma}_C)}{(\bar{\gamma}_B - \bar{\gamma}_C)(\bar{\lambda}_A - \bar{\lambda}_C) - (\bar{\lambda}_B - \bar{\lambda}_C)(\bar{\gamma}_A - \bar{\gamma}_C)} \tag{4-5}$$

$$R_C = 1 - R_A - R_B \tag{4-6}$$

If the plots of groundwater fall outside of the three end-member model, the contribution ratio for the outliers would be estimated by the method descripted by Liu et al. (2004).

Same as Wakui and Yamanaka (2006), O^{18} and D are used as two tracers in the EMMA (Fig. 4.2). The river, precipitation and paddy field water are three potential recharge sources of groundwater. It should be noted that the δ values of precipitation used in this study is weighted mean values by monthly precipitation but not arithmetic mean values which used in the previous study.

4.2.3 Error Analysis

Considering the uncertain concentration of end-members and the resultant mixtures, the mean contribution ratio and standard error of the estimated contribution ratio was computed by error propagation analysis (Phillips and Gregg, 2001). If we assume the independence of the concentration/ composition measurements of the three sources and the mixture, then a first order Taylor series approximation for variance of R_A evaluated at the mean is:

$$\begin{aligned}\sigma_{R_A}^2 = &(\frac{\partial R_A}{\partial \bar{\gamma}_M})^2\sigma_{\bar{\gamma}_M}^2 + (\frac{\partial R_A}{\partial \bar{\gamma}_A})^2\sigma_{\bar{\gamma}_A}^2 + (\frac{\partial R_A}{\partial \bar{\gamma}_B})^2\sigma_{\bar{\gamma}_B}^2 + (\frac{\partial R_A}{\partial \bar{\gamma}_C})^2\sigma_{\bar{\gamma}_C}^2 \\ &+(\frac{\partial R_A}{\partial \bar{\lambda}_M})^2\sigma_{\bar{\lambda}_M}^2 + (\frac{\partial R_A}{\partial \bar{\lambda}_A})^2\sigma_{\bar{\lambda}_A}^2 + (\frac{\partial R_A}{\partial \bar{\lambda}_M})^2\sigma_{\bar{\lambda}_B}^2 + (\frac{\partial R_A}{\partial \bar{\lambda}_M})^2\sigma_{\bar{\lambda}_C}^2\end{aligned} \quad (4\text{-}7)$$

where the σ_{R_A} is standard error of contribution ratio estimation with 95% confidence intervals for R_A; $\sigma_{\bar{\gamma}_M}^2$, $\sigma_{\bar{\gamma}_A}^2$, $\sigma_{\bar{\gamma}_B}^2$ and $\sigma_{\bar{\gamma}_C}^2$ represent variances of $\bar{\gamma}$ for mixture *M*, and sources *A*, *B* and *C*, respectively; $\sigma_{\bar{\lambda}_M}^2$, $\sigma_{\bar{\lambda}_A}^2$, $\sigma_{\bar{\lambda}_B}^2$ and $\sigma_{\bar{\lambda}_C}^2$ represent variances of $\bar{\lambda}$ for mixture *M*, and sources *A*, *B* and *C*, respectively. The σ_{R_B} and σ_{R_C} can be determined by switching the *A*, *B* and *C* subscripts in Eq. 4-7. If a correlation exists between tracer γ and tracer λ, then the Eq. 4-7 can be modified as:

$$\begin{aligned}\sigma_{R_A}^{2'} = &\sigma_{R_A}^2 + 2\frac{\partial R_A}{\partial \bar{\gamma}_M}\frac{\partial R_A}{\partial \bar{\lambda}_M}\sigma_{\bar{\gamma}_M,\bar{\lambda}_M} + 2\frac{\partial R_A}{\partial \bar{\gamma}_A}\frac{\partial R_A}{\partial \bar{\lambda}_A}\sigma_{\bar{\gamma}_A,\bar{\lambda}_A} \\ &+2\frac{\partial R_A}{\partial \bar{\gamma}_B}\frac{\partial R_A}{\partial \bar{\lambda}_B}\sigma_{\bar{\gamma}_B,\bar{\lambda}_B} + 2\frac{\partial R_A}{\partial \bar{\gamma}_C}\frac{\partial R_A}{\partial \bar{\lambda}_C}\sigma_{\bar{\gamma}_C,\bar{\lambda}_C}\end{aligned} \quad (4\text{-}8)$$

where $\sigma_{\bar{\gamma},\bar{\lambda}}$ is the covariance between $\bar{\gamma}$ and $\bar{\lambda}$ for populations *A*, *B*, *C*, and *M*. If the correlations are assumed to be zero, then $\sigma_{R_A} = \sigma_{R_A}^{'}$. An excel spreadsheet to perform the

calculations for the source proportions and their variances, standard errors, and 95% confidence intervals for three end-member model can be accessed at http://www.epa.gov/wed/pages/models.htm (Phillips and Gregg, 2001).

The standard deviations of measured δ values were used to represent the variances of δ values for groundwater and river water samples (Table 4.1). As a mixing process probably exits in the unsaturated zone before water infiltration from precipitation and paddy field water to the groundwater table, the variances of δ values of local precipitation and paddy field water was assumed to equal to the mean standard deviations of river water samples. The standard error caused by the variances of δ values of each end-member and mixture was calculated, respectively. Then the mean value of calculated standard errors was used as the error of contribution ratio caused by the uncertainty of EMMA at wells in the Nasunogahara area.

4.3 Results

The estimated mean contribution ratios and their possible errors are shown in Fig. 4.3. The errors are very large for estimated contribution ratios of river and precipitation, which ranged from 33% to 58% and from 42% to 72%, respectively. However, the estimated contribution ratio of paddy field water is relatively not sensitive to the uncertainty composition of end-members and mixtures. The errors of contribution ratios of paddy field water ranged from 12-19%. The contribution ratios of paddy field water are low (≤12%) at most of sites except G4, where the contribution ratio of paddy field water is 32%. Even with high standard errors, the general tendency of contribution ratios of river and precipitation still can be distinguished from Figure 4.3. The rive seepage were occurred at G1, G3, G4, G5, and G6. The precipitation is a very important recharge source at G7, G30, G44 and G45. The spatial distribution of mean contribution ratios is shown in Figure 4.4, indicating that the river contribution is high near river channel and becomes low gradually with distance from the channel.

4.4 Discussion

As mentioned above, the contribution ratios of river waters are very high at wells near river channels and decrease with distance from the channels. It suggests that the distance from river channels is a very important factor controlling river water relative contribution. However, the estimated contribution ratio at G6 is larger than that at G5, where is nearer the Sabi River channel than G6 (Fig. 4.1). The isotopic signature also shows that the isotope signature of G5 is closer to the Sabi River than G6 (Fig 4.2). Therefore, the Sabi River contribution ratio is probably overestimated at G6. The location of G6 is close to the Kuma River and the isotopic signature of G6 is also close to the isotopic signature of the Kuma River, indicating that the infiltration of the Kuma River water probably occurred at G6. The occurrence of the Kuma River water induces the overestimated contribution ratio of the Sabi River water at G6.

Although the Sabi River is an intermittent river, the contribution ratio of the river water is very high to wells near the river channel. The contribution ratio even reaches to 68% at G4. In other words, the groundwater near the channel is very sensitive to the water quality and quantity of the Sabi River. The high permeability of sediments along the Sabi River channel is probably the main reason caused high river seepage. In addition, the geological setting, i.e. the impermeable fault increases the contribution ratio of river water more or less through resisting mountain block recharge and aquifer lateral recharge to aquifers in the alluvial fan. The contribution ratios of river and precipitation show symmetric characteristics with respective to the Sabi River, which is agree with the symmetric distribution characteristics of local topography and surface geology (Fig. 3.4). Therefore, the symmetric surface topography and alluvial sediments are probably very important factors controlling the symmetric distribution of river seepage.

In most of sits, the estimated contribution ratios of paddy field water are less than 5%. The largest estimated contribution ratio from paddy field water (32%) occurs at G4, where is nearby paddy field. The results indicate that the contribution of paddy field water infiltration is relatively small in the midstream part of the Nasunogahara area. Although the rice paddy field accounts for

about 40% land use in the Nasunogahara area, most of the paddy field distributed at the downstream part and along river channels (Fig. 3.3). Accordingly, relatively smaller area of paddy field distribute around the sampling wells causing small contribution ratios of paddy field water. The low permeability of paddy field soil and short irrigation period (4 months) are probably other reasons inducing the small contribution ratios of paddy field water. In addition, the large amount of seepage from rivers somewhat reduces the relative contribution of paddy filed water.

The direct infiltration of precipitation is the main recharge source of groundwater. The mean contribution ratio of precipitation is 54%, and the contribution ratio up to 97% at G45. The variable contribution ratios of precipitation and paddy field water among different sites indicate that land use is a very important factor impacting the groundwater recharge system. Furthermore, the land use also potentially modifies the spatial distribution of contribution ratios of river waters.

The large standard error indicates that the EMMA is sensitive to the uncertainty of end-members and mixture in the study area. It reflects the shortcoming of qualitatively analysis of tracer methods, which are usually based on the some assumptions. Violating any assumption mentioned in section 4.2.2 could cause large errors. In addition, time lag from sources to wells could also impact the results of EMMA. However, even with the large standard error in the estimated contribution ratios, the EMMA still gave a general tendency of contribution ratios of recharge sources for the Nasunogahara area. It will be very useful for understanding the recharge mechanism of this area and constructing the conceptual model for numerical simulation. It could also provide useful information for integrated water resources management.

4.4 Summery

River seepage is a very important recharge source for local groundwater system along river channels in the Nasunogahara area. Especially, the seepage along the Sabi River channel is very large and the contribution ratio of Sabi River water up to 68% at G4. The distance from river

channels, hydraulic property of river bed sediments, symmetric surface topography and alluvial sediments are three potential factors controlled river seepage. In addition, the geology and land use modify the spatial distribution of the contribution ratio of river water more or less. Direct infiltration from local precipitation is the main recharge source in the midstream of Nasunogahara area. The contribution ratio of the paddy field water is small at most of sites (≤12%) of the midstream of Nasunogahara area, which is probably caused by small rice planting area in the midstream part, low permeability of paddy field soil and short irrigation period.

Although the results of EMMA companied with high standard errors, this method is still provides useful information for understanding recharge mechanism of local groundwater system and the influence of river seepage on local groundwater system in the Nasunogahara area. To further increase the reliability of EMMA, combined use of the other approaches such as numerical simulation is very necessary.

Table 4.1 Isotopic compositions of groundwater, river water, precipitation and paddy field water in the Nasunogahara area (annual mean values, from Wakui and Yamanaka, 2006).

	Groundwater										River			Paddy[b] field water	Precipitation[c] (Weighted mean)
	G1	G3	G4	G5	G6	G7	G30	G31	G44	G45	Sabi	Naka	Houki		
$\delta^{18}O$ (‰)	-8.99	-9.19	-8.10	-8.90	-8.74	-8.71	-8.23	-8.77	-8.66	-8.28	-9.57	-9.21	-9.41	-4.98	-8.39
δD (‰)	-58.7	-59.76	-54.84	-58.2	-57.7	-57.07	-54.54	-57.39	-56.79	-54.76	-61.9	-59.9	-60.9	-39.8	-55.26
[a]Std_$\delta^{18}O$	0.21	0.13	0.22	0.20	0.21	0.15	0.17	0.18	0.11	0.17	0.53	0.2	0.52	0.42	0.42
[a]Std_δD	1.49	1.34	0.80	1.70	1.36	1.94	1.31	1.29	1.77	1.72	3.9	1.72	4.34	3.32	3.32
Sampling Number	13	13	13	13	13	13	9	6	13	13	13	13	13	4	12
Correlation Coefficient of $\delta^{18}O$ and δD	0.91	0.14	0.98	0.60	0.67	0.51	0.33	0.89	0.18	0.18	0.93	0.69	0.91	0.90	0.98

[a] Std denotes standard deviation, which was calculated excluding the abnormal values at G1 and G4 in July 2004 and at the Sabi River in August 2004.

[b] The δ values are monthly mean values and standard deviations are mean standard deviation of river waters.

[c] The weighted mean δ values of precipitation are weighted by monthly precipitation and standard deviations are mean standard deviation of river waters.

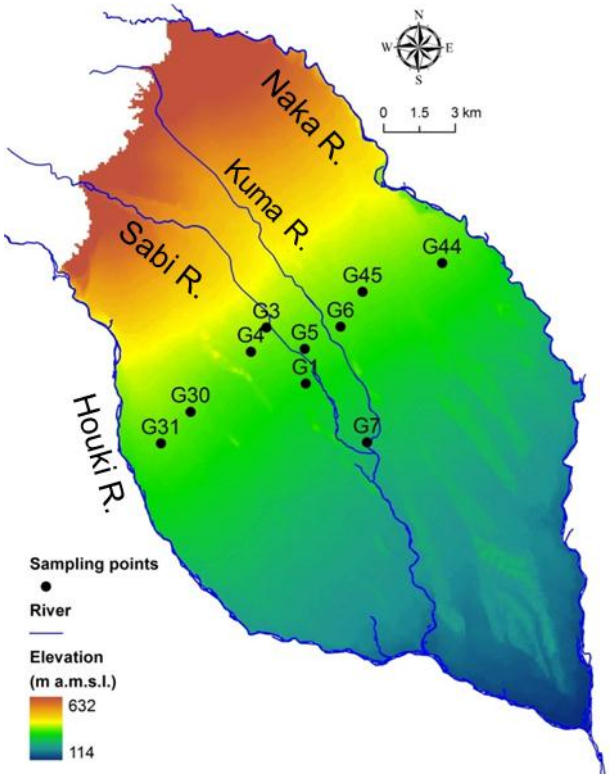

Figure 4.1 Groundwater sampling locations for the Nasunogahara area during the period from February 2004 to February 2005 (after Wakui and Yamanaka, 2006).

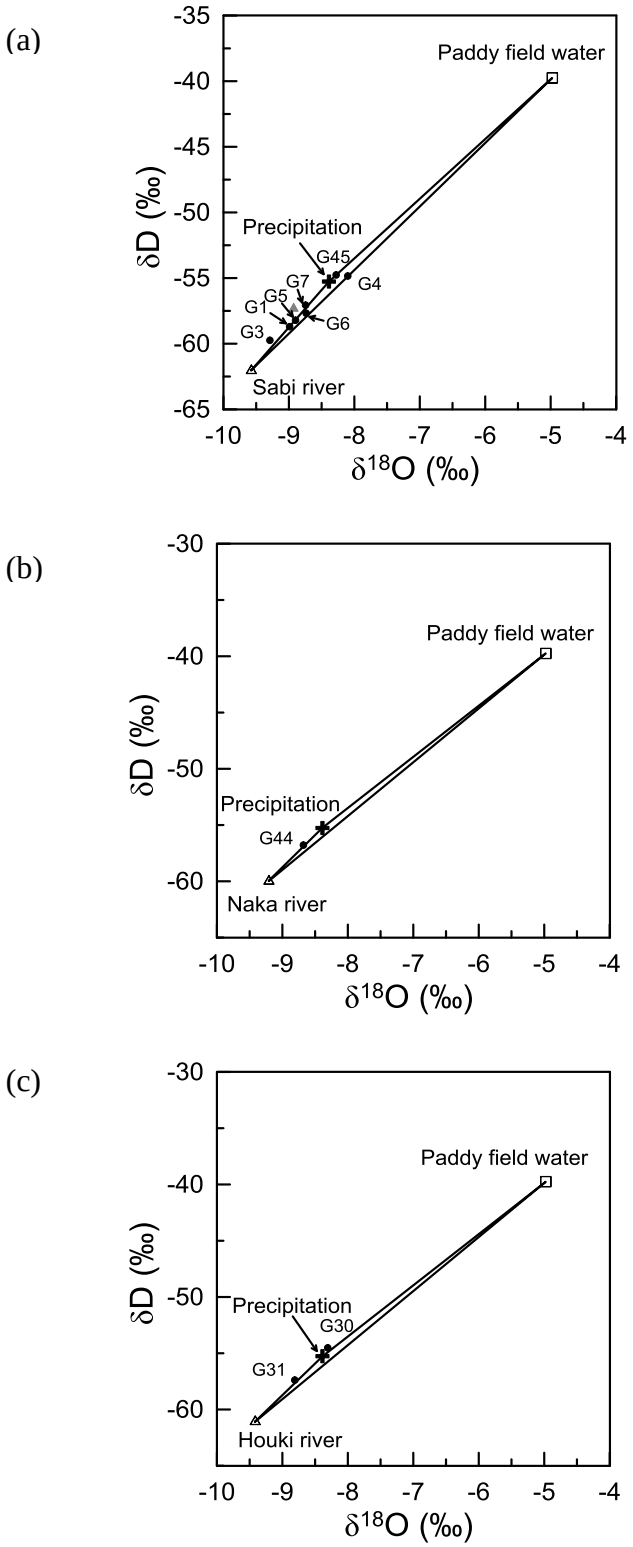

Figure 4.2 Isotopic compositions of groundwater and its potential sources (after Wakui and Yamanaka, 2006). (a) the Sabi River influence area, the filled gray triangle represents the isotopic signature of Kuma River water; (b) the Naka River influence area; and (c) the Houki River influence area.

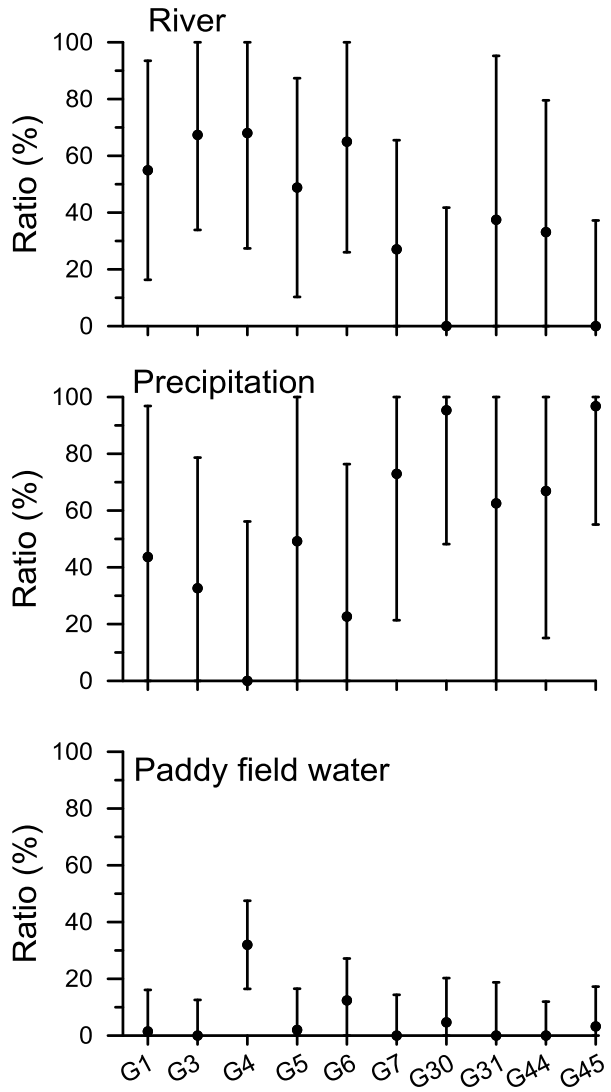

Figure 4.3 The mean contribution ratio of each recharge source and their corresponding standard errors for groundwater samples in the Nasunogahara area.

(a)

(b)

(c)

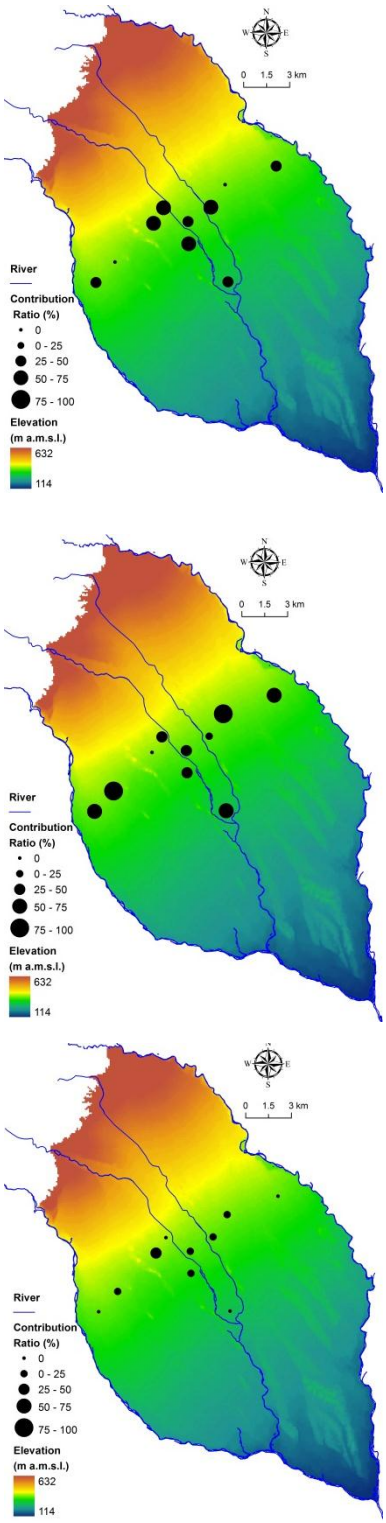

Figure 4.4 The spatial distribution of contribution ratios of (a) river, (b) precipitation, and (c) paddy field water estimated by EMMA for the Nasunogahara area.

Chapter 5
Numerical simulation for the Nasunogahara area

5.1 Introduction

Although the contribution ratios of recharge sources to groundwater were clarified in Chapter 4, the detailed spatial and temporal characteristics of groundwater- river interaction is still not very clear. The specific objectives of this chapter are: (1) to reveal the spatial and temporal characteristics of groundwater recharge and discharge in Nasunogahara area; (2) to certify the validity of using stable isotope tracers as additional simulation terms other than hydrometric data to numerical model for addressing the first objective.

5.2 Methodology

5.2.1 Numerical modeling codes

Groundwater flow was simulated using a three-dimensional groundwater flow modeling program MODFLOW-2000 (Harbaugh et al. 2000), a U.S. Geological Survey block-centered finite-difference computer code. A commercial pre- and post- processor software program, Visual MODFLOW Pro (Ver 4.2; Waterloo Hydrogeologic Inc.), was used to construct the modeling. The groundwater flow is described by the following equation:

$$\frac{\partial}{\partial X}(K_X \frac{\partial h}{\partial x}) + \frac{\partial}{\partial Y}(K_y \frac{\partial h}{\partial y}) + \frac{\partial}{\partial Y}(K_z \frac{\partial h}{\partial Z}) + W = S_S \frac{\partial h}{\partial t} \qquad (5\text{-}1)$$

where K_x, K_y and K_z are the values of hydraulic conductivity along the x, y, and z coordinate axes and are assumed to be parallel to the major axes of hydraulic conductivity [LT^{-1}]; h is the potentiometric head [L]; W is a volumetric source/sink term [L^3T^{-1}], which is used to simulate well discharge, leakage through confining units, streambed leakage, recharge, and water removed from the aquifer by drains; S_s is the storage coefficient of the porous material [L^{-1}]; and t is time [T].

The flow equation was solved by the WHS (Waterloo Hydrogeologic Solver) solver, which is faster and more stable than other standard MODFLOW solver packages such as Strongly Implicit Procedure Package and Preconditioned Conjugate-Gradient Package (Ravazzani et al., 2011). The WHS solver uses a Bi-Conjugate Gradient Stabilized acceleration routine with stone incomplete decomposition as preconditioning method for groundwater flow partial differential equations.

To simulate solute transport in aquifers, we used a MT3DMS code (Zheng and Wang, 1999), an improved version of Modular 3-D Transport model (MT3D) (Zheng, 1990) for simulating transport of multispecies, included with the Visual MODFLOW Pro. The MT3DMS code is developed based on the assumption that changes in the concentration field will not affect the flow field significantly and has a comprehensive set of options and capabilities for simulating advection, dispersion/diffusion, and chemical reactions of contaminants in groundwater flow systems under general hydrogeological conditions. It solves the transport equation after the flow solution has been calculated from groundwater flow model (i.e., MODFLOW). The general advective-dispersive equation describing the fate and transport of contaminant of species *k* in the 3-D transient groundwater flow systems is:

$$\frac{\partial}{\partial x_i}(\theta D_{ij}\frac{\partial C^k}{\partial x_j}) - \frac{\partial}{\partial x_i}(\theta v_i C^k) + q_s C_s^k + \sum R_n = \frac{\partial(\theta C^k)}{\partial t} \qquad (5\text{-}2)$$

where C^k is the dissolved concentration of species k [ML^{-3}]; θ is the porosity of the subsurface medium and it is dimensionless; t is time [T]; x_i is the distance along the respective Cartesian coordinate axis [L]; D_{ij} is the hydrodynamic dispersion coefficient tensor [L^2T^{-1}]; V_i is the seepage or linear pore water velocity [LT^{-1}] and related to the specific discharge or Darcy flux through the relationship of $V_i=q_i/\theta$; q_s is the volumetric flow rate per unit volume of aquifer representing fluid sources (positive) and sinks (negative) [T^{-1}]; C^k_s is the concentration of the source or sink flux for species k [ML^{-3}]; and $\sum R_n$ is the chemical reaction term [$ML^{-3}T^{-1}$].

For solving the solute transport equation, the Visual MODFLOW pro provides 3 kinds of solution methods: the Particle-tracking Based Eulerian-Lagrangian method, Standard

Finite-difference method, and the third-order Total-Variation-Diminishing method (TVD). The Finite-difference methods, such as Upstream Finite Difference (UFD) method, and TVD method are more computationally efficient than particle-tracking methods. In this study, the UFD method with implicit Generalized Conjugate Gradient Solver was used to solve the solute transport equation.

At river banks, two main water sources are (1) river water, depleted of heavy isotopes, originating upstream, and (2) groundwater, which comes mainly from the local rainfall (Lambs, 2004). Based on this principle, the stable isotope of oxygen and hydrogen were used as tracers in the transport simulation. The ^{18}O and D were treated as two contaminants and the absolute value of δ values were input into the transport model as concentrations of contaminants. We assumed that no isotope fractionation occurred during the process of water from recharge sources to observation wells. Therefore, the chemical reaction term was ignored in the simulation, and the Eq. 5-2 could be modified as follows.

$$\frac{\partial}{\partial x_i}(\theta D_{ij}\frac{\partial C^k}{\partial x_j}) - \frac{\partial}{\partial x_i}(\theta v_i C^k) + q_s C_s^k = \frac{\partial(\theta C^k)}{\partial t} \qquad (5\text{-}3)$$

5.2.1 Model construction and parameters

a) Model domain and grid design

The modeled area is 20 by 30 km, which contains the entire Nasunogahara area shown in Fig. 3.1b. The simulation used variable cells areas of 250 m×250 m, 250 m×500 m and 500 m×500 m and contained 29520 cells in 82 rows, 60 columns, and 6 layers (Fig. 5.1a). Layer 1 is the focused simulation layer which corresponds to the unconfined aquifer, where gravel and sand are domain. Layer 2 corresponds to the first aquitard where pumice and clay with sand and gravel are present. Layer 3 to 6 corresponds to confined aquifers/aquitards. Surrounding mountains and hills were assigned as inactive cells. Based on the local hydrogeology setting (section 3.1.1), variable thickness ranging from 2 to 107 m was assigned to Layer 1 in the active model domain. Uniform

thicknesses were assigned to Layers 2 to 6 and they are 10 m, 20 m, 15 m, 30 m, and 50 m, respectively (Fig. 5.1b and c).

b) Boundary setting and input data

Flow Boundaries

The Naka River and the Houki River are assigned as constant head boundaries using Time-Variant Specified-Head package (Leake and Prudic, 1991) in the model. The daily observed river stage in Kurobane gaging station (140°07′07″ E, 36°51′25″ N) of the Naka River during the simulation period was used to simulate the hydraulic head of constant head boundaries. The Sabi River was treated as a stream boundary using Streamflow-Routing Package (Prudic, 1989). The inflow of the first uppermost segment of the stream boundary was calculated by a sample river tank model and verified by a previous study (Wakui, 2007). The river bed conductance was determined by a trail-and-error method. Springs were simulated as a sink term of groundwater by using drain boundaries with fixed head in time and variable in space.

Since an impermeable fault separates Nasunogahara area from the Shimotsuke Mountains in the northwest area of the model domain, a no-flow boundary was assigned for the northwestern boundary of the model domain. This setting is similar as previous studies (Elhassan et al. 2001; Fujinawa, 1981). The present study assumed that the bedrock or deep aquifers below Layer 6 do not have contribution to groundwater flow in the simulated aquifers. Therefore a no-flow boundary was adopted for the bottom of the model.

The Recharge Package was assigned to the uppermost active aquifer to simulate spatially distributed recharge from precipitation and paddy field water to the groundwater system. The daily net recharges of precipitation and paddy field water were estimated by a tank model, which considered the spatial distribution of paddy field land use and the irrigation time in the study area (Fig. 5.2). The parameters used in the tank model were from previous studies (Wakui, 2007; Yamanaka and Wakui, 2009). The groundwater recharge from the paddy field during the irrigation period was considered as paddy field water recharge, while during the rest of the year

was considered as precipitation recharge. The recharge at paddies and at non-paddy field was estimated for each mesh at a daily time step. According to the estimated net recharge from both paddy field and non-paddy field, the model domain of MODFLOW was divided into 4 recharge zones and the corresponding recharge was shown in Fig. 5.2.

Mass Transport Boundaries

Three general types of boundary conditions are considered in the MT3DMS transport model: (a) concentration known along a boundary (Dirichlet Condition), (b) concentration gradient known across a boundary (Neumann Condition); and (c) a combination of (a) and (b) (Cauchy Condition) (Zheng and Wang, 1999). In the Visual MODFLOW pro, the above three types of boundary conditions were modified through combing the water flow boundary settings. The detailed boundary settings in the transport model for the Nasunogahara area are list as follows.

The Sabi River was set as a constant concentration boundary, which acts as a contaminant source providing solute mass to the model domain in the form of a known concentration. Corresponding with constant head boundaries, point source boundaries were assigned to the Naka River and the Houki River. The point source boundary condition specifies the concentration of each species entering or leaving the model through the constant head boundary condition grid cells specified in the flow model. For the impermeable boundary and drain boundary, a default setting that concentration gradient is equal to zero (i.e., a special case of the second-type boundary condition) was accepted. The recharge concentration boundary condition (i.e., the source term of the governing equation), which specifies the concentration of each species accompanying the recharge flux specified in the flow model, was assigned to the recharge boundary.

c) Initial conditions

A steady state simulation was done for achieving the initial conditions of the transient (non-steady state) simulation. The observed hydraulic heads and δ values of ^{18}O and D in February 2004 were used as initial heads in the model under steady state condition. Then, the calculated

hydraulic head and concentrations of ^{18}O and D were applied as initial conditions in the model under transient condition.

d) Hydraulic and transport parameters

Considering the heterogenetic and anisotropic properties of the aquifers, Layer 1 was subdivided into 21 parameter zones (Fig. 5.3). For the other layers, one parameter zone was set accompanying with one layer. It was assumed that the horizontal conductivity is isotropy and vertical conductivity was less than horizontal conductivity in each parameter zone. The hydraulic conductivities and specific yield parameters were initially assigned on the basis of the hydraulic parameters estimated by Elhassan et al. (2001) and Wakui (2007). The other hydraulic parameters and transport parameters were initially assigned based on the empirical values and systems defaults. Then, the hydraulic parameters were modified through model calibration with the help of Visual PEST (Doherty, 1998), a graphical nonlinear parameter estimation and predictive analysis package. The conductances of stream and drain boundaries were determined through calibration by a trail-and-error method. Table 6.1 summarized the determined parameters through hydraulic and isotopic calibrations.

e) Head and concentration observation wells

For Nasunogahara area, field investigations were done monthly from February 2004 to February 2005 (Wakui and Yamanaka, 2006) and almost bimonthly from April to September 2006 (Wakui, 2007). Groundwater tables were measured and samples were taken for 10 wells (Fig. 4.1) in the 1st field survey and 17 wells (Fig. 5.4) in the 2nd field survey. River waters and paddy field waters were sampled during two field investigation periods. The precipitation was collected monthly from February 2004 to September 2006. Stable isotopes of all water samples were analyzed in two investigation periods. Both the observed hydrometric data and the measured isotopic data in two investigation periods were used to calibrate water flow and transport model.

5.3 Results

5.3.1 Calibration results

The model was calibrated twice under transient conditions during two field investigation periods for acquiring reliable calibration results. The first calibration period is from March 2004 to February 2005 with monthly observation data and the second calibration period is over the period between April and October 2006 with almost bimonthly observation data. As the observation wells were mainly located in the midstream of the Nasunogahara area during the 1st simulation period (Fig. 4.1), the hydraulic and transport parameters of the downstream of the Nasunogahara area were mainly decided based on the 2nd calibration and then input to the 1st simulation. However, the observation period was longer and observation frequency was higher in the 1st simulation period than in the 2nd simulation period. Therefore, the hydraulic and transport parameters of the upstream and midstream parts of the Nasunogahara area were mainly determined based on the calibration results of the 1st simulation and slightly modified by the 2nd simulation. A method of trial and error was used to determine the parameters for these two simulations. Both of the hydraulic head and δ values were used as the calibration terms in these two simulations.

The comparison of observed and computed values was shown in Fig. 5.5 for the 1st simulation and in Fig. 5.6 for the 2nd simulation. The degree of conformity between simulated and observed data was examined using residual mean (RM) and root mean squared error (RMS). The RM values of hydraulic head for the 1st and 2nd simulations were -0.1 m and -0.18 m respectively and the RMS values were 1.03 m and 1.61 m. For $\delta^{18}O$, the RM values were -0.01‰ and -0.02‰ and the RMS values were 0.48‰ and 0.26‰ respectively. The RM and RMS values of δD were -0.03‰ and 2.1‰ for the 1st simulation and -0.4‰ and 1.9‰ for the 2nd simulation. The results indicated that the model could represent hydrologic conditions and transport conditions very well for the Nasunogahara area. The reliability of the model was future evaluated through comparing the observed and simulated temporal variation in hydraulic head and δ values (Fig. 5.7 and Fig. 5.8). The results implied that the model could effectively reproduce the temporal variations of hydraulic

head and δ values in the field. Therefore, the model was considered to be calibrated satisfactorily and could be applied to solve some physical problems for the Nasunogahara area.

5.3.2 Sensitivity analysis for hydraulic parameters

Since the Nasunogahara area is surrounded by natural boundaries (i.e., rivers and faults) and the inputs of river stages were observed data, uncertainty of boundary settings is thus expected to be limited. Therefore, a set of sensitivity analyses of hydraulic parameters rather than boundary settings were performed.

For examining the sensitivity of hydraulic head and δ values to hydraulic parameters, the parameter of sensitivity was defined as follows:

$$Sens_{head} = RMS_{head(n)} - RMS_{head(0)} \tag{5-4}$$

$$Sens_{\delta^{18}O} = RMS_{\delta^{18}O(n)} - RMS_{\delta^{18}O(0)} \tag{5-5}$$

$$Sens_{\delta D} = RMS_{\delta D(n)} - RMS_{\delta D(0)} \tag{5-6}$$

$$Sens = 1 \times Sens_{head} + 1 \times \frac{(10 \times Sens_{\delta^{18}O} + Sens_{\delta D})}{2} \tag{5-7}$$

where *Sens* is sensitivity; *RMS* is root mean squired error; subscript *head* is hydraulic head, subscripts $\delta^{18}O$ and δD are δ values of ^{18}O and D, respectively; subscripts *n* and *0* represent simulation case No. *n* and No. 0, respectively.

Here, it was assumed that the total sensitivity equals to the sensitivity on hydraulic head plus the sensitivity on stable isotopes. Since values of δ^{18}O has approximately one order lower magnitude than those of δD, the sensitivity of δ^{18}O was weighted by 10 and then took the average of 10 times sensitivity of δ^{18}O and sensitivity of δD as the sensitivity of stable isotopes.

The control case is defined as that obtained by the calibration (i.e., nearly the best). Totally 16 cases except the control case were runs for sensitivity analysis and the parameter settings for each case were described in Table 5.2. If the *Sens* has positive values, performance of the case No. *n* is worse than that of control case and vice versa. As shown in Fig. 5.9, parameters with higher sensitivity are as follows in descending order: (1) hydraulic conductivity of aquifers, (2) specific

yield and storage of aquifers, (3) vertical hydraulic conductivity of streambed and (4) conductance of drain boundary. For a same case, the sensitivity of the hydraulic head was different from that of δ values (Fig. 5.10). For example, the sensitivity of hydraulic head in Case 2 was positive, while the sensitivity of the δ values was negative. In other words, the simulation results of hydraulic head in Case 2 were worse than those of control case, though the simulation results of δ values were better. Case 14 showed nearly no sensitivity for hydraulic head, while it showed slight sensitivity for δ values, providing information to find a sets of suitable parameters for the simulation. Therefore, use of δ values as additional terms for calibration other than hydraulic head could give more reliable calibration results than use of only hydraulic head.

5.3.3 Spatial and temporal variation of groundwater tables in unconfined aquifer

During the simulation period, the largest monthly mean precipitation (338.3 mm) occurred in July and the second highest monthly mean temperature (23°C) was also occurred in this month. Thus, simulation results in July were chosen to represent the groundwater-river interaction in the wet season. The simulation results in January, in which the smallest monthly mean precipitation (20 mm) and lowest monthly mean temperature (0.6°C) occurred, were chosen to represent the dry season conditions.

Figure 5.11 shows the spatial distributions of groundwater tables in unconfined aquifer in 15th July 2004 and 15th January 2005. The groundwater table was almost parallel with ground surface in the midstream and downstream of the Nasunogahara area, agreeing with previous studies on the Nasunogahara area (Sasaki et al., 1958; Yamamoto and Terada, 1980; Hiyama and Suzuki, 1991). However, it was found that the groundwater table seasonally changed significantly in the upstream of Nasunogahara area especially near the Sabi River region. In the wet season (Fig. 5.11a), the isolines of groundwater table elevations curved very sharply and were dense around the Sabi River, but they became smooth and sparse in the dry season. The amounts of stream seepage and spring discharge along the Sabi River from March 2004 to February 2005 (Fig. 5.12) were computed using the MODFLOW Zone Budget Package. It was indicated that the seepage from the

Sabi River mainly occurred in the upstream segments, and approximately 80% was occurred within 3.5 km from the uppermost point of the Sabi River in the model domain. The Sabi River changed from a losing river to a gaining river from upstream to downstream. A large amount of river seepage in the upstream area increased groundwater tables in the wet season, that is, the sharply curved, dense isolines around the upstream of the Sabi River were due to river seepage.

5.3.4 Spatial and temporal variation of δ values in unconfined aquifer

The spatial and temporal variations of $\delta^{18}O$ and δD values in unconfined groundwater in Nasunogahara area were graphically expressed in Fig. 5.13 and Fig. 5.14, respectively. From these two figures, it is clear to find that the δ values in the upstream part were lower than in the downstream part. Since the surface elevation variation within the model domain was approximately 518 m, the isotopic altitude effect of precipitation within the model domain was not very significant and was not considered in the model inputs. Therefore, the lower δ values in the upstream part were probably caused by seepage from rivers.

5.3.5 Recharge and discharge amount of groundwater

In Nasunogahara area, precipitation, paddy field water and river water are three main recharge sources for the groundwater system, while rivers and springs are two main discharge paths. The mass balance package was used to compute the recharge and discharge amounts during the 1st calibration period from March 2004 to February 2005 and the results were shown in Fig. 5.15. The river seepage was 210.3 million m^3 during the 1-yr simulation period, accounting for 29% of total recharge of groundwater and the seepage of the Sabi River (116.5 million m^3) was larger than that of both the Naka River and the Houki River (93.9 million m^3). The Sabi River was a losing river while the Naka River and the Houki River were gaining rivers from the viewpoint of net recharge as a whole during the 1-yr simulation. The seasonal variation of river seepage was remarkable especially for the Sabi River. The Sabi River changed from losing condition in the wet season to gaining condition from the viewpoint of net recharge as a whole. The seepage from the Sabi River in the wet season (15.7 million m^3/month) was about 4 times of that in the dry season

(3.9 million m^3/month), while the seepage of Naka River and Houki River was almost constant (8.5 million m^3/month).

The discharge of rivers was 476.2 million m^3, accounting for 62% of total discharge. Even the net discharge of both the Naka River and the Houki River was 287.1 million m^3, which accounted for 49% of total net discharge. The discharge of the Sabi River (95.3 million m^3) was far smaller than the Naka River and the Houki River (380.9 million m^3). However, the seasonal change of river discharge was almost stable even for the Sabi River. The monthly discharge was 8.7 million m^3 in July and 7.3 million m^3 in January for the Sabi River and 33.1 million m^3 in July and 31.5 million m^3 in January for the Naka River and the Houki River. The spring was the second dominant discharge path, of which the discharge amount was 294.3 million m^3. The discharge of springs varied from 31.4 million m^3 in July to 18.4 million m^3 in January.

5.3.6 Spatial and temporal variation pattern of contribution ratio for each recharge source

If the groundwater is a mixture of different sources with fixed composition, the contribution ratio of each source could be estimated by the following equation:

$$R_n = C_n / (C_1 + C_2 + ... + C_m) \qquad (5\text{-}8)$$

where R_n is the contribution ratio of recharge source n, C is the simulated concentration of each recharge source, subscripts 1, 2, …n,…m represent the 1st, 2nd, …n-th,…, m-th recharge sources of groundwater when local groundwater system has m recharge sources in total. It is worth to mention that the estimated contribution ratio in this study is defined as the proportion of different recharge sources in the groundwater, that is, how many percentage of groundwater sourced from the recharge source. Since the groundwater includes not only the recently recharged groundwater but also historically recharged groundwater, the proportion of both of the recent recharge and the historical recharge from the source are included in the contribution ratio of the recharge source. From the viewpoint of recharge paths, the contribution of the recharge source consists of the contributions of both direct infiltration and transporting water from the recharge source.

The MT3DMS with calibrated transport and flow parameters was used to compute the contribution ratios of recharge sources of groundwater. The initial concentration of groundwater was set to be zero. For one species corresponding to one recharge source, its concentration in water from the source was assigned as 100 mg/L (i.e., equivalent to percentage) and the concentration of the other waters was set to be 0 mg/L. The simulation should be run under sufficiently long period until the concentration of groundwater in the model domain become constant. In this study, the simulation was run for 10 years and the result was checked whether it was constant.

In the Nasunogahara area, the main recharge sources of groundwater can be clarified into three: precipitation, rivers and paddy field water. The water infiltration through paddy field was considered to be paddy field water origin in irrigation period and as precipitation origin in non-irrigation period. After 10 years model running, the relative contributions of three sources were calculated based on Eq. 5-8 and shown in Fig. 5.16 for the wet season and Fig. 5.17 for the dry season. The results indicate that the river seepage mainly occurred along river channels and in the upstream of the Nasunogahara area. The distribution of river-recharged groundwater with more than 50% contribution ratios extended to 2.5 km from the channel in the upstream, while less than 1 km in the downstream. Due to the influence of the river seepage, the contribution from precipitation infiltration was dominant at zones between river channels. The contribution ratio of precipitation in most of areas except cells adjacent river channels was no less than 50%, indicating the precipitation was the most important recharge source in the Nasunogahara area. The paddy field water infiltration mainly occurred in the downstream of the Nasunogahara area, reflecting the distribution of paddy field (Fig. 3.3). It is obvious that the contribution ratio of paddy field water increased during the irrigation period (wet season). However, the relative contribution of paddy field water was no more than 50% even during the irrigation period. Based on above mentioned results, it is easy to understand that why the groundwater quality classification zone (Fig. 3.5) was parallel with respect to rivers but slightly different near the Sabi

River, indicating the groundwater quality in the Nasunogahara area was controlled by the river seepage but modified by the land use.

The mean contribution ratios of recharge sources of the unconfined groundwater in the whole model domain during the 1st simulation period were: precipitation 59%, river water 25% and paddy field water 16%. As shown in Fig. 5.18, it is clearly that the monthly mean contribution ratio of paddy field water increased from March to July and then gradually decreased from August to February. On the contrary, the monthly mean contribution ratio of precipitation decreased from March to July and then gradually increased from August to February. The monthly mean contribution ratio of river water was relatively stable. However, the contribution ratio of river water increased along river channel in river-recharge dominated area (i.e., contribution ratio ≥ 50%) from January to July while decreased in other areas (Fig. 5.19). Due to the changes of river water contribution, the relative contribution of precipitation decreased along river channels except the Kuma River, of which the infiltration was not consider in this study, and increased far from rive channels from January to July. The precipitation contribution ratio was also decreased in the paddy field area and increased in the non-paddy field area from January to July. Generally, the seasonal variation of relative contribution of recharge sources is larger in the downstream than in the upstream area. However, the seasonal change of contribution ratios along the intermittent reach of the Sabi River was more than 10%. The variation of contribution ratios of recharge sources also could be found at point scale (Fig. 5.20). The river water contribution gradually decreased and paddy field water contribution gradually increased at G1 and G7 from March to July. However, the variation patterns were different among sites.

5.4 Discussion

The comparison results of the simulation with the EMMA are shown in Fig 5.21. In general, the results by two approaches agree with each other. The estimated contribution ratios by Visual

MODFLOW Pro (i.e., numerical simulation approach) are included within the error range by the EMMA (i.e., tracer approach), indicating both of the results are reliable. Although the difference in estimated contribution ratios between the two approaches is up to 40% at G6, the river contribution ratio estimated by the simulation approach is almost within the error range estimated by the EMMA. As mentioned in Chapter 4, the groundwater at G6 is probably overestimated by the EMMA due to the influence of the Kuma River, the calculated value by the simulation approach should be the reasonable contribution ratio of Sabi River water to the groundwater at G6. However, the estimated contribution ratio of paddy field water by the simulation approach is 10% lower than that of the EMMA at G4 and is 10% higher at G7. The difference of estimated contribution ratios of paddy field water is probably caused by (1) the input error of location and area of paddy field to the numerical model and (2) the same setting of hydraulic properties for paddy field and non-paddy field in the numerical model. Even though with 10% errors between the estimated relative contribution of paddy field water by the simulation approach and the tracer approach, the spatial and temporal variations of paddy field water infiltration still could be represented by the results from the numerical simulation very well (Figs. 5.16 and 5.17).

As shown in Fig. 5.16 and Fig. 5.17, the spatial distribution of relative contribution of paddy field water is highly corresponded with the distribution of paddy field (Fig. 3.3). The contribution ratio of paddy field water is obviously increased in the irrigation period (Fig. 5.18 and Fig. 5.19). The paddy field accounts for 40% of total land use in the Nasunogahara area. However, the mean contribution ratio of the paddy field water to unconfined groundwater in the whole model domain is only 15%. The relative contribution of paddy field water is even less than 50% in paddy fields during the irrigation period. These evidences suggest that limited distribution and the short irrigation period are two very important factors restrict the paddy field water contribution to groundwater.

As we mentioned in the section 6.3.3, the downstream of the Nasunogahara area is the main discharge zone of the local groundwater system. Field investigation also found that many springs occur at the downstream of the Nasunogahara area. The local groundwater discharge system also potentially restricts the contribution of paddy field water to groundwater.

The seasonal change of contribution ratio of paddy field water in the point scale (Fig.5. 20) was generally fit the overall trend, that is, the ratio increased in the irrigation period. Since the recharge amount of precipitation and river water was also increased in the wet season, the seasonal variation of contribution ratio of paddy field water at some sites, such as G31 and G45 was very small. As the contribution of paddy field water consisted of not only the recently infiltrated water but also historically infiltrated water, the monthly variation of contribution ratio of paddy field water is thus influence by both the irrigation period and the residence time. The relatively long residence time could result in relatively stable contribution ratio of paddy field water. In addition, the time lag effect of recharge events, i.e., the spending time of water flow from the recharge source to the groundwater, was also could influence the seasonal variation of the contribution ratio.

5.5 Summery

A 3-D water flow and transport model was built for Nasunogahara area. The model was calibrated using a trail-and-error method by both of observed hydraulic head and stable isotope compositions from March 2004 to February 2005 and from April to October 2006. Based on the calibration results, the sensitivity analysis for parameters was done to examine the sensitivity of hydraulic head and δ values to the variation of selected parameters. The results indicate that using δ values as additional calibration terms other than hydraulic head could give more reliable simulation results than only using hydraulic head as calibration terms. The main simulation results are shown as follows.

The river water is the dominant recharge source along rive channels. The river seepage was 210 million m^3 from March 2004 to February 2005, which accounted for 29% of total recharge of groundwater. The mean contribution ratio of river water to the unconfined groundwater of the whole model domain was 25%. Among rivers, the annual seepage from the Sabi River, of which middle reach is intermittent, is larger than both the Naka River and the Houki River, which are permanent. From the viewpoint of net recharge/discharge, the Sabi River works as a losing river while the Naka River and the Houki River are gaining rivers. However, the Naka River and the Houki River also recharge groundwater at upstream area. The river seepage distributes along channels and nearly symmetric with respect to the Sabi River. The spatial distribution of river-recharge dominated area, where contribution ratio of river water ≥50%, is larger in the upstream part of the Nasunogahara area than in the downstream part. For the Sabi River, approximately 80% seepage was occurred within 3.5 km from the uppermost point of the river in the model domain. The seasonal change of river seepage is very significant especially for the Sabi River. The Sabi River changed from a losing river in July to a gaining river in January and the monthly seepage in July is 4 times larger than that in January.

The precipitation is the dominant recharge source at sites far from river channels in the Nasunogahara area. The mean contribution ratio of precipitation in the unconfined aquifer of the whole model domain is 59%. The paddy field water infiltration is significant in the downstream area but the mean contribution ratio of paddy field water in the unconfined aquifer is only 16%. Even the contribution ratio of paddy field water is less than 50% in paddy fields during the irrigation period. The contribution ratio of paddy field water was obviously higher in the irrigation period than that in non-irrigation period. Limited distribution and the short irrigation period are two main reasons restrict the paddy field water contribution to groundwater. In addition, the relative distribution of paddy field respective to the local groundwater flow system also potentially affects the paddy field water infiltration in the Nasunogahara area.

Table 5.1 Calibrated values of hydraulic and transport parameters in numerical model for the Nasunogahara area.

Parameter type	Layer	Final value	Reference range	Unit	References
Horizontal hydraulic conductivity (Kx, Ky)	1-6	3.46-311.04	0.15-400	m/d	Elhassan et al. 2001; Wu et al. 2010;
Vertical hydraulic conductivity (Kz)	1-6	0.0069-0.14	3×10^{-5}-12	m/d	Mikita et al. 2011; Wu et al. 2010
Specific storage (Ss)	2-6	5×10^{-6}-9×10^{-4}	7×10^{-6} - 1.4×10^{-3}	1/m	Kelly, 2004; Mikita et al. 2011
Specific yield (Sy)	1-6	0.0065-0.1	0-0.27		Johnson, 1967; Elhassan et al. 2001
Streambed Kz	1	6.912-38.016		m/d	
Drain conductance (Simulated springs)	1	0.024-0.2376		1/d	
Effective porosity	1-6	0.1-0.2			

Table 5.2 The simulation cases for sensitivity analysis.

Case Number	Changed parameters
0	Control case (Calibrated parameters)
1	K_x and K_y of Layer 1 increased 20%
2	K_x and K_y of Layer 1 decreased 20%
3	K_z of Layer 1 increased 20%
4	K_z of Layer 1 decreased 20%
5	S_y of Layer 1 increased 20%
6	S_y of Layer 1 decreased 20%
7	K_x and K_y of Layer 2-6 increased 20%
8	K_x and K_y of Layer 2-6 decreased 20%
9	K_z of Layer 2-6 increased 20%
10	K_z of Layer 2-6 decreased 20%
11	S_s of Layer 2-6 increased 20%
12	S_s of Layer 2-6 decreased 20%
13	K_z of stream boundary increased 20%
14	K_z of stream boundary decreased 20%
15	Conductance of drain boundary increased 20%
16	Conductance of drain boundary decreased 20%

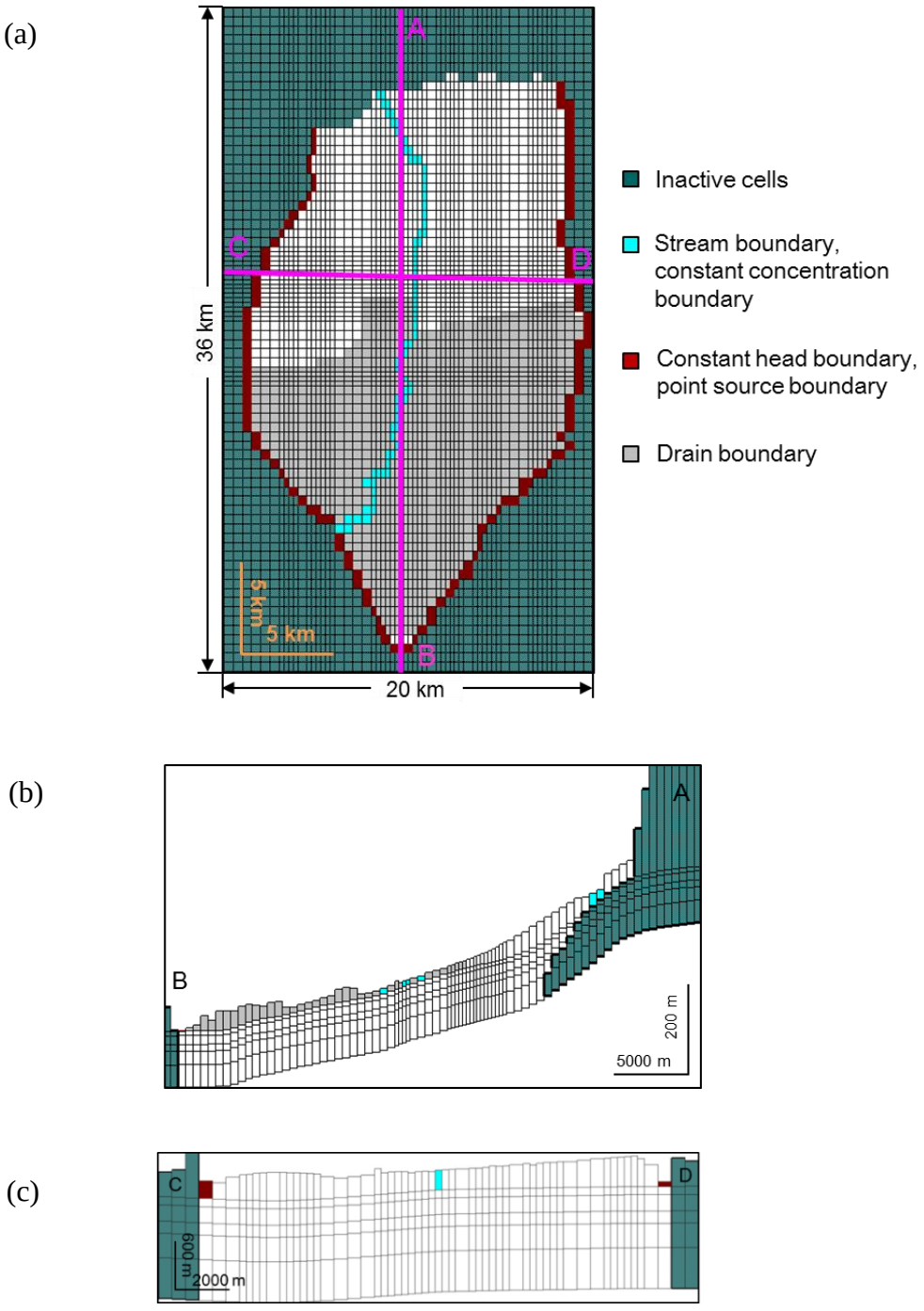

Figure 5.1 The model domain with grid design and boundary settings for the Nasunogahara area; (a) grid discretization and boundary settings in Layer 1, (b) cross section A-B and (c) cross section C-D showing vertical layer structure and boundary settings.

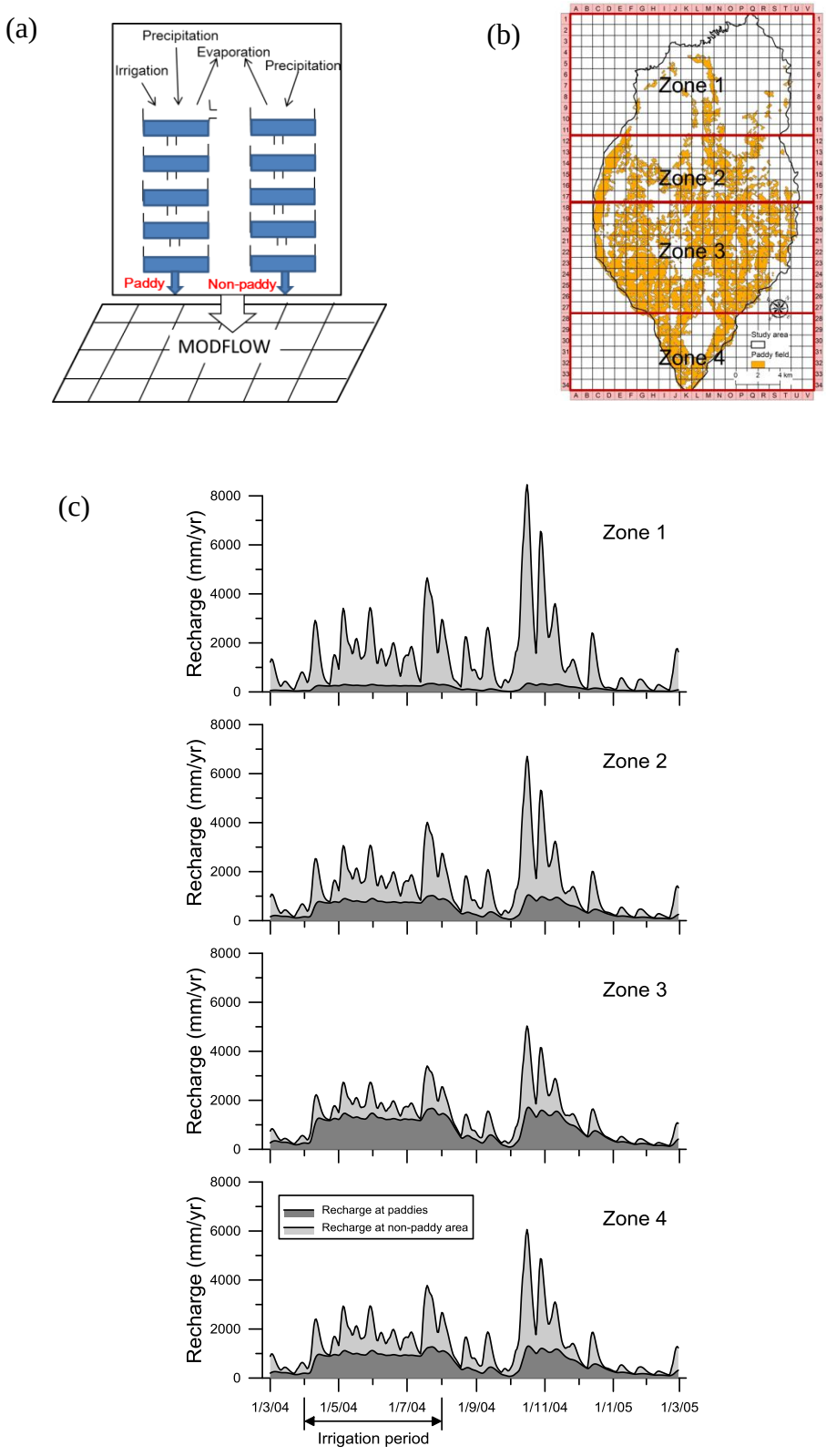

Figure 5.2 (a) The conceptual diagram for recharge estimation, (b) land use map with mesh division for estimating recharge in the tank model and zone division for recharge input in MODFLOW and (c) estimated recharge at paddies and at non-paddy field at 4 recharge zones for MODFLOW.

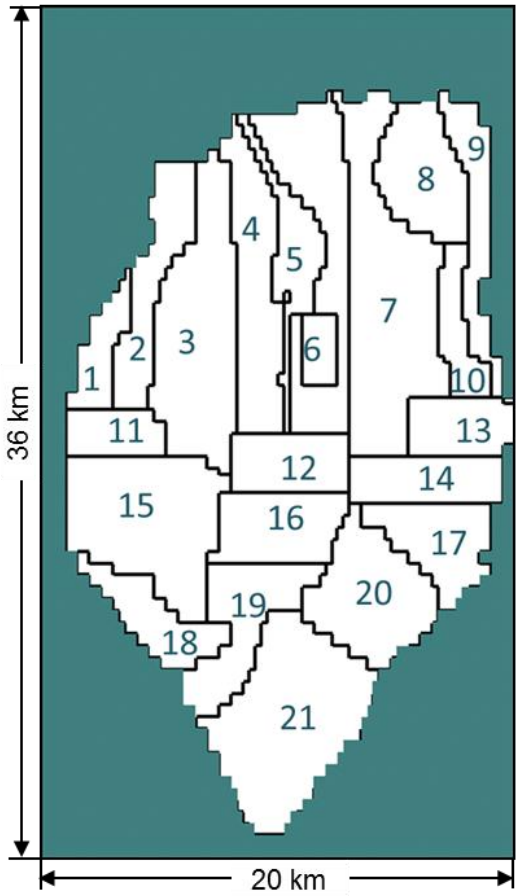

Figure 5.3 Parameters setting zones in Layer 1 of the numerical model for the Nasunogahara area.

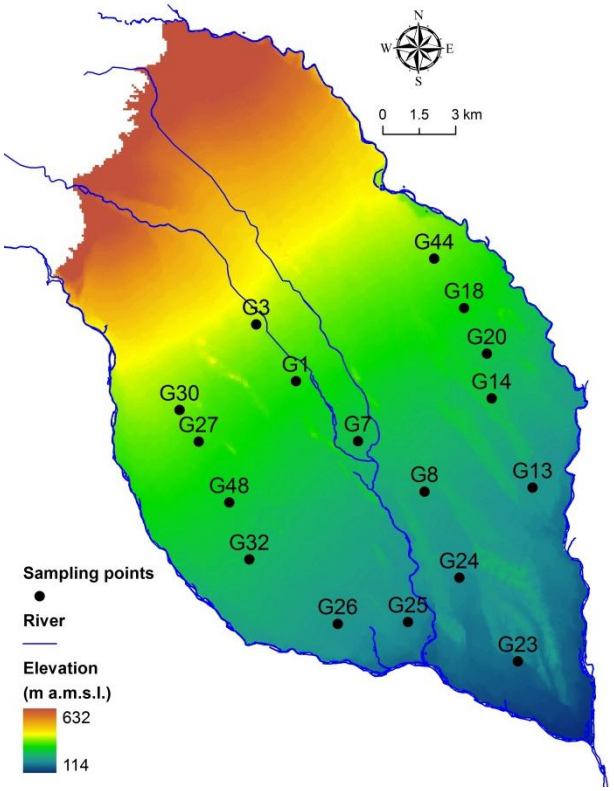

Figure 5.4 Groundwater sampling locations in the Nasunogahara area during the period from April to September 2006 (after Wakui, 2007).

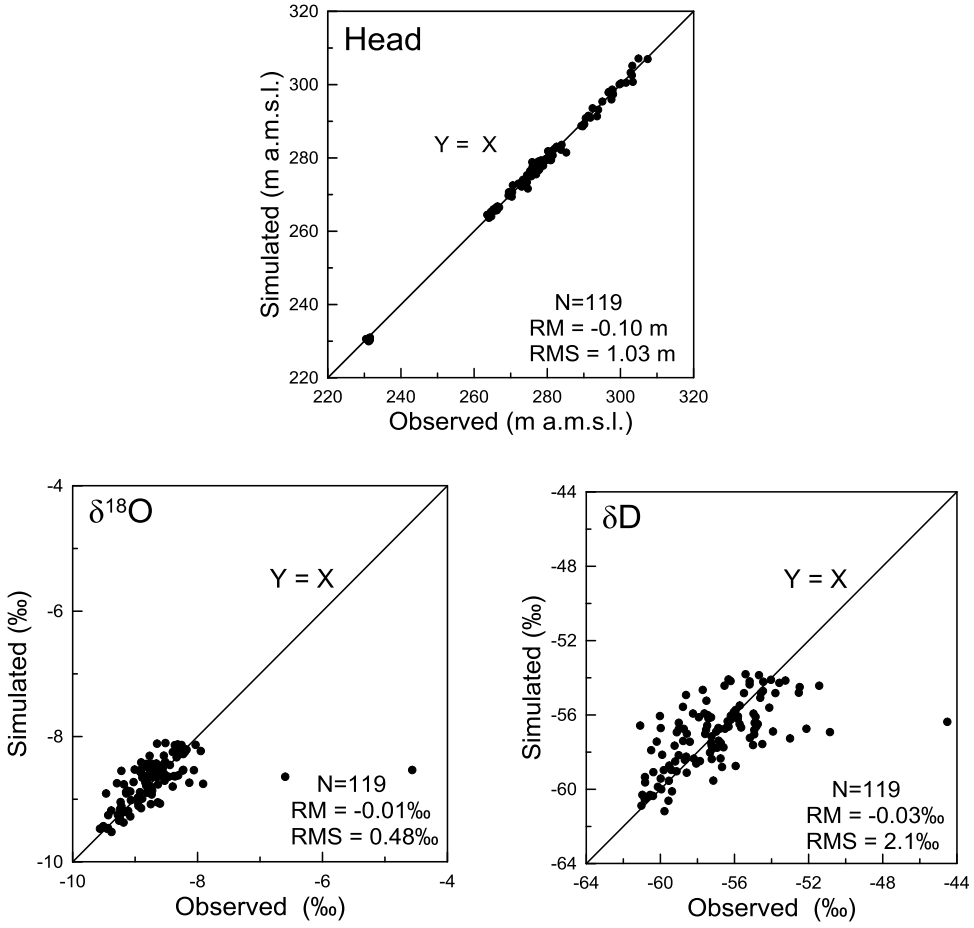

Figure 5.5 Comparison between observed and simulated groundwater head and δ values of ^{18}O and D in transient simulation of the Nasunogahara area for the 1st period from March 2004 to February 2005. The *N* represents the pointed numbers, *RM* is residual mean and *RMS* is root mean squared errors.

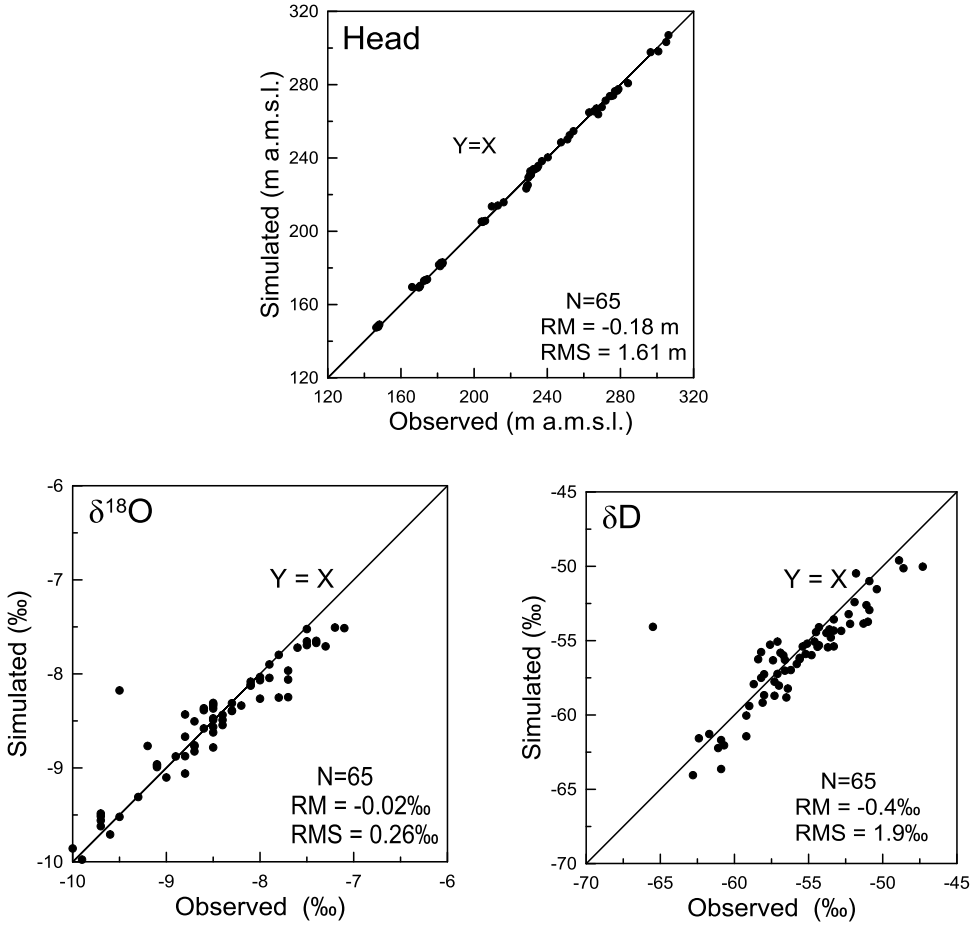

Figure 5.6 Same as Fig. 5.5, but for the 2nd period from April to October 2006.

(a)

(b)

(c)

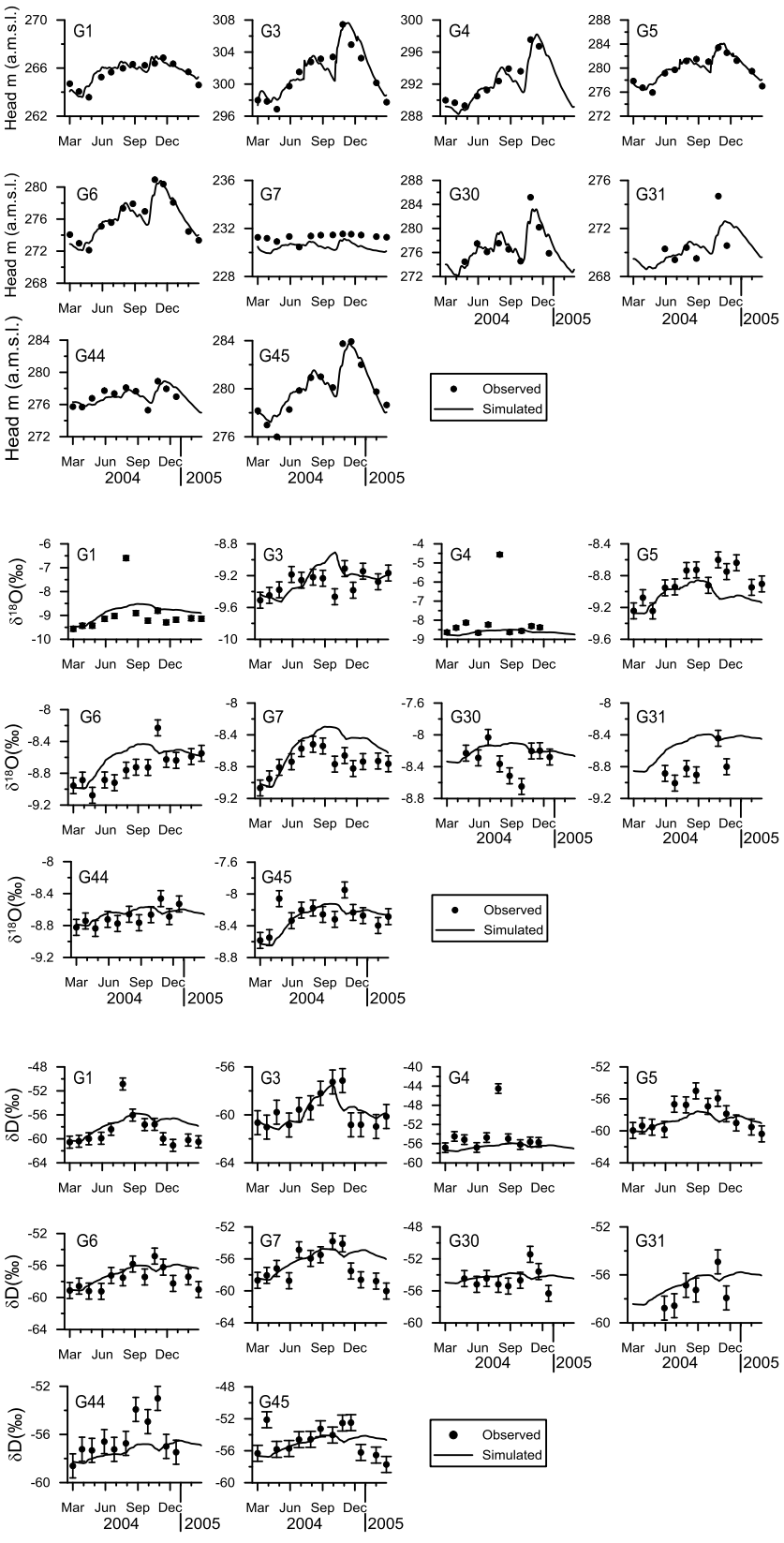

Figure 5.7 Temporal variations of observed and simulated (a) groundwater head, (b) $\delta^{18}O$ and (c) δD in transient simulation of the Nasunogahara area for the 1st period from March 2004 to February 2005.

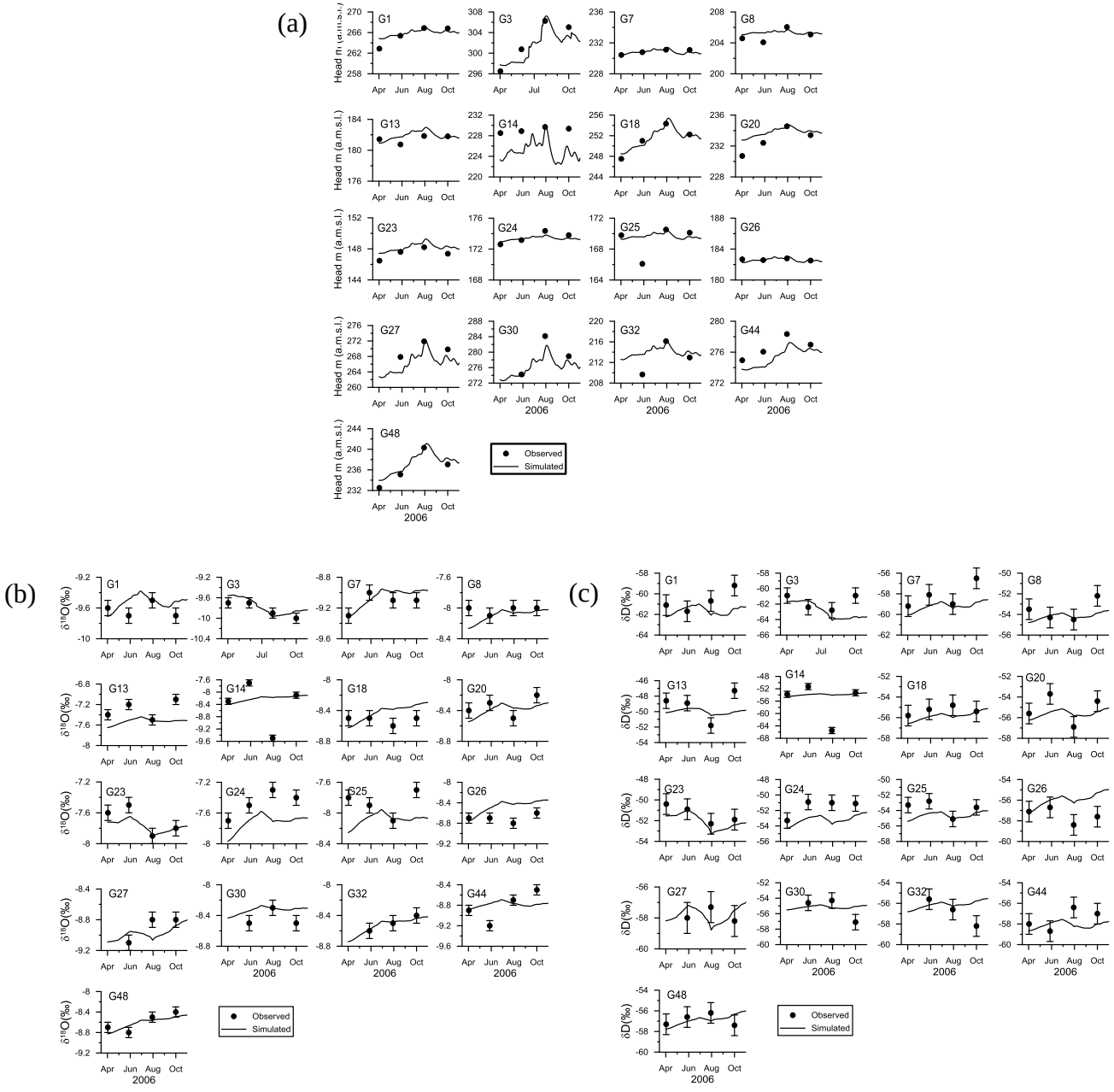

Figure 5.8 Same as Fig. 5.7, but for the 2nd period from April to October 2006.

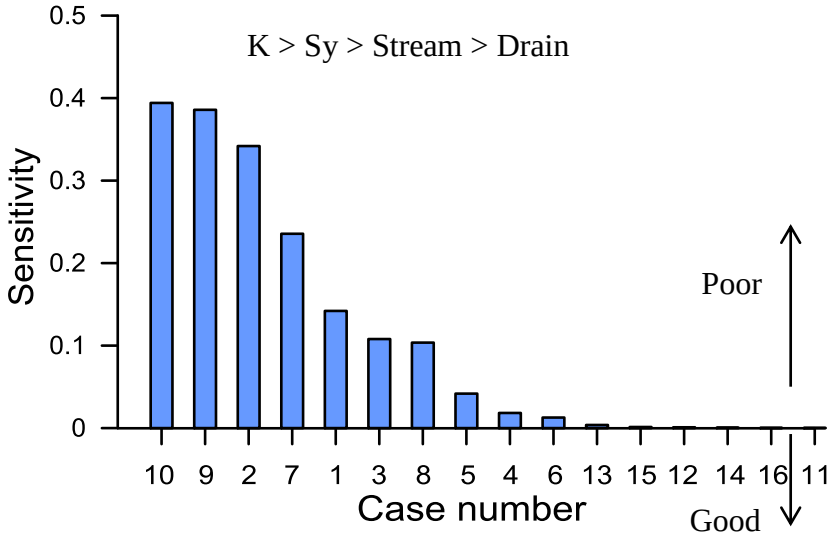

Figure 5.9 Comparison of total sensitivity among simulation cases for the Nasunogahara area. The larger the sensitivity value, the worse results of the corresponding simulation. The corresponding parameter changes are described in Table 5.2.

(a)

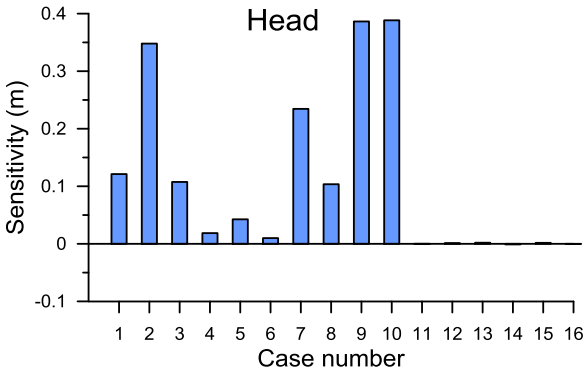

(b)

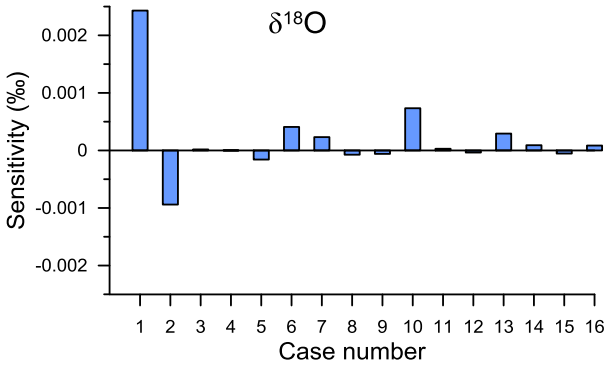

(c)

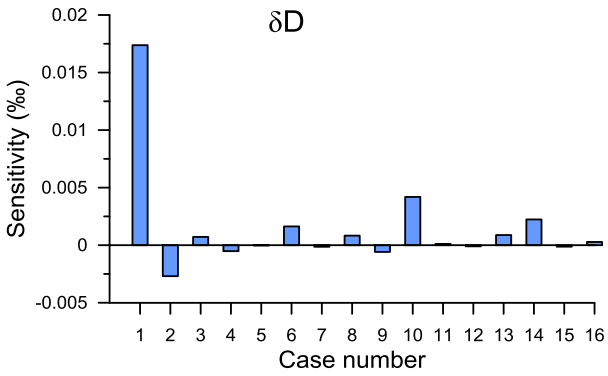

Figure 5.10 Sensitivity of (a) hydraulic head, (b) $\delta^{18}O$ and (c) δD.

(a)

(b)

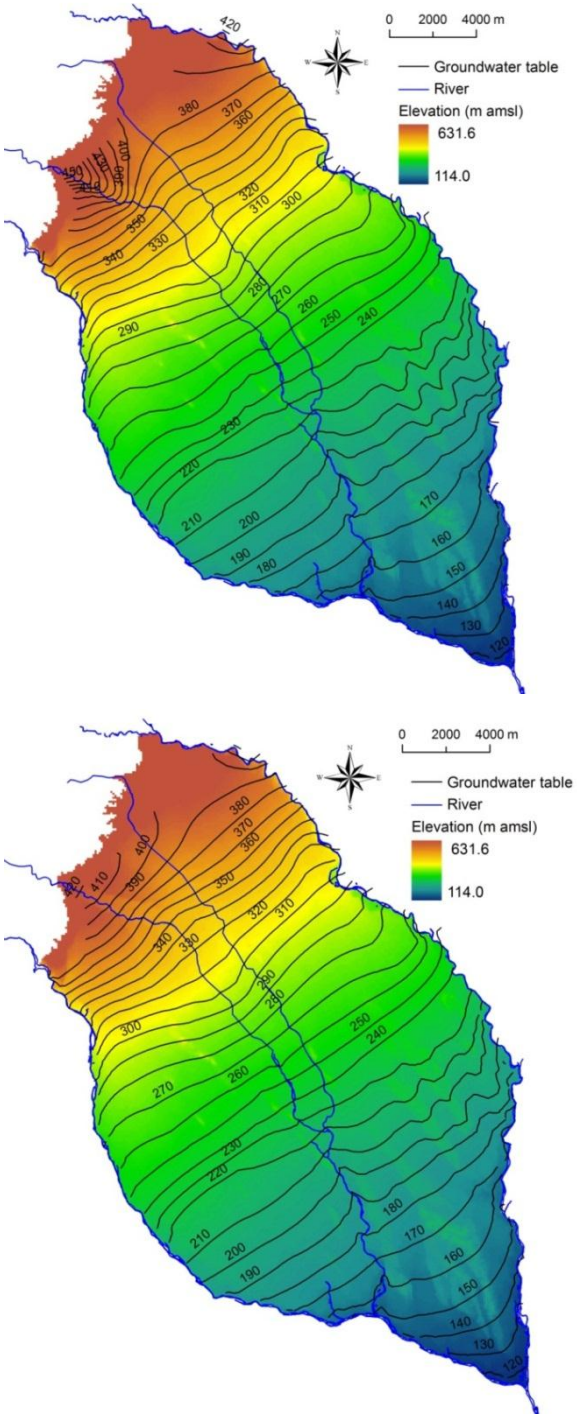

Figure 5.11 Spatial distribution pattern of simulated groundwater levels in unconfined aquifer on (a) 15th July 2004 (wet season) and (b) 15th January 2005 (dry season) for the Nasunogahara area.

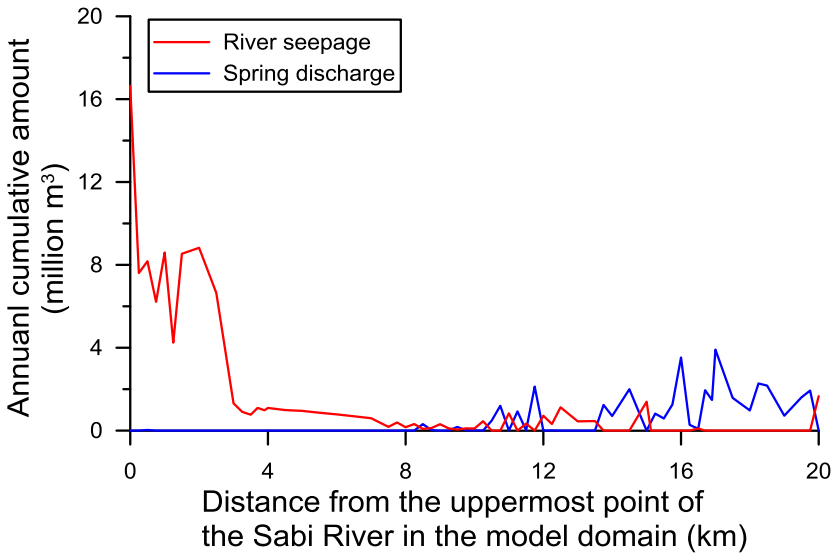

Figure 5.12 River seepage and spring discharge amounts along the Sabi River from March 2004 to February 2005.

(a)

(b)

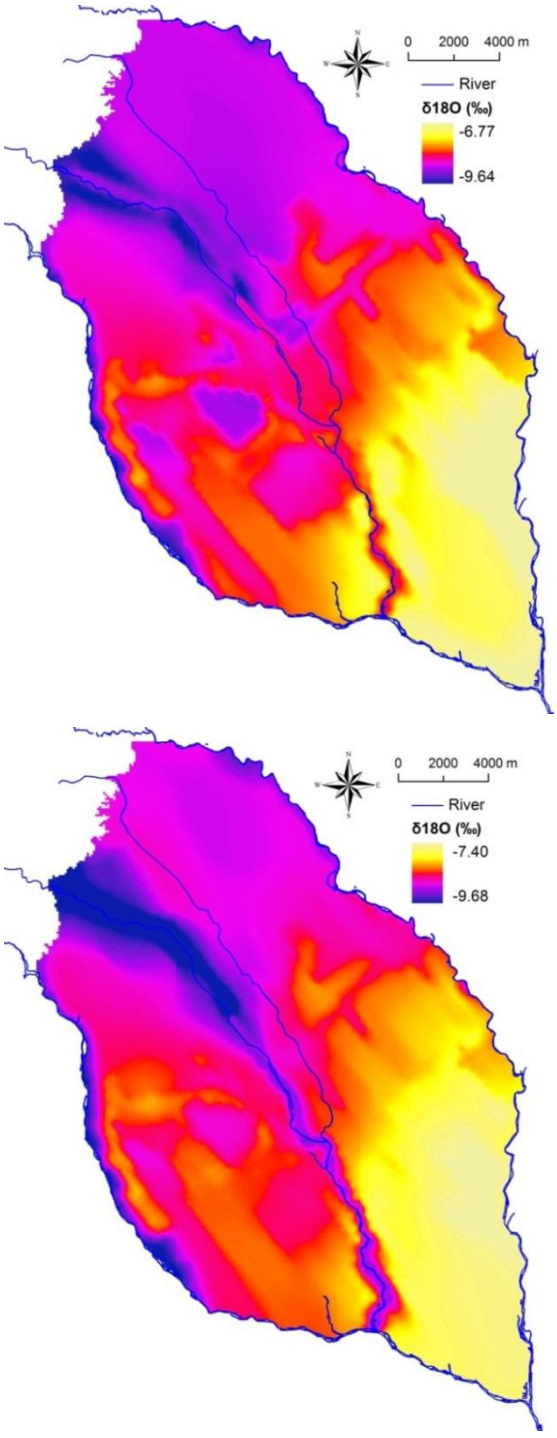

Figure 5.13 Spatial distribution of $\delta^{18}O$ of groundwater in unconfined aquifer on (a) 15th July 2004 (wet season) and (b) 15th January 2005 (dry season) for the Nasunogahara area.

(a)

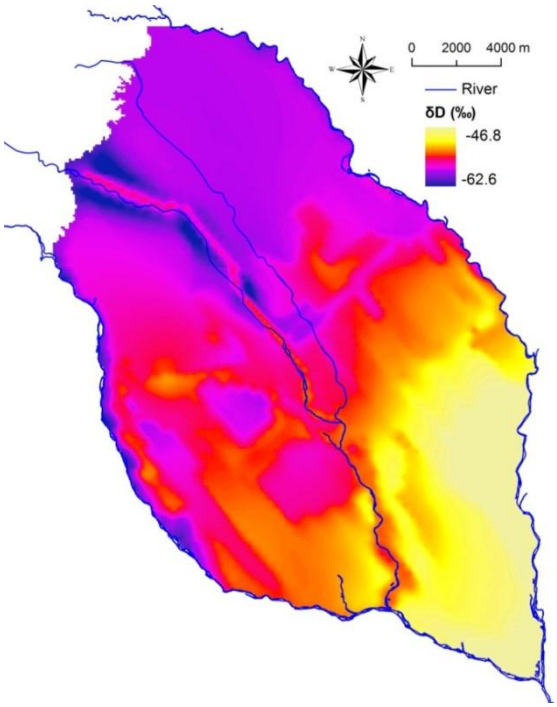

(b)

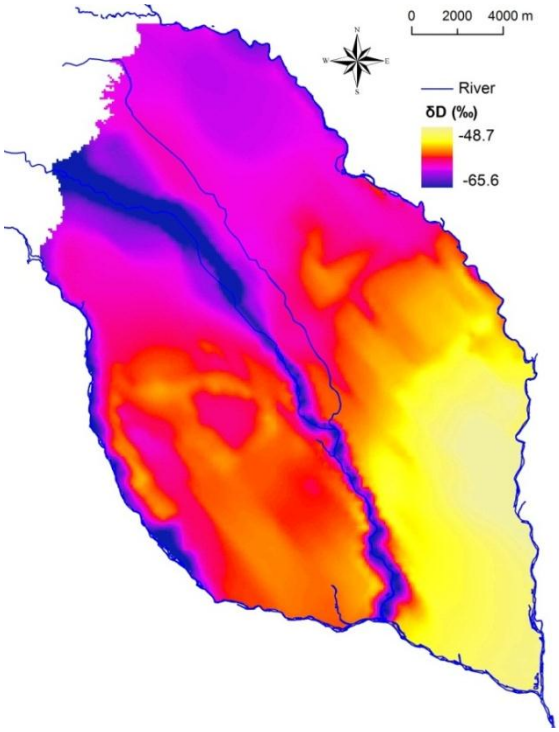

Figure 5.14 Spatial distribution pattern of δD of groundwater in unconfined aquifer on (a) 15th July 2004 (wet season) and (b) 15th January 2005 (dry season) for the Nasunogahara area.

(a)

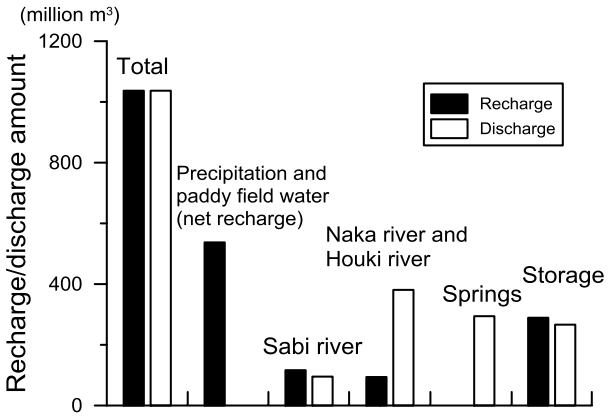

(b)

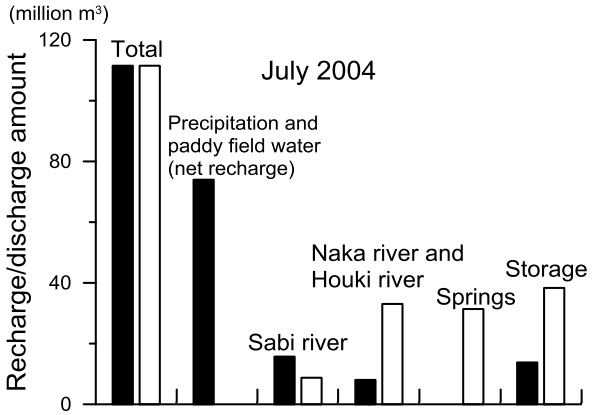

(c)

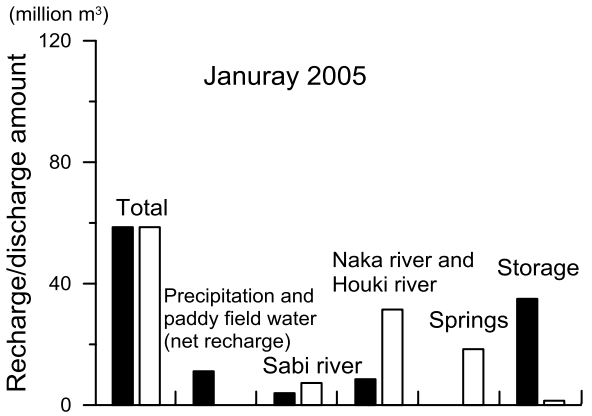

Figure 5. 15 Amounts of recharge and discharge for the whole of the Nasunogahara area (a) from March 2004 to February 2005; (b) on 15th July 2004 (wet season); and (c) on 15th January 2005 (dry season).

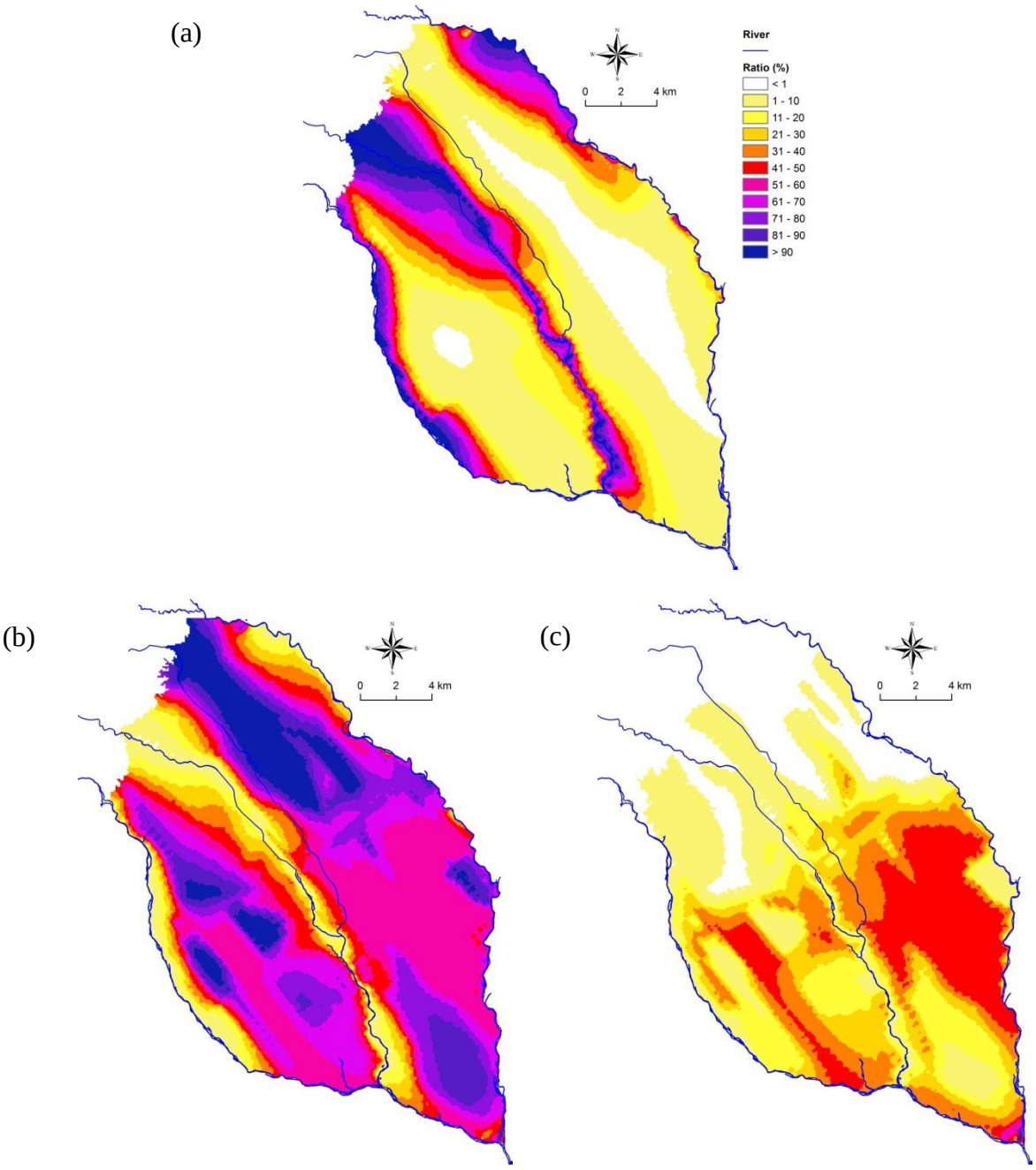

Figure 5.16 Spatial distribution pattern of contribution ratio of (a) river water, (b) precipitation and (c) paddy field water to groundwater in the wet season (15th July 2004) for the Nasunogahara area.

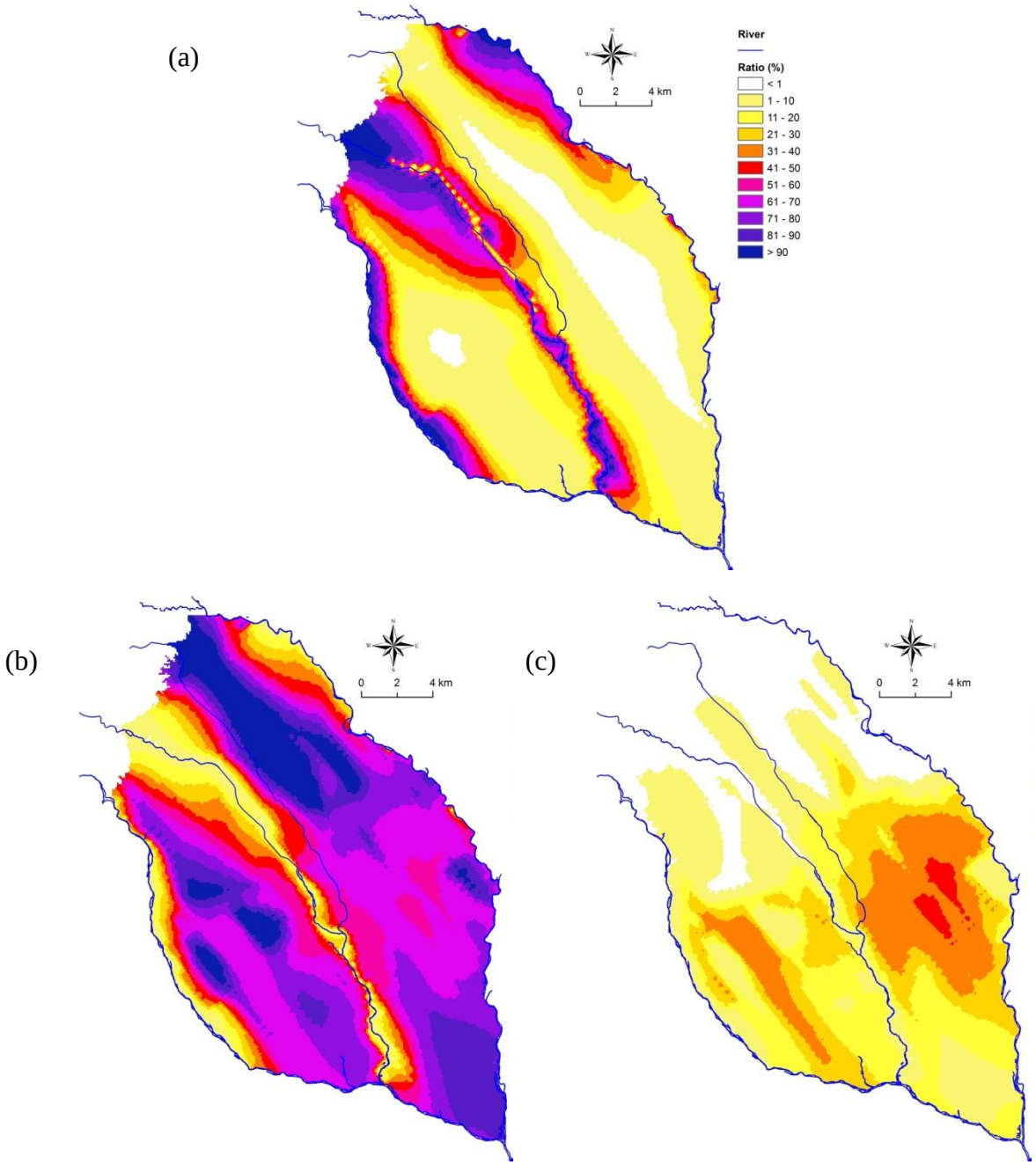

Figure 5. 17 Same as Fig. 5.16, but in the dry season (15th January 2005).

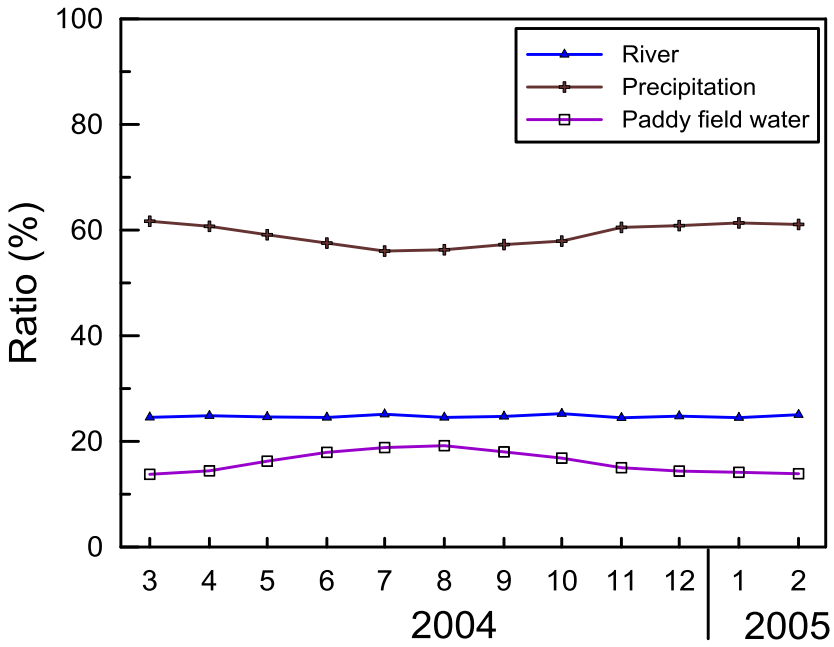

Figure 5.18 Monthly variation of mean contribution ratios of recharge sources in the whole model domain for the Nasunogahara area during the period between March 2004 and February 2005.

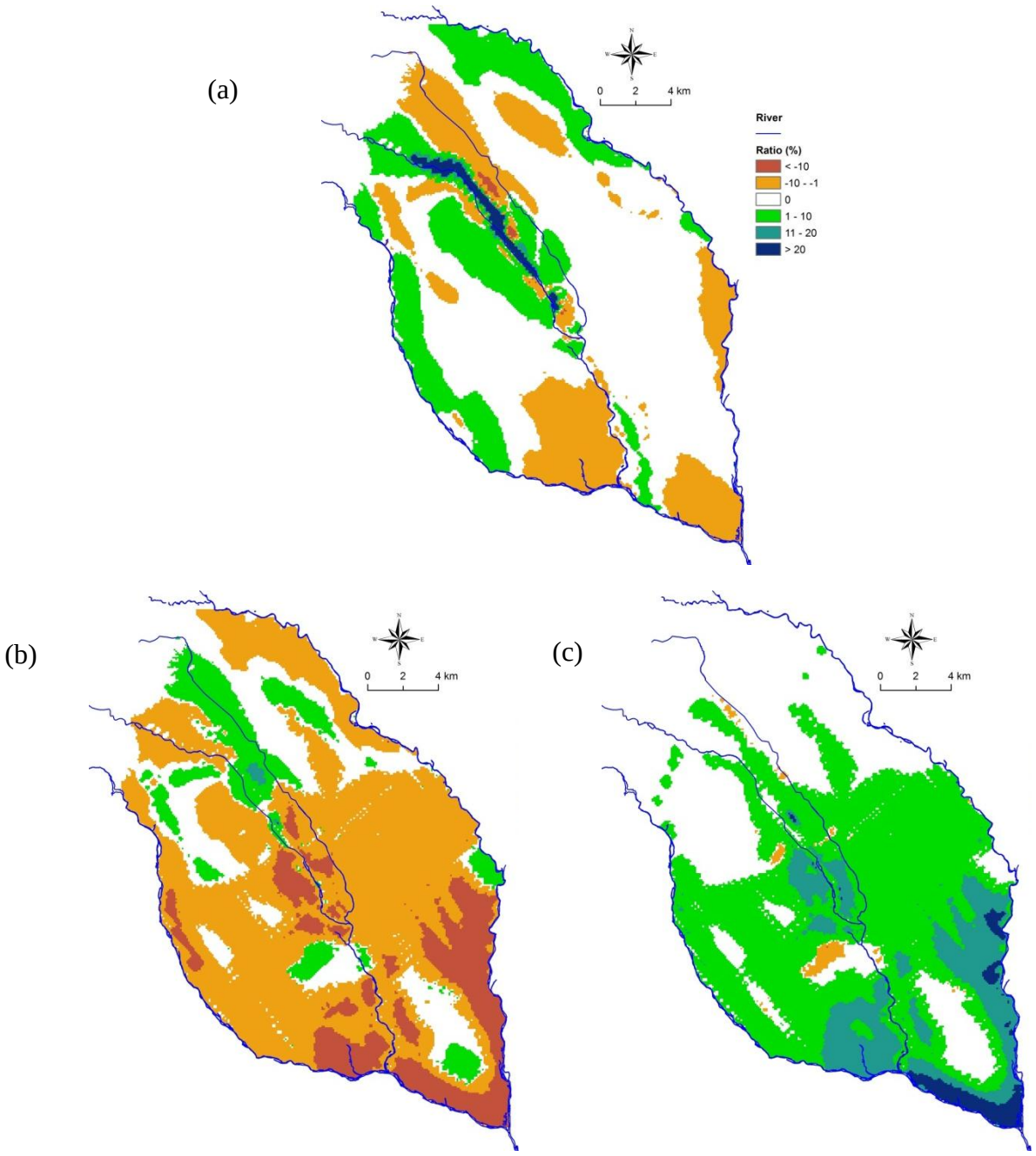

Figure 5.19 The changes in contribution ratio for (a) river water, (b) precipitation, and (c) paddy field water from July, 2004 (wet season) to January, 2005 (dry season) for the Nasunogahara area. Positive values represent the contribution ratios increased from dry season to wet season and vice versa.

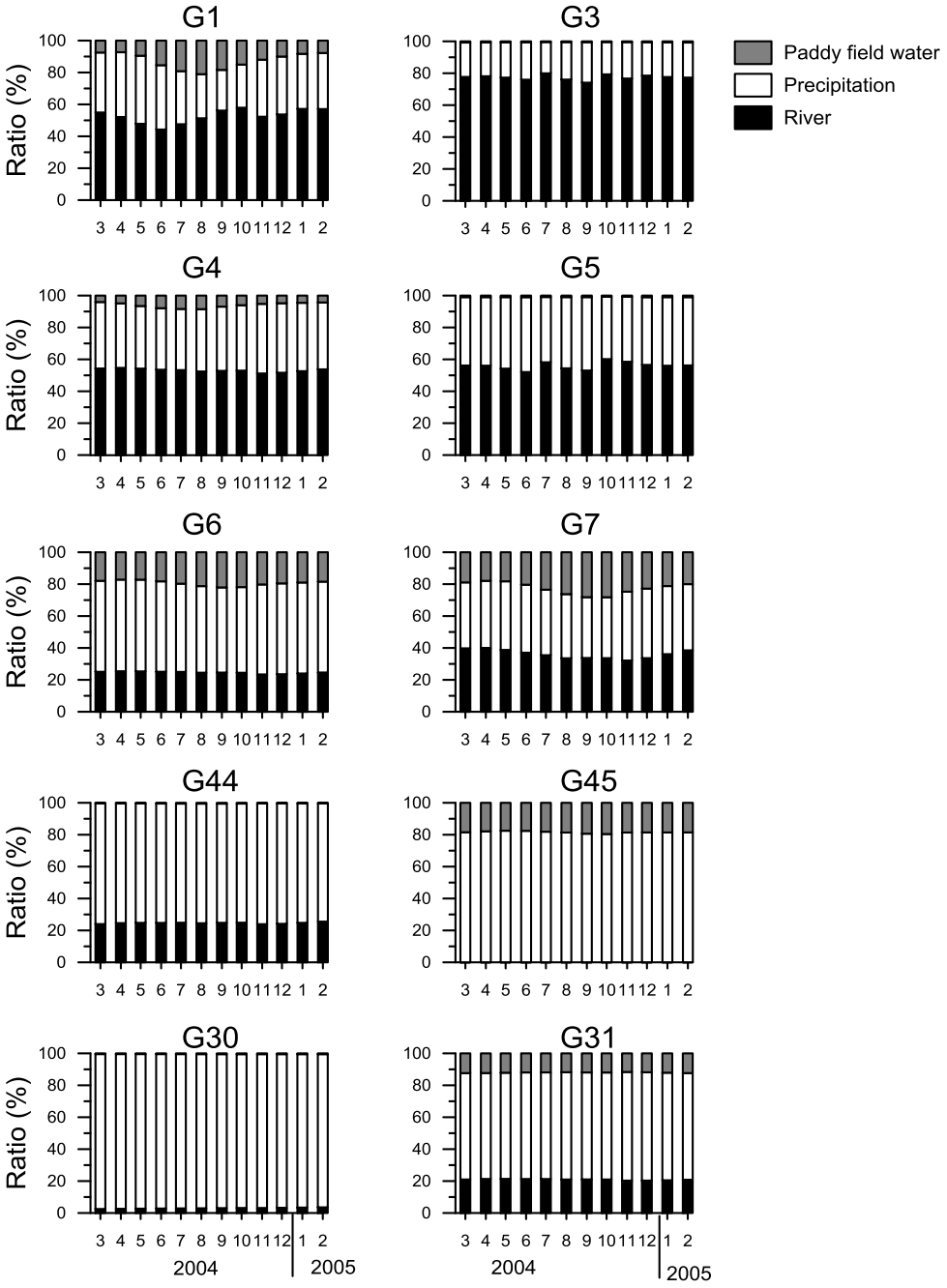

Figure 5.20 Month to month variation of contribution ratios for the three recharge sources to groundwater at selected wells in the Nasunogahara area.

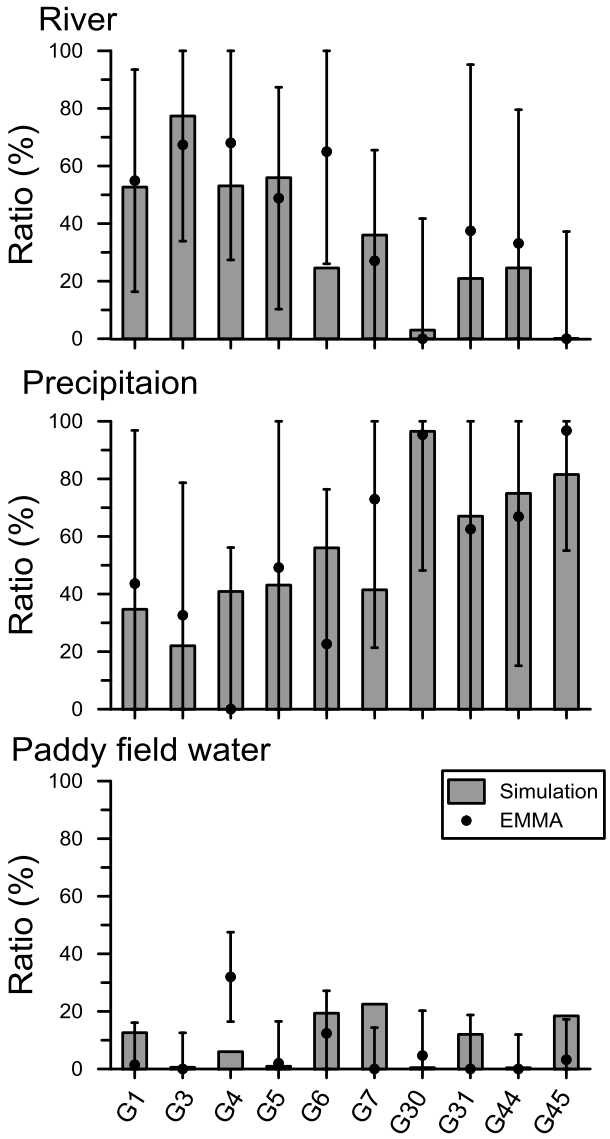

Figure 5.21 Comparison of the estimated contribution ratios between the numerical simulation and the EMMA for the Nasunogahara area.

Chapter 6
Tracer approach for the Ashikaga area

6.1 Introduction

The Ashikaga area is situated between the Ashio Mountains and the Kanto plain, and the Watarase River flows into the region parallel to the mountain-plain boundary. Syncline geological settings and long-term groundwater abstraction are the main characteristics of the Ashikaga area.

The specific objectives of this chapter are to identify recharge sources of groundwater in the Ashikaga area and quantitatively evaluate their contribution ratio using stable isotopes and hydrochemistry, with a special emphasis on the spatial extent of river-recharged groundwater and its controlling factors.

6.2 Material and Methods

6.2.1 Data sets

Precipitation samples were collected monthly during a 1-yr period from November 2010 to October 2011. Field surveys were carried out six times approximately bimonthly during the period. Overall, 12 groundwater samples were collected from private wells and four river water samples were collected at each sampling point (Fig. 6.1). Water temperature, EC and pH were measured in situ with portable instruments. Additionally, groundwater samples from 17 municipal wells utilized by seven water purification plants were collected monthly from December 2010 to October 2011. All samples were subjected to isotope analysis. In addition, hydrochemical analysis was conducted using 23 groundwater samples collected from private wells and seven river water samples in September 2010 and April 2011, and 8 groundwater samples from municipal wells in September 2010.

The isotopic and chemical compositions of the water samples were analyzed at the Terrestrial Environment Research Center, University of Tsukuba. The hydrogen and oxygen stable isotopic composition of the water samples were determined using a liquid water isotope analyzer (L1102-i, Picarro, Santa Clara, CA, USA) based on wavelength-scanned cavity ring-down spectroscopy (WS-CRDS; Gupta et al., 2009). The isotopic ratios of ^{18}O and D were expressed as $\delta^{18}O$ and δD, respectively, relative to the Vienna Standard Mean Ocean Water. The analytical errors were 0.1‰ for $\delta^{18}O$ and 1‰ for δD (Yamanaka and Onda, 2010) for samples collected from November 2010 to July 2011, while they were 0.2‰ for $\delta^{18}O$ and 2‰ for δD for samples collected after August 2011 owing to replacement of the analyzer. Cation and anion concentrations were measured using an ion chromatograph (LC-10AP, Shimadzu, Tokyo, Japan) with an analytical precision of ±1 mg/L. The bicarbonate concentration was measured by the titration method using sulfuric acid. The accuracy of the hydrochemical analyses was checked using an electrical balance. Samples with relative errors greater than 5% were reanalyzed.

6.2.2 End-member mixing analysis

Although oxygen and hydrogen stable isotope compositions of water have the potential for use in tracing both sources and flow paths in groundwater systems (Nakaya et al., 2007). While the hydrochemical data, such as chloride can be used to complement isotopic information. Chloride is a very conservative tracer, and Subyani (2004) demonstrated its usefulness as a tracer to evaluate groundwater recharge in alluvial sediments. The combination use of isotopic tracers and hydrochemical tracers become more important when any one species of tracers cannot distinguish all the recharge sources very well.

In the Ashikaga area, Watarase River water, local precipitation and mountain block recharge were clarified as three mainly recharge sources of groundwater, which constituted three end-members A, B, and C of Eq. 4-4, 4-5, and 4-6 (section 4.2.2). The detailed process of how to distinguish recharge sources was shown in following sections. The use of isotopic tracers allows to tracer the river and local precipitation, while chloride tracer is helpful to identify the mountain

block recharge. Therefore, the isotopic tracers and chloride tracer were used in the Ashikaga area and both $\delta^{18}O$ vs. Cl and δD vs. Cl were applied.

6.2.3 Error analysis

The uncertainty of the EMMA caused by the uncertain concentration of end-members and the resultant mixtures in the Ashikaga area was estimated by error propagation analysis (Phillips and Gregg, 2001). The detail uncertainty analysis method was descripted in section 4.2.3. The standard deviations of the δ values and Cl^- concentration of groundwater (including AW9 as mountain block recharge) and Watarase River water were used as a measure of the uncertainty. The potential error of long-term mean δ values of local precipitation was estimated to be the different between long-term mean δ values and weighted mean δ values for precipitation during the sampling period. The uncertainty in Cl^- concentration for local precipitation and some groundwater samples were assumed to be 0.5 mg/L, which is the mean standard deviation of Cl^- concentrations of known groundwater samples. The difference between estimated contribution ratios by $\delta^{18}O$ and by δD was also compared.

6.3 Results

6.3.1 Stable Isotope signatures in precipitation and surface waters

The isotopic compositions of precipitation change temporally in response to rainout history and various factors such as temperature effect and amount effect (Clark and Fritz, 1997). The amount effect tends to be high at low latitudes, whereas seasonal variations at high latitude are generally ascribed to temperature effect (Dansgaard, 1964). A sharp transition from amount effect dominated variations to temperature effect dominated variations occurs at 30° latitude for both the northern and southern hemispheres (Bowen, 2008).

Figure 6.2 shows the temporal variations in $\delta^{18}O$, δD and d-excess (= $\delta D - 8\times\delta^{18}O$) in precipitation, Watarase River water and groundwater from private and municipal wells for the study period. The values for precipitation ranged from -13.03 to -5.16‰ $\delta^{18}O$, -86.1 to -26.0‰ δD

and 6.2 to 23.4‰ d-excess. The δ values were not significantly correlated with mean temperature or precipitation amount, at least on a monthly basis, indicating that seasonal variability of the isotopic composition in precipitation was somewhat complicated in the study area. Specifically, these variations were likely influenced by both temperature and precipitation amount, as well as other factors such as distance from the coast and wind direction. Conversely, d-excess was negatively correlated with temperature ($r = -0.87$, $p < 0.001$). A similar tendency was reported by Waseda and Nakai (1983), who stated that it was caused by seasonal shifting of the water vapor source between the Pacific and the Sea of Japan. In contrast to the high variability in δ values of precipitation, those of river water and groundwater remained nearly constant. Although the d-excess of river water and groundwater showed weak variation, its phase was not in agreement with that of precipitation. These features suggest that the mean residence times of river water and groundwater are considerably long (at least > 1 year).

As expected from the seasonal changes in the d-excess of precipitation, the local meteoric water line (LMWL) differed remarkably between the warm period (April-September; $\delta D = 8.65\delta^{18}O+14.8$, $r^2 = 0.98$) and the cool period (October-March; $\delta D = 8.42\delta^{18}O+23.8$, $r^2 = 0.98$). The LMWL in warm period is very similar to the global meteoric water line (GMWL; $\delta D = 8\delta^{18}O+10$; Craig, 1961), with a slightly higher slope (Fig. 6.3). The observed isotopic compositions of river water and groundwater (except for AW7) were plotted along the LMWL for the warm period, indicating that precipitation in the warm period is a more effective recharge source than precipitation during the cool period. The arithmetic means of $\delta^{18}O$ and δD of water from the Watarase River were lowest among all samples collected during the study period. The weighted (based on monthly precipitation) mean $\delta^{18}O$ and δD of precipitation were -9.26‰ and -62.5‰, respectively. Total precipitation during the period was 236 mm (20%) higher than the climatic normal, in part because an extraordinary amount of rainfall occurred in May, July and September, 2011. Therefore, the 1-year observation period may be insufficient to provide a representative isotopic signature of the local precipitation. If the climatic normals (1981-2010) of

monthly precipitation are used to calculate the weighted mean δ values, significantly higher values ($\delta^{18}O$ = -8.58‰ and δD = -57.4‰) are obtained. Since the extraordinary amount of rainfall should have reduced the observed δ values of precipitation, long-term mean values in this area are expected to be higher.

A close relationship existed between the mean δ values of river water and the mean elevation of the catchment corresponding to each sampling point (Fig. 6.4), which reflects the well-known altitude effect (Dansgaard, 1964; Clark and Fritz, 1997). Accordingly, the low δ values of the Watarase River water (AR1) are due to the high elevation of its recharge zone. The isotopic lapse rate was calculated to be -0.25‰ per 100 m for $\delta^{18}O$ and -1.7‰ per 100 m for δD. The global average isotopic lapse rate reported by Poage and Chamberlain (2001) is -0.28‰ per 100 m for $\delta^{18}O$, which is similar to the results reported here. Based on our isotopic lapse rate and the mean elevation of the entire study area, the long-term mean $\delta^{18}O$ and δD of the local precipitation are approximately -8.26‰ and -56.6‰, respectively. Although these values are higher than the observed weighted mean values for the study period, they are consistent with our expectations. Thus, we adopted these estimated values rather than those based on only 1-year observations as the isotopic signature of the local precipitation.

6.3.2 Stable isotope signatures in groundwater

The arithmetic mean values of groundwater $\delta^{18}O$ and δD at each well during the study period ranged from -9.48‰ to -7.83‰ and from -65.0‰ to -55.5‰, respectively (Table 6.1). With the exception of AW7, the mean δ values of groundwater were between those of Watarase River water and the estimated local precipitation values. The isotopic composition of groundwater at AW7 (with the lowest d-excess) was plotted on the right-hand side of the meteoric water lines at a distance, suggesting that it was affected by kinetic fractionation, probably due to evaporation from water or ground surfaces. The lowest $\delta^{18}O$ and δD values were found in well AT3, which is only 0.68 km from the Watarase River. The $\delta^{18}O$ and δD of groundwater on the south side of the Watarase River ranged from -9.48 to -8.45‰ and from -65.0 to -58.9‰, respectively. Conversely,

the values on the north side ranged from -9.22 to -7.83‰ and from -63.0 to -55.5‰, respectively. The values were generally more negative on the south (i.e., plain) side than the north (i.e., mountain) side, which is seemingly contrary to the altitude effect. As shown in Figure 6.5, a strong relationship between δ values and the distance from the Watarase River was observed for each well on the south side. In addition, relatively low δ values were found at wells near the Watarase River on the north side. These findings suggest that the Watarase River contributes a significant amount of water to aquifers, especially on its south side.

6.3.3 Hydrochemical characteristics

The EC reflects the total dissolved ion concentrations in water bodies, and to a certain extent, the length of flow paths and residence times underground (Song et al., 2006). The EC values of groundwater ranged from 11.9 to 44.4 mS/m, while those of river water ranged from 8.3 to 18.1 mS/m (Table 6.1). The lowest EC for groundwater was found at AW11, which was a very shallow well situated in the foothills, suggesting a shallow flow path along the hillslope with a relatively short residence time. The highest EC for groundwater was found at AW7, where the d-excess value was lowest, indicating an evaporative enrichment effect.

The groundwater pH ranged from 6.11 to 7.53, with the highest value being observed at the deepest well (AW6, 150 m). The depths of the other private wells and some municipal wells (AT1, AT2, AT3, and AT5) were less than 12 m, while that of AW9 is unknown. Lower pH values (e.g., < 6.0) were found in very shallow wells in the foothills (AW 11).

The trilinear diagram suggests that Ca-HCO_3 is the dominant hydrochemical facies in the study area (Fig. 6.6), which is common to ordinary groundwater systems. However, for AW9 and AW6, the proportion of Ca^{2+} relative to the total cations (in meq/L) is lower and that of Na^{+} is higher than for the other wells. These characteristics are similar to those for tributaries of the Watarase River and may reflect geology specific to their recharge areas. Groundwater in the foothills (AW9, AW11 and AW12) and from a deep well (AW6), as well as water from the tributaries (AR2, AR3 and AR4) was characterized by poor SO_4^{2-} content. Conversely, water samples from the Watarase

River and the adjacent groundwater had relatively high SO_4^{2-} contents. Because the absolute SO_4^{2-} concentration was greater in groundwater than in water from the Watarase River, the SO_4^{2-} likely originated from sediments deposited by the river rather than the river water itself.

NO_3^- was detected in all river water and groundwater samples except for AW7 and AW9. These findings suggest a certain measure of contamination by fertilizers, sewage and acid deposition. The absence of NO_3^- indicates that the water has never been contaminated or that natural attenuation of nitrate (i.e., denitrification) has occurred in the system.

6.3.4 End-member mixing analysis

Figure 6.7 shows a plot of annual (arithmetic) mean δ values against Cl^- in river water and groundwater. Data for all groundwater samples except AW7 are plotted within a triangle. Watarase River water is clearly the end-member corresponding to the lower left vertex of the triangle. Local precipitation had estimated long-term mean δ values and low chloride concentrations and was therefore likely the end-member forming the upper left vertex. Because the chloride concentration of precipitation is not highly variable in space, the chloride concentration of 0.5 mg/L for precipitation at a nearby city (Miyoshi, 2012; personal communication) was used. The δ values and Cl^- concentration of this end-member were similar to those of samples collected from the tributaries (except AR4). The third end-member appears to have moderate δ values and a high Cl^- concentration, which is similar to AW9. As mentioned above, the hydrochemical characteristics of groundwater at AW9 suggest a deep, long flow path. Therefore, this end-member is considered to be the mountain block recharge component. The medium δ values of this end-member indicate that mountain block groundwater was recharged at an elevation between those of the upper Watarase River watershed and the present study area. The reasons for the high Cl^- in the mountain block groundwater are discussed later.

It should be noted that the AW7 groundwater and AR4 river water differed from the other samples. The isotopic signatures of groundwater at AW7 suggest evaporative enrichment with kinetic fractionation (Section 5.3.2). However, the high Cl^- concentration of this sample cannot be

explained solely by such enrichment, indicating mixing with high Cl^- water. According to Miyazaki et al. (2005), the Cl^- concentration of paddy field water ranged from 0.15 to 1.46 mmol/L (5.3 to 51.7 mg/L) at an area adjacent to the present study area. Moreover, the d-excess of paddy field water is generally low because of direct evaporation from water surfaces (Wakui and Yamanaka, 2006). Thus, it is likely that groundwater at AW7 is affected by paddy field water. Indeed, paddy fields comprise one of the dominant land uses in areas north of AW7. Anaerobic environments below paddy fields may have enhanced denitrification. Although river water at AW4 had similar characteristics, its d-excess was not very low. Therefore, this water may be affected by sewage rather than paddy field water. Consequently, data for AW7 are not suitable for the EMMA.

Except for AW7, the groundwater δ values and Cl^- concentrations can be used for the EMMA assuming three end-members: Although γ_C and λ_C cannot be determined exactly, those for groundwater at AW9 were used as approximations.

The estimated contribution ratios and their possible errors are shown in Fig. 6.8. The errors ranged from 3 to 10% for all wells except AW11. The difference in estimated ratios between $\delta^{18}O$ and δD ranged from 0 to 13%. Taken together, these findings suggest that the results of the EMMA are considerably reliable, with a 10% error range. Although river seepage contribution ratio of 16% is found at AW11, which is located far from the river, the potential error of ±17% at this well is relatively large. As mentioned above, the hydrochemical characteristics of groundwater at AW11 indicate its shallow flow path and relatively short residence time. Therefore, the observed δ values of the water should be affected by the lower δ values of precipitation in the study period rather than the long-term mean values used for the EMMA. Thus, this error can be attributed to the difference in the time scale deterring γ_B, and the contribution of the Watarase River water at AW11 should be nonexistent.

6.3.5 The relationship between well screen depths and river water contribution ratios

The depths of most of observed shallow wells are ranged from 2 to 11 m below surface. We assumed that the screen depths of shallow wells were one meter higher than the well depths. The

relationship between estimated screen depth of shallow wells and river contribution ratio and precipitation contribution ratio of wells were shown in Fig. 6.9. The results indicated that the river contribution ratio increased with the increasing screen depth of shallow wells. However, the relative contribution of precipitation decreased with the increasing screen depth. The same changed trends of river contribution ratio and precipitation ratio with screen depth also could be seen in the deep municipal wells (Fig. 6.9), of which the mean screen depths were calculated from borehole loggings.

6.4 Discussion

Even with the errors in the estimated contribution ratios (Fig. 6.8), the general characteristics of their spatial distribution patterns (Fig. 6.10) do not change very much, indicating that the results obtained are fairly insensitive to errors. These findings suggest that the contribution ratio from the Watarase River water was extremely high (up to 94%) at wells adjacent to the river channel. However, the distribution of contribution ratios of river seepage was asymmetric with respect to the Watarase River channel. As shown in Figure 6.11, the contribution of river seepage decreased with increasing distance from the river on both the south and north sides. The river recharged systems as far as 5 km to the south and 1.6 km to the north. The steeper slope of the ground near the mountain is expected to produce faster groundwater flow from the mountain to the river and thus reduce groundwater flow from the river to the north. Thus, the distance can be considered an important factor controlling the contribution ratio of the river water to the groundwater, while the relationship between these factors is modified by topographic conditions such as slope.

Direct infiltration of local precipitation is greatest in the foothills (AW11 and AW12) and areas far from the Watarase River in the plain (AW5). Even at areas along the Watarase River (AT5, AT7 and AW8), the contribution ratio of direct infiltration is ≥50%. The absolute value of the recharge rate by local precipitation should not differ greatly among locations; therefore, reducing the local precipitation contribution will indicate the additional recharge by the river and/or mountain block

groundwater. The spatial distribution pattern of the contribution ratios obtained from the EMMA indicates where such additional recharge occurs and how the recharge waters flow.

The contribution of the mountain block groundwater to aquifers (mountain block recharge) was remarkably high at the central portion of the study area north of the Watarase River (AW9, AW8 and AT5). In contrast, the contribution of the river water at AW8 and AT5 was nonexistent or negligible, despite the proximity to the river. The AW9, AW8 and AT5 were situated around the estimated axis of the syncline and had layers of chert and sandstone (Fig. 3.8), which suggests that the syncline structure promoted the mountain block recharge at a particular area around the wells while hindering the flow of water from the river channel to the mountain side and precipitation infiltration. These results agree with those of Ben-Itzhak and Gvirtzman (2005), who found that groundwater could flow from mountain aquifers to rift valley aquifers along synclinal axes. The high Cl^- concentration observed at AW9 may reflect dissolution of the rocks or solute enrichment by transpiration (not evaporation), which does not induce isotopic fractionation. Since the Na^+, Mg^{2+} and HCO_3^- concentrations were also high at AW9, dissolution of the rocks may be a major cause of high Cl^-. Although this appears to violate the third assumption of the model, the EMMA results are still valid for tracing the mixing of groundwater in the plain aquifer since such sediment is less easily dissolved.

As mentioned above, the major factors controlling the contribution ratio of the river water at each well are the distance from the river, slope, and hydrogeological conditions such as syncline structure. The groundwater pumping rate at each well may be another potential factor influencing the groundwater recharge and flow system (Kelly, 2002; Yamanaka et al., 2011b). Although Fig. 6.12 suggests a positive correlation between pumping rate and the river water contribution ratio for some municipal wells (AT3, AT4, AT6 and AT7), the higher contribution ratios are a reflection of the shorter distance from the river (Fig. 6.11) rather than the sole effect of the pumping rate. Although groundwater pumping may enhance the absolute rates of total recharge, the EMMA did not provide strong evidence of its effect on river channel seepage.

Based on the above results, the main recharge source for municipal wells (except AT5) is the Watarase River. The contribution ratios of river water generally exceed 50%. The greatest contribution ratio for municipal wells was 94%, which was observed at the well with the largest pumping rate (AT3 in Fig. 6.12). Therefore, the domestic water supply system in this area depends strongly on the quantity and quality conditions of the Watarase River. For example, if upstream river water is regulated by dams or contaminated by accidents, water from municipal wells may be affected, while hydraulic drawdown due to pumping at the wells can be mitigated by river seepage. Conversely, even though AT5 is located very close to the river channel and has high pumping rate, the contribution of Watarase River water to this aquifer is suppressed by mountain block recharge. Thus, this well is not strongly influenced by Watarase River conditions. Furthermore, at direct-recharge-dominated sites, shallow groundwater should be more sensitive to artificial alteration of land use and cover. These findings should be helpful for integrated management of groundwater and surface water resources.

6.5 Summary

Isotope and hydrochemistry analysis indicated that direct infiltration by precipitation, Watarase River seepage and mountain block recharge are the three main recharge sources in the study area. The isotopic signatures revealed an obvious altitude effect, as well as mean residence times of river water and groundwater > 1 year.

The EMMA using stable isotope and chloride tracers was shown to be useful for estimation of the contribution ratio of different recharge sources with sufficiently low error (≤ 10%). The results demonstrated that the Watarase River contributes a great amount of water to aquifers along its channel, with the contribution ratio reaching as high as 94%. However, the spatial extent of river-recharged water differs, with the water influencing aquifers for 5 km from the channel and 1.6 km on the plain side and mountain side, respectively. Mountain block recharge is one of the dominant components in a limited area in the foothills. A syncline structure was found to play an

important role in transmitting mountain block recharge, and mountain block recharge was shown to suppress river channel seepage into the mountain side aquifers and precipitation infiltration. The distance from the river channel, topography, and hydrogeological settings such as syncline were identified as the three major factors controlling the river water contribution ratio. In addition, the contribution ratio of river water to groundwater is also slightly varies with depth.

Table 6.1 The analyzed hydrochemical and isotopic items of groundwater and river samples in the Ashikaga area.

Well ID	Hydrochemistry										Isotope	
	EC	pH	Na^+	K^+	Ca^{2+}	Mg^{2+}	Cl^-	SO_4^{2-}	HCO_3^-	NO_3^-	$\delta^{18}O$	δD
	ms/m		mg/L	mg/L	mg/L	mg/L	mg/L	mg/L	mg/L	mg/L	‰	‰
AW1	17.1	6.40	13.5	1.6	20.1	2.9	6.3	23.7	55.5	9.3	-9.43	-64.4
AW2	22.8	6.52	20.1	2.1	32.3	4.9	9.3	29.4	71.1	13.4	-9.31	-63.9
AW3	29.4	6.62	16.4	2.3	42.2	6.8	8.2	45.7	101.5	14.6	-9.05	-62.7
AW4	27.3	6.51	24.0	2.9	37.1	10.4	9.1	36.7	101.2	2.7	-8.97	-62.4
AW5	19.9	6.29	11.5	2.8	32.5	3.9	5.5	28.4	76.9	3.3	-8.45	-58.9
AW6	16.8	7.53	17.5	1.5	18.5	4.4	7.6	13.1	73.6	4.7	-8.92	-61.3
AW7	44.4	6.73	23.9	1.7	34.5	13.5	21.8	18.1	168.9	0.0	-7.83	-55.5
AW8	26.0	6.35	20.4	1.9	32.7	5.2	13.6	27.9	94.7	13.9	-8.53	-59.0
AW9	36.6	6.66	43.9	2.3	27.2	11.7	26.0	2.8	156.7	0.0	-8.92	-61.0
AW10	21.2	6.36	19.7	2.7	25.2	3.4	8.2	25.5	74.2	10.8	-9.22	-63.0
AW11	11.9	6.11	5.9	0.9	18.3	2.6	1.5	8.9	57.6	6.9	-8.55	-57.8
AW12	15.3	6.46	8.6	2.6	23.9	6.6	3.8	10.2	94.7	9.6	-8.39	-56.6
AT1			11.4	2.1	34.6	4.9	11.2	33.3	98.7	16.7	-9.18	-62.8
AT2			8.3	1.6	33.4	5.3	8.5	37.3	106.7	15.3	-9.14	-62.9
AT3			9.6	2.3	24.3	2.8	5.5	18.0	48.4	7.6	-9.48	-65.0
AT4			9.3	1.6	23.9	3.3	6.2	18.5	58.2	8.3	-9.09	-62.3
AT5			15.3	2.5	44.5	6.8	13.3	33.7	107.9	14.3	-8.57	-58.9
AT6			7.1	1.7	23.1	3.4	4.6	15.9	61.9	9.9	-8.92	-61.3
AT7			7.0	1.5	25.3	3.6	3.0	10.2	63.8	5.5	-8.89	-60.8
AR1	12.6	7.37	15.6	1.7	22.3	2.6	6.0	19.5	38.6	6.0	-9.50	-65.2
AR2	10.6	6.86	18.9	1.0	11.3	2.5	4.2	10.5	47.2	4.8	-8.40	-57.7
AR3	8.3	7.10	12.5	0.8	11.2	1.4	2.7	3.8	41.4	7.8	-8.58	-58.8
AR4	18.1	7.19	16.8	2.1	20.0	3.3	8.1	14.3	65.6	7.3	-8.13	-55.7

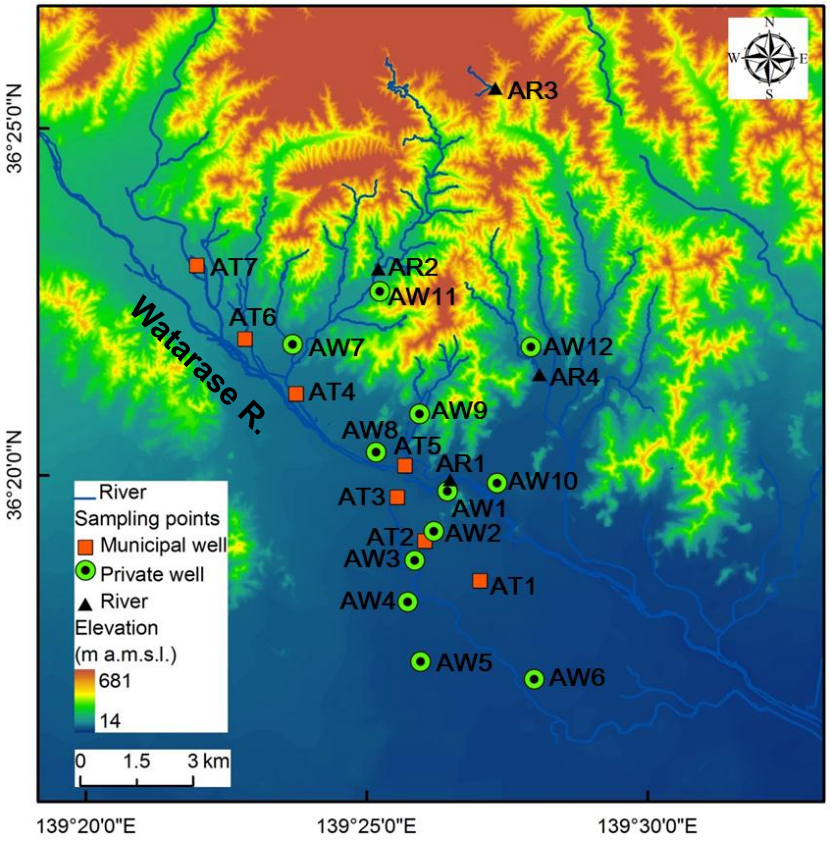

Figure 6.1 Groundwater and river water sampling locations in the Ashikaga area.

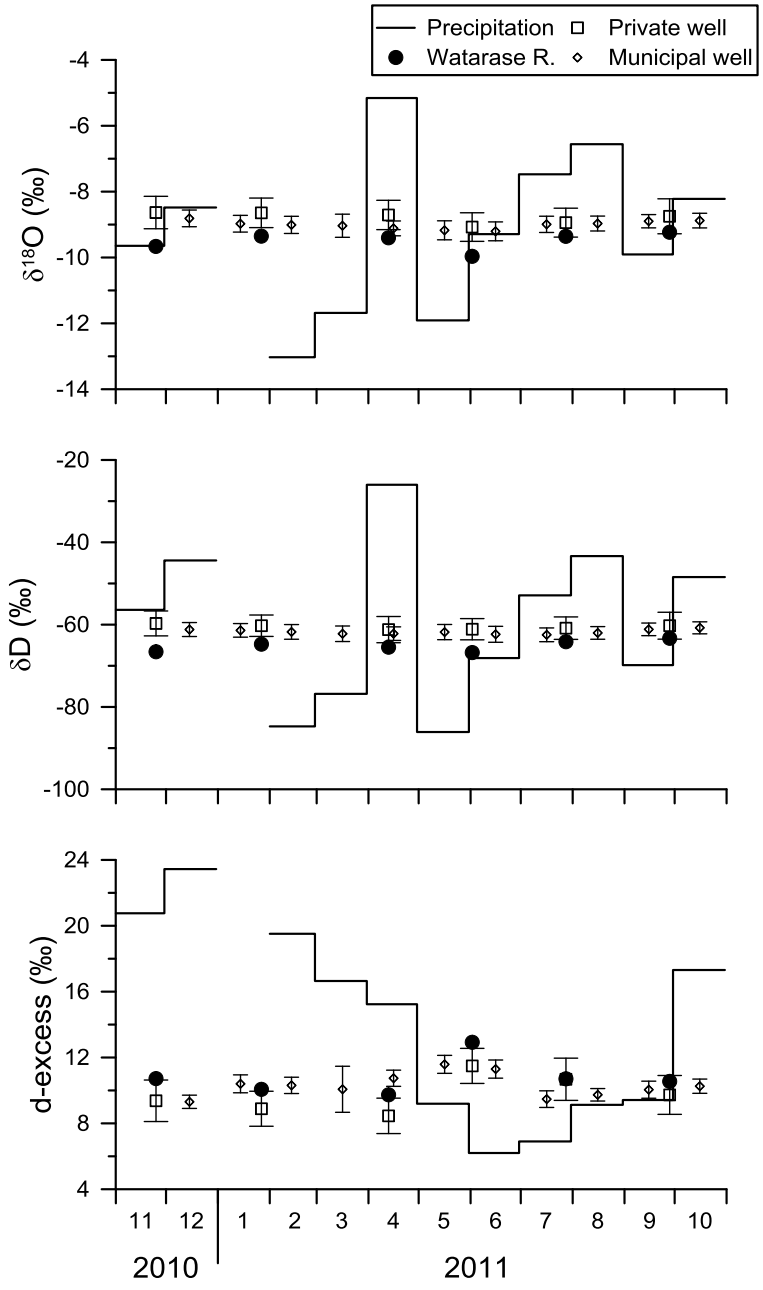

Figure 6.2 Temporal variations of $\delta^{18}O$, δD and d-excess in precipitation, Watarase River water and groundwater during the study period.

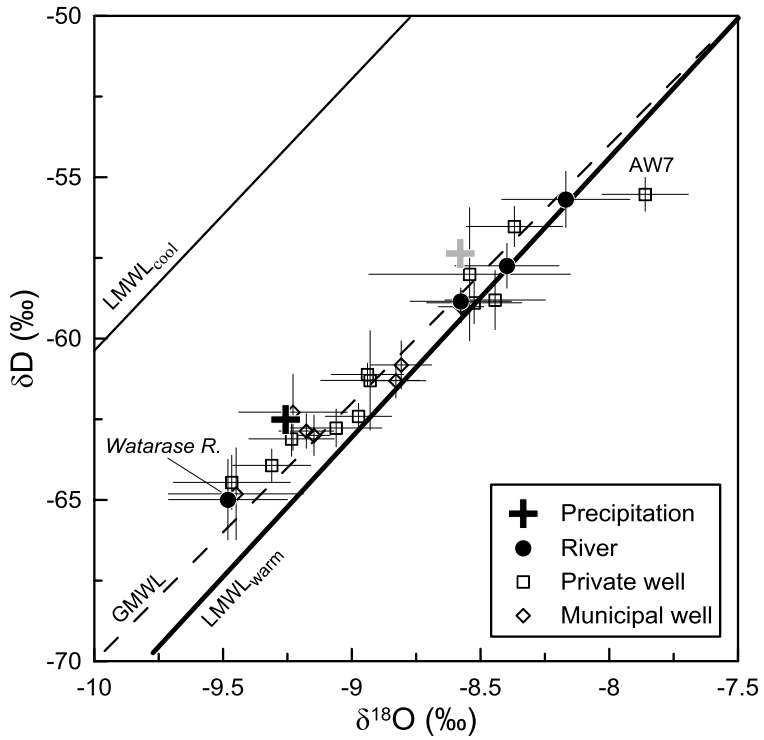

Figure 6.3 Plot of $\delta^{18}O$ vs. δD of river and groundwater samples. The global meteoric water line and local meteoric water lines (in cool season and warm season) are added. Black cross is weighted (by monthly precipitation amount) mean precipitation and gray cross represent mean precipitation weighted by long-term mean precipitation amount.

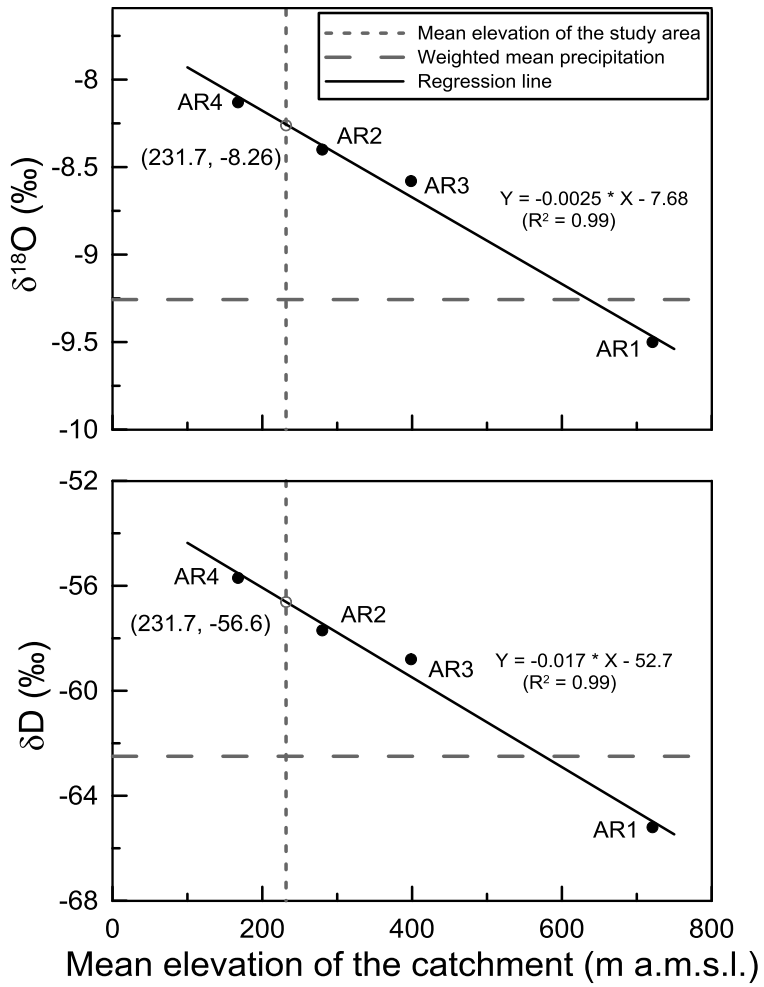

Figure 6.4 Mean $\delta^{18}O$ and δD of river water vs. mean elevation of the catchment. The gray open circles represent estimated long-term mean δ values of precipitation corresponding to the mean elevation of the study area and the gray error bars are estimated standard deviation for long-term mean δ values of precipitation.

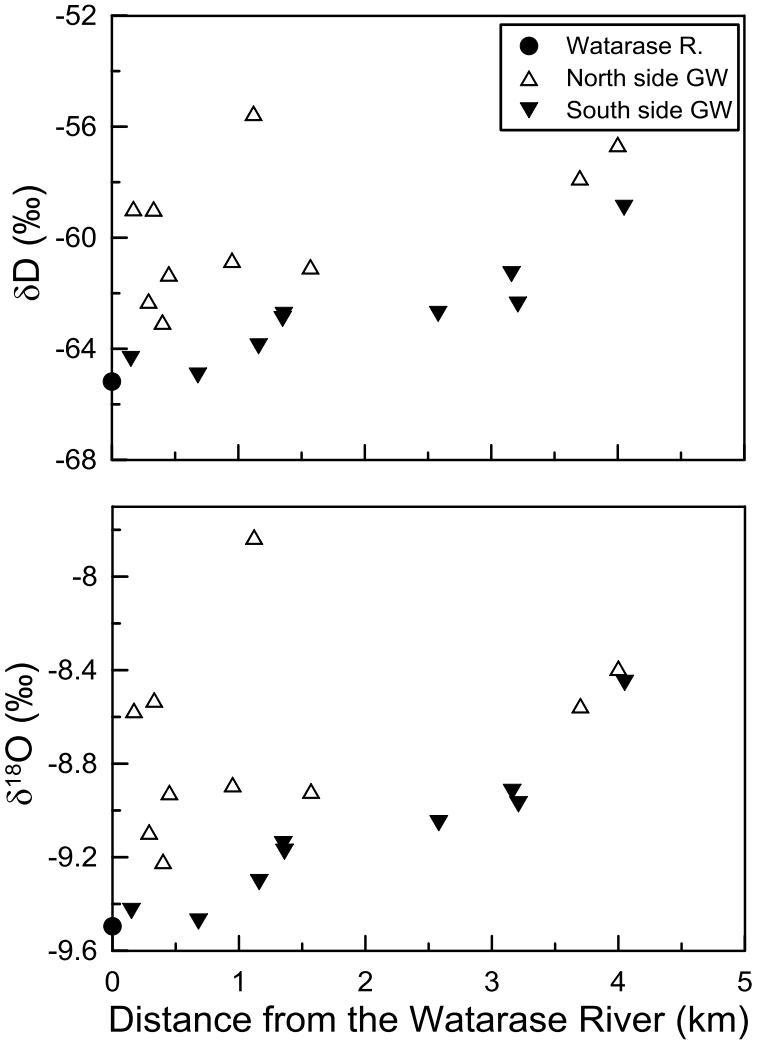

Figure 6.5 Annual mean $\delta^{18}O$ and δD of groundwater and their relationship with distance from the Watarase River. The annual mean $\delta^{18}O$ and δD of Watarase River water was also plotted for reference.

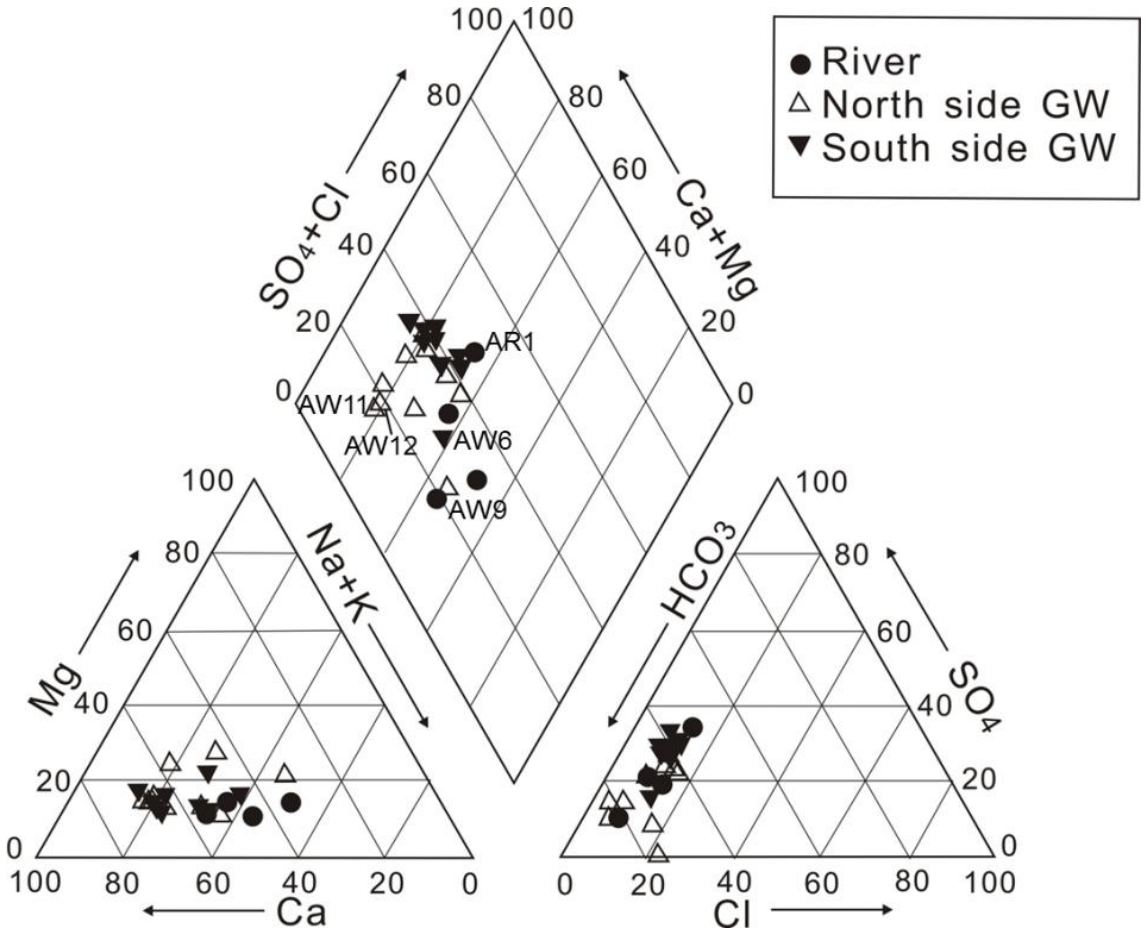

Figure 6.6 Piper diagram of groundwater and river water samples in the Ashikaga area.

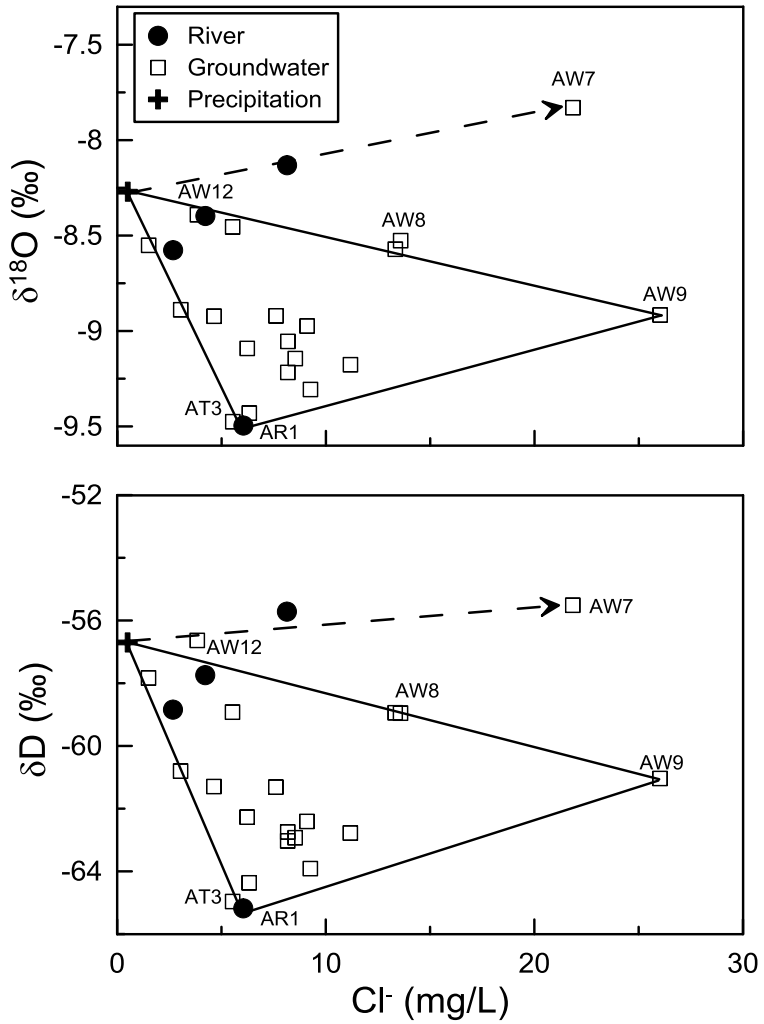

Figure 6.7 Relationship of arithmetic mean annual $\delta^{18}O$, δD and Cl^- concentration in river water and groundwater.

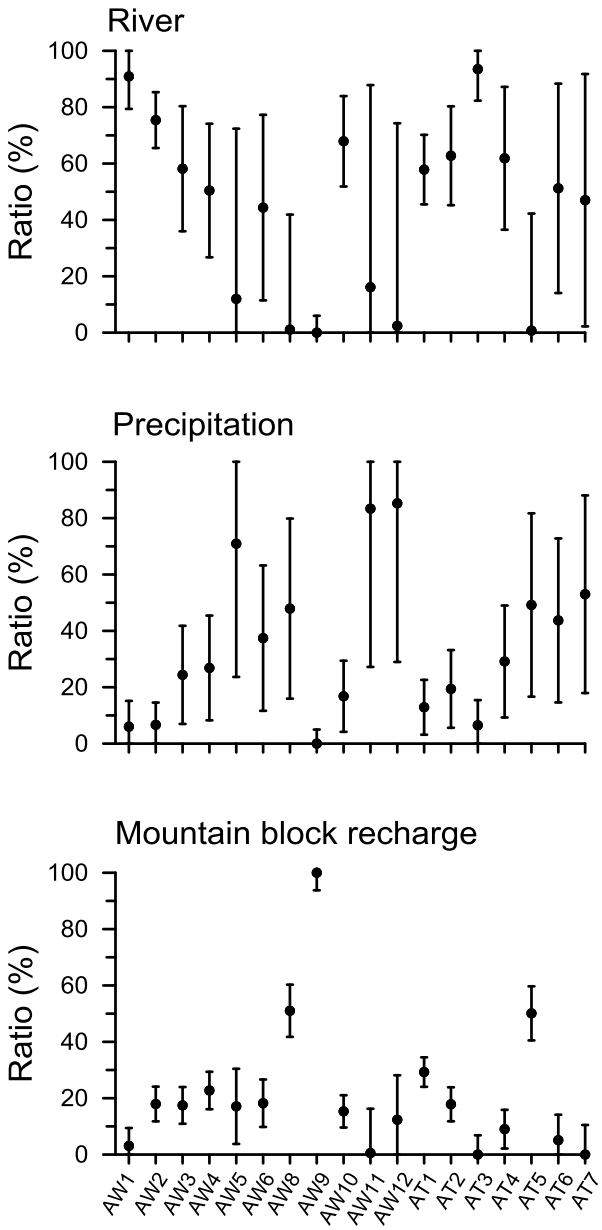

Figure 6.8 The contribution ratios and corresponding estimation errors of recharge sources for wells in the Ashikaga area.

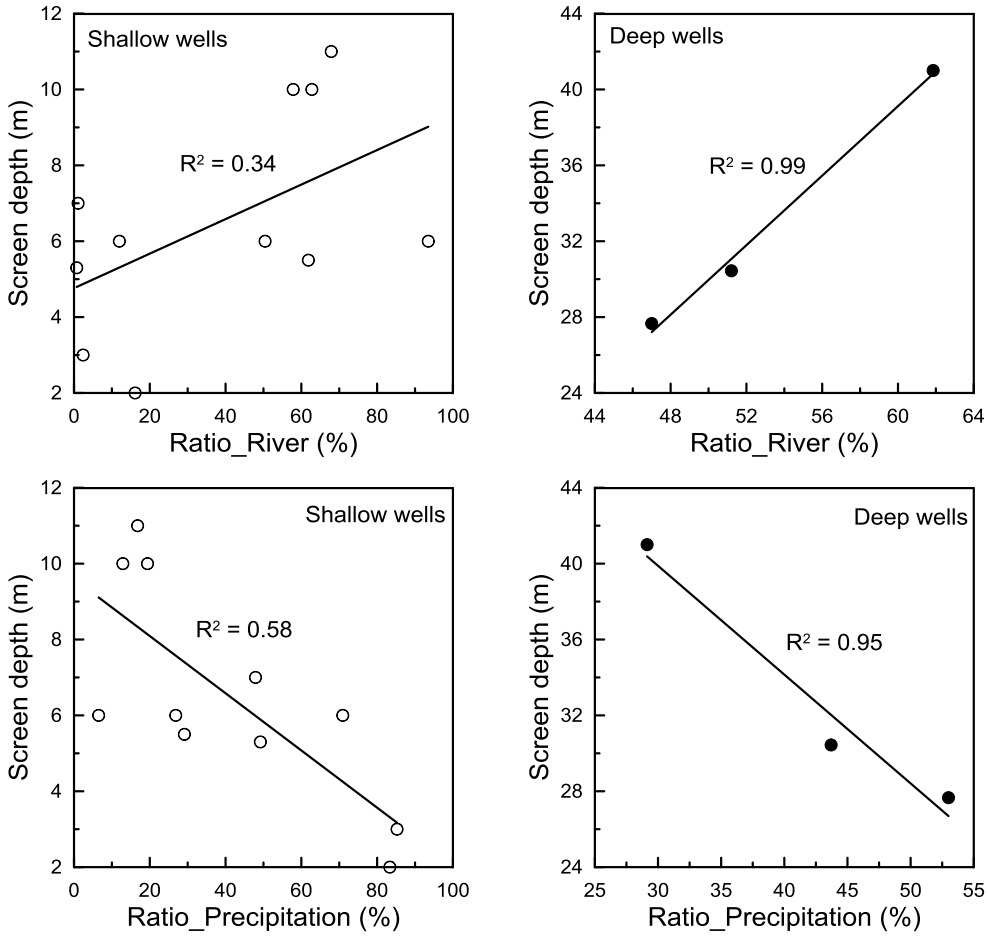

Figure 6.9 The relationship between screen depth and contribution ratios of river water and precipitation for selected wells in the Ashikaga area.

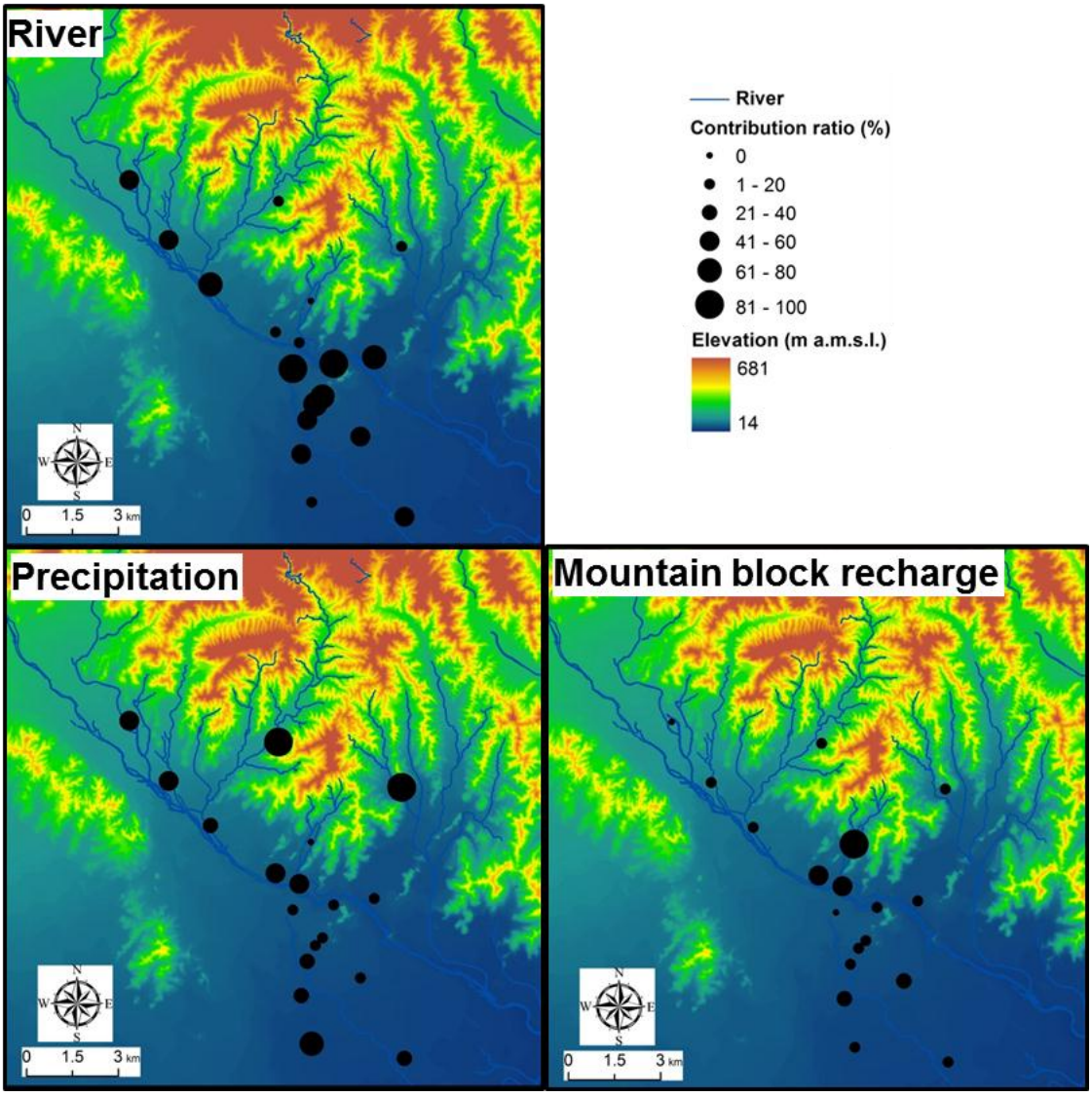

Figure 6.10 Spatial distribution of contribution ratios of groundwater recharge sources for the Ashikaga area.

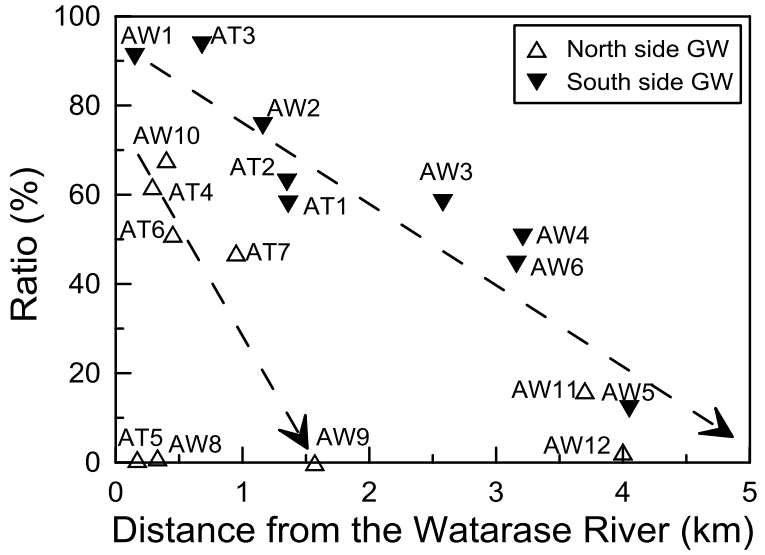

Figure 6.11 Relationship of river water contribution ratio and distance from the Watarase River.

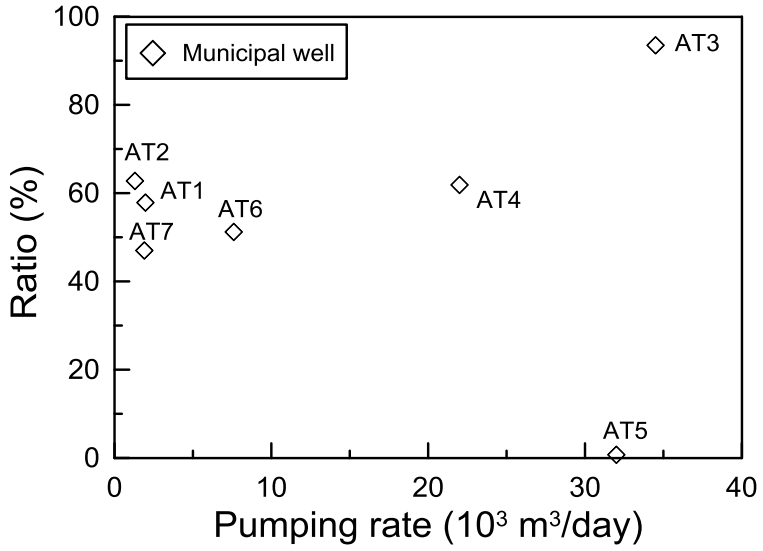

Figure 6.12 Relationship of river water contribution ratio and pumping rate for the Ashikaga area.

Chapter 7
Numerical simulation for the Ashikaga area

7.1 Introduction

The contribution ratios of three major recharge sources for the Ashikaga area were estimated using tracer approach in Chapter 6. Although the uncertainty analysis of the EMMA showed that the uncertain concentration of mountain block recharge was not sensitive to the calculated contribution ratio, the sensitivity of the uncertain location of mountain block recharge still need to be examined. The specific objectives of this chapter are (a) to make clear the detailed spatiotemporal variations of recharge sources in the Ashikaga area considering the uncertain location of mountain block recharge and (b) to reveal the discharge characteristics of the Ashikaga area. The influence of long-term pumping on river seepage is also further examined. The simulation results in 15th January and 15th July 2010 were selected to represent the conditions in the dry season and wet season, respectively.

7.2 Methodology

7.2.1 Numerical modeling codes

MODFLOW-2000 (Harbaugh et al. 2000) was used to simulate groundwater flow and MT3DMS (Zheng and Wang, 1999) was used to simulate the solute transport. A detailed description of these two codes was shown in section 5.2.1.

7.2.2 Model construction and parameters

a) Model domain and grid design

For decreasing the influence of uncertainty of the boundary setting on simulation results, a larger area was chosen as the model domain (Fig 7.1). The surface grid interval was 1000 m, 500 m, 250 m and 125 m (Fig. 7.2a). Totally 5 layers were set to simulate aquifers (Fig. 7.2b). Layer

1 is the focused layer, which corresponding to the unconfined aquifer is composed of gravel, sand and loam. Layer 2 represents the first aquitard, which consists of gravel, sand, clay and silt. Layers 3 to 5 correspond to deep aquifers, where gravel, sand, clay and loam are present. The thicknesses of layers were determined by interpolation using Kriging method based on the borehole logs in Fig. 3.8. The thickness of Layer 1 ranged from 2 to 130 m.

b) Head and concentration observation wells

The sampling wells shown in Fig. 6.1 were used as concentration observation wells. Since hydrometric data at these wells were not available, some observed data from previous studies were used (Fig. 7.3). The data of wells W, SW, S were obtained from Water Information System of Japan (http://www1.river.go.jp/). The W, SW and S represent data from observation points, Yabuzuka (139°17′49″ E, 36°21′32″ N), Ojima (139°17′11″ E, 36°15′15″ N) and Oura (139°28′04″ E, 36°15′54″ N), respectively. For the wells W and S, monthly observation data in 2005 were utilized, while the observation data are available only in February, July, August and November for the well SW. The mean groundwater table in these four months of 2003, 2007, 2008 and 2009 were used as observed head at SW. The daily groundwater table of wells 49, 50 and 136 were from Groundwater Level Chronology in 2004. The groundwater table with 10-days interval at wells 49, 50 and 136 were used in the model as observed hydraulic head.

A clearly linear relationship exists between the elevations of the ground surface and groundwater table at head observation wells (Fig. 7.4a). Also, the elevation of ground surface has a good liner relationship with elevation of well bottom at concentration observation wells (Fig. 7.4b). In addition, the elevation of groundwater table increased with the increasing elevation of well screens (Fig. 7.4c).

c) Boundary settings and input data

Flow Boundaries

Constant head boundaries were assigned to represent the groundwater tables in the south, east and north sides. The daily observed river stage in the Futto gaging station of Tone River

(139°23′00″ E, 36°14′27″ N) during the simulation period was used to simulate the hydraulic head of constant head boundaries in the south side of the first layer. The constant head setting was determined considering the linear relationship between elevations of ground surface and groundwater table as well as possible seasonal variation of groundwater table (Table 7.1).

The Watarase River was set as a stream boundary using the Streamflow-Routing Package (Prudic, 1989). The river stage was set using the observation data at gaging station of Ashikaga (139°26′41″ E, 36°20′02″ N) (http://www1.river.go.jp/). Since the volumetric flow rate was only available before 2001, a statistical analysis was done to calculate the relationship between the river stage and volumetric flow rate from 1992 to 2001 (Fig 7.5). The estimated volumetric flow rate based on the results of statistical analysis was used as inflow at the first uppermost segment of the Watarase River. The river bed conductance was given as an assumed value and then modified by trail-and-error method (Table 7.2). The small rivers in the model domain were simulated as a sink term of groundwater by using drain boundary with fixed head in time and variable in space.

A general boundary was set for simulating the mountain block recharge. Based on the calculated isotopic lapse rate, the δ values of AW9, and the mean elevation of the study area, the elevation of recharge source for AW9 was estimated to be more than 500 m a.m.s.l., that is, elevation of the source of the mountain block recharge should be higher than 500 m a.m.s.l. From topographic map, it is found that there are two mountains with elevation of some 600 m a.m.s.l. at the northwest of the study area. Therefore, we set that an additional source for general boundary was 600 m, and the distance from the additional source to the model domain was 8 000 m. The conductance was assigned to be 0.1 m/d.

We assumed that the bedrock and deep aquifers below Layer 5 do not have contribution to groundwater flow in the unconfined aquifer. Therefore, no-flow boundary was adopted for the bottom of the model. The Recharge Package was assigned to the uppermost active aquifer to simulate spatially distributed recharge from precipitation and paddy field water to the groundwater

system. The infiltration rate of the precipitation and paddy field water were given as assumed infiltration rates and then modified by calibration (Table 7.2). The groundwater recharge from the paddy field during the irrigation period was considered as paddy field water recharge, while during the rest of the year was considered as precipitation recharge. The recharge input was at a monthly time step and the estimated monthly recharge at paddy field area and at non-paddy field was shown in Fig. 7.6.

The pumping wells in the model were set at locations of seven municipal wells and their pumping rates were determined considering the government website of Ashikaga area (http://www.city.ashikaga.tochigi.jp/site/jougesuidou/) as shown in Table 7.3. A deep well AW6 is also a small pumping well for supplying water to a small village; its pumping rate was set to be 500 m^3/d.

Mass Transport Boundaries

The constant concentration boundary was set accompanying with stream boundary, general head boundary and north side of constant head boundary. Point sources were set accompanying with the south, west and east sides of constant head boundary. As the concentration for the stream boundary, δ values of the Watarase River water were used, while the concentrations for the constant concentration boundaries and point source boundary were assigned using δ values at wells AW11, AW12 and AW5 in the northwest, northeast and other sides, respectively. The estimated δ values for an elevation of 600 m were assigned to the constant concentration at the general head boundary.

Simulation cases

Four cases with changed north boundary were done to simulate the uncertain boundary in the north side (Fig. 7.7). Case 1 was assumed that the general head boundary only around well AW9 and in all the layers. The north side boundaries of Layers 3 to 5 were assigned as no flux boundaries except the general head boundary. Case 2 was hypothesized that the whole north side boundary is the general head boundary in Layers 3 to 5, while the first and second layers were

set as constant head boundary. The settings of Case 3 are same as Case 2, but the general head boundary was set to Layers 2 to 5. Case 4 is based on Case 3 and Case 1, assuming that the north boundary of Layers 2 to 5 and grids around well AW9 in Layer 1 are general head boundary.

d) Initial conditions

Steady state simulations having the same boundary settings with the transient simulations were run to determine the initial conditions of the transient simulations. Since the observed hydraulic head data are limited to some wells, we estimated groundwater table at the other wells by the following procedure. The elevation of the groundwater table is assumed to be 1 m higher than the elevation of corresponding well bottom. Then, the groundwater table can be estimated to be the elevation of well bottom plus 1 m. The mean observed hydraulic head of observation wells and the estimated groundwater table at 10 concentration wells were used as initial heads in the model under steady state condition. The observed δ values of private wells in September, AW4 in November, and municipal wells in December 2010 were applied as initial concentrations in the steady state simulation. Then, the calculated hydraulic head and concentrations of ^{18}O and D from the steady state simulation were applied as initial conditions in the model under transient condition.

e) Hydraulic and transport parameters

Nineteen parameter zones were set in the Layer 1 to simulate the hydraulic heterogeneity of the unconfined aquifer (Fig 7.8). For the deep layers, one parameter zone was set accompanying with the plain sediment in each layer. In addition, one parameter zone (Zone 5) was assigned to simulate the aquifers or mountain block at foothills in the deep aquifers. The hydraulic parameters and transport parameters were initially assigned based on the empirical values and systems defaults. Then, the parameters were modified for Case 1 using available field data and through model calibration with the help of Visual PEST (Doherty, 1998). The conductance values of the stream, drain and general head boundaries were determined through calibration by the trail-and-error method. Table 7.2 summarized the determined parameters through hydraulic and

isotopic calibrations. For all the other cases, the hydraulic and transport parameters were same as the calibrated parameters by Case 1.

7.3 Results

7.3.1 Calibration results and sensitivity analysis for boundary settings

Figure 7.9 shows the observed and calculated hydraulic head in 4 cases. The root mean squared errors of observed and computed hydraulic head in 4 cases ranged from 1.3 to 1.6 m. Case 3 has the lowest RMS and Case 2 has the largest RMS. However, the lowest RMS of $\delta^{18}O$ (0.26‰) is in Case 1 and Case 2 (Fig. 7.10). The RMSs of observed and calculated δD are same (1.3‰) for 4 cases, while the residual mean in Case 1 is the lowest (0.1‰, Fig. 7.11). The results indicate that the agreement of simulated and observed data in Case 1 is better than in the other cases, even though the model is not very sensitive to the north boundary changes.

As shown in Fig. 7.12, the temporal variation of simulated hydraulic head in Case 1 generally agrees with observed hydraulic head. Moreover, the temporal variations of $\delta^{18}O$ and δD at the shallow wells were reproduced very well (Fig. 7.13 and Fig, 7.14). However, the simulated δ values at the deep wells (AW6, AT4, AT6, and AT7) are slightly different from the observed data. Use of mean screen depths for representing the multiple screens of the deep wells is probably one reason to cause the difference. In addition, the same initial concentration setting was assigned to the deep aquifers as the unconfined aquifer, which is probably another reason.

7.3.2 Comparison of the contribution ratios estimated by simulation and EMMA

The contribution ratios of the Watarase River, precipitation, mountain block recharge and paddy field water were computed using the method mentioned in section 6.3.6. The estimated annual mean contribution ratios were compared with the results of EMMA (Fig. 7.15). The correlation coefficient between the estimated ratios by the numerical simulation and the EMMA for Case 1 is larger than three other cases, indicating that Case 1 provides the best one. Therefore,

it can be inferred that the boundary settings in Case 1 are the closest to the true distribution of mountain block recharge.

7.3.3 Spatial and temporal variation of groundwater tables in unconfined aquifer

The spatial distribution of hydraulic head (Fig. 7.16) demonstrates that the groundwater flow from northwest and north to southeast and south in the Ashikaga area. The contour lines are very steep at the valleys in the north side (i.e., mountain side) and very smooth in the southeast side (i.e., plain side), indicating that the groundwater flow is potentially faster in the mountain side than in the plain side. The groundwater flows from the mountains through the Watarase River to the plain. The Watarase River acts as a recharge source of groundwater in the plain side, and a discharge sink of groundwater in the mountain side. In addition, the distribution of contour lines is symmetric with respect to the Watarase River at the upstream and most downstream reach, and asymmetric at the midstream reach.

7.3.4 Spatial and temporal variation of δ values in the unconfined aquifer

Generally, the δ values of groundwater along the Watarase River channel are lower than that in the foothills and the plain area far from the channel. The δ values in areas near mountains also have low values (Fig. 7.17). It is clear that seasonal change in δ values at an area in the southwest is very remarkable. In such an area, the δ values are obviously higher than the surrounding areas. The location of the high δ values corresponds to the location of paddy field dominated area (Fig 3.7), indicating the paddy field water infiltration during the irrigation period modified the δ values of groundwater under paddy field.

7.3.5 Recharge and discharge amount of groundwater

In Ashikaga area, the groundwater receiving recharge from precipitation via two paths: direct infiltration and lateral recharge through shallow aquifers of boundary margins along mountains. As shown in Fig. 7.18, the direct infiltration of precipitation and paddy field water was 417.9 million m^3 during the simulation period, accounting for 7% of total recharge and 66% of total net recharge. The direct infiltration amount increased from null in January to 81.6 million m^3 in July,

2010, which accounted for 83% of total net recharge. The lateral recharge accounted for 91% of total recharge and 24% of total net recharge. The Watarase River played as a losing river from the viewpoint of net recharge during the whole simulation period. The seepage of the Watarase River was 98.4 million m^3 in total, 7.3 million m^3 in January and 6.5 million m^3 in July. Although the seepage of the Watarase only accounts for 2% of total recharge, the relative contribution of river seepage was 8% in total, 29% in January, and 2% in July from the viewpoint of net recharge. The mountain block recharge was 7.9 million m^3 in total, 0.6 million m^3 in January, and 0.6 million m^3 in July, accounting for 1%, 4% and 1% of total net recharge, respectively.

The tributaries of the Watarase River and the Tone River and pumping wells are main discharge paths in the model domain. The discharge of tributaries was 714.5 million m^3 and pumping wells was 43.4 million m^3, accounting for 94% and 6% of total net discharge, respectively. The pumping amount was constant with 0.6 million m^3 per month. However, the ratio of groundwater pumping was varied from 7% in January to 5% in July from the viewpoint of total net discharge. The discharge of the Watarase River was 46.3 million m^3 in total, 2.8 million m^3 in January and 4.1 million m^3 in July.

7.3.6 Spatial and temporal variation pattern of contribution ratio for each recharge source

The spatial distribution of contribution ratios of recharge sources to groundwater in dry season and wet season in Ashikaga area is shown in Fig.7.19 and Fig. 7.20, respectively. The river seepage occurs mainly along the river channel. However, the spatial distribution of river-recharged groundwater is obviously asymmetric with respect to the Watarase River. Spatial extent of river-recharged groundwater with more than 50% contribution ratio reaches to 4 km from the river in the south side. On the other hand, the extent of river seepage in the north part is far smaller than in the south side ($\leq$ 1 km). However, the river seepage is almost symmetric with respective to the channel at the upstream of the Watarase River and the most downstream reach. The extent of river recharged groundwater with more than 50% contribution ratio at the

symmetric reach is 1.5 km from the channel, which is smaller than the extent of asymmetric reach. The mountain block recharge mainly distributes in the north side surrounding AW9. The distribution of paddy field water infiltration highly related to the distribution of paddy field (Fig. 3.7). It is clear that contribution ratio of paddy field water is remarkable in some regions of the south side of the Watarase River where the paddy field is the dominate land use.

The mean contribution ratio of river, precipitation, mountain block recharge and paddy field water for the unconfined aquifer in the whole model domain during the simulation period was 10%, 81%, 3%, and 6%, respectively (Fig. 7.21). The contribution ratio of Watarase River water in Layer 1 along some reaches of the channel is lower in the wet season than in the dry season (Fig. 7.22). However, the river contribution ratio at river-influenced-area except river channel increased from dry season to wet season. Same as river seepage, the relative contribution of mountain block recharge decreased at mountain block boundary, while it increased at mountain-block-recharge-influenced-area. For the infiltration of paddy field water, the contribution ratio obviously increased in the wet season. The contribution ratio of precipitation increased at the sites where the relative contribution of the other recharge source decreased and vice versa. However, the seasonal variations of contribution ratio for all the recharge sources were no more than 10% in most of the study area.

The month to month variation of contribution ratios of recharge sources at shallow concentration observation wells are shown in Fig. 7. 23. In general, the seasonal variation range of contribution ratios is no more than 7% in the observation wells. The contribution ratios of river increased from November and then decreased from July, while the contribution ratios of precipitation decreased and then increased. However, such a tendency was opposite at well AT5 probably because of the occurrence of mountain block recharge. Although the paddy field water is the dominant recharge source in the southeastern area and some other sites in the south side of the Watarase River, the contribution of paddy field water in the concentration observation wells are no more than 10% except AW5 (Fig. 7.23).

7.4 Discussion

Estimated river water contribution ratio at AW10 and 4 deep wells (AW6, AT4, AT6 and AT7) are different between the numerical simulation and the EMMA (Fig. 7.15a). AW10, AT4, AT6 and AT7 are located in the north side of the Watarase, while the AW6 is the only one deep well in the south side. The precipitation recharge through shallow aquifers at the margins of model domain accounts for 24% of total net recharge of the whole model domain. Does the lateral recharge was overestimated in the numerical simulation and then lead to underestimated river water contribution? To answer this question, an additional simulation was done. As shown in Fig. 7.24, the boundary setting of the north boundary in the first layer of Case 5 was modified according to the boundary setting of Case 1. In Case 5, constant head in the northern boundary of Layer 1 only assigned in the grids near AW11 and AW12, where the occurrence of groundwater was observed at foothills. Then, the spatial distribution of relative contribution of Watarase River water was calculated for Case 5. As shown in Fig. 7.25, the estimated spatial distribution of river water contribution in Case 5 is same as the results of Case 1. The extent of river-recharged groundwater in the north side (i.e. mountain side) of the midstream of the Watarase River in Case 5 didn't become larger with the decreased lateral recharge. However, the lateral recharge could modify the isotopic signatures of well waters. As shown in Fig. 7.26, the δ values at AW6, AT6 and AT7 plotted between weighted mean δ values of precipitation and long-term mean δ values of precipitation, and AW10 and AT4 are plotted near weighted mean δ values of precipitation. If the lateral recharge has the same signature with weighted mean δ values of precipitation and the groundwater storage has the same signature with long-term mean δ values of precipitation, it would be possible that groundwater at AW6, AT6 and AT7 is the mixture of waters precipitated in the study period and before the study period.

The groundwater pumping is a potential cause to enhance river seepage. However, the enhancement of river seepage at municipal wells in the north side was not found from the results of numerical simulation (Fig. 7.27). In the south side, the contribution ratio of river was

relatively high at AT1, AT2 and AT3. Although pumping rate at AT3 is large, while that at AT1 and AT2 is very small. On the other hand, relationship between river water contribution ratio and distance from the Watarase River is very clear in the south side (Fig. 7.28), indicating that the distance from the river is one major factor controlling the relative contribution of river seepage. Consequently, the enhancement of river seepage by groundwater pumping was not always proved by the results of numerical simulation.

The relationship among ground surface, groundwater table, and the locations of mountains and the Watarase River indicates that the mountain block recharge and steep slope of hills at the midstream of the Watarase River, which induced fast groundwater flow, is probably the major reason restricting the groundwater flow from river channel to the north side (Fig. 7.29). It is clear that the slop of groundwater table is stepper in the right side (i.e. mountain side) of the Watarase in the cross section of B-B' than the cross sections of A-A' and C-C'. Although the slope of hills are also very steep in the upstream and downstream area of the Watarase, the distance from hills to the channel is longer at the upstream and downstream reaches than the midstream reach.

The paddy field water contribution was detected only at four wells. The contribution ratios were 6% at AW4, 27% at AW5, 10 % at AW6 and 1% at AW7. It is worth to note that AW6 is a deep well with depth of 150 m. The 20% of river water contribution and 10% of paddy field water contribution at this well indicate the river water and paddy field water are capable of recharging deep aquifers in the Ashikaga area. The isotopic and hydrochemical signatures of groundwater at AW7 indicate that the groundwater at this site was significantly affected by the paddy field water, while the estimated contribution ratio of paddy field water at AW7 was very small in the simulation. The difference between tracer and modeling approaches is probably caused by uncertainty or sub-grid-scale heterogeneity in the input conditions such as hydraulic properties and/or land use. However, the general tendency of relative contribution of groundwater recharge sources reproduced by the numerical model still agrees with that from the

tracer approach for both aspects of spatial distribution and seasonal variation. Thus, combined use of tracer approach and numerical modeling approach could avoid or decrease the errors.

The month to month variation of contribution ratio of paddy field water at point scale, such as AW5 in Fig. 7.23, was relatively stable during the simulation period. This was probably caused by the rainstorm event occurred in July and September 2011. The rainstorm event induced large amount of precipitation infiltration during the irrigation period for paddy field area. The relatively long residence time and long time lag also diminished the seasonal variation of the contribution ratio of paddy field water at point scale. However, the contribution ratio of paddy field water at large scale is obviously increased from dry season to wet season (i.e. irrigation period) (Fig. 7.22).

7.5 Summery

Four cases of simulations with different boundary settings in the north side were done to simulate the groundwater and river interaction in the Ashikaga area. The models were run from September 2010 to October 2011 and both of the hydrometric and isotopic calibrations were done. The calibration results indicate that the Case 1 was the best one. The Case 1 also provided the best calibration results in agreement with the results of EMMA, clarifying that the mountain bock recharge occurred around AW9 in both shallow and deep aquifers.

The groundwater flows from north/northwest to south/southeast in the Ashikaga area. The Watarase River not only acts as a recharge source for the groundwater on the south side of the river but also as a discharge path for the groundwater on the north side of the river. The Watarase River was a losing river from the viewpoint of net recharge in the whole. The river seepage is the second dominant recharge source in the model domain. Precipitation was the main recharge source in the model domain, which was constituted by direct infiltration and aquifer lateral recharge. The groundwater was mainly discharged by the tributaries. In addition, the groundwater withdraws at municipal wells accounts for 6% of total net discharge.

The distribution of river-recharged groundwater with 50% contribution ratio is asymmetric with respect to the channel on the midstream of the Watarase River but almost symmetric at the upstream and downstream reach. The extent of the river-recharge-dominated area in the asymmetric zone is up to 4 km from the channel in the south side but less than 1 km in the north side. The estimated mean contribution ratio of river, precipitation, mountain block recharge and paddy field water in the unconfined aquifer of the whole model domain is 10%, 81%, 3%, and 6%, respectively. This result indicates that the precipitation is the dominant recharge source and the river seepage is remarkable in the model domain. The paddy field water is an important recharge source in areas, where paddy field is the dominant land use. However, for the observation wells, the contribution ratio of paddy field water is considerably low (≤ 10%) or null, except for AW5 (27%) and AW7. The mean contribution ratio of mountain block recharge is low but the contribution ratio of mountain block recharge at the mountain block recharge boundary is very remarkable.

The seasonal variation range of contribution ratio generally does not exceed 10%. The contribution ratio of river and paddy field water increased from dry season to wet season, while the contribution ratio of precipitation decreased. The relative contribution of mountain block recharge increased at mountain-block-recharge-dominated area and decreased at mountain block recharge boundary from dry season to wet season. The contribution ratio of river water decreased with distance from the river channel. The mountain block recharge in the middle reach of the Watarase River was clarified to suppress river water flow from channel to mountain side. Clear evidence of enhanced river seepage by groundwater pumping was not confirmed from the results of numerical simulation.

Table 7.1 Assumed hydraulic heads at constant head boundaries in numerical model for the Ashikaga area

Layer group	North	South	West	East
L1 and L2	BOT+0.1*Z+M (M: 0.38-3.41)	Stage of Tone River	1.03*(BOT+Z)+M (M: 7.93-11.63)	1.03*(BOT+Z)+M (M: 3-3.82)
L3, L4 and L5	0.44*(BOT+0.5*Z)+M (M: 16.9-18.06)			

BOT is bottom elevation of corresponding layer, *Z* is thickness of corresponding layer, *M* is a constant.

Table 7.2 Values of hydraulic and transport parameters used in numerical model for the Ashikaga area.

Parameter type	Layer	Final value	Reference range	Unit	References
Horizontal hydraulic conductivity (K_x, K_y)	1-5	9.5-330	0.15-400	m/d	Elhassan et al. 2001; Wu et al. 2010
Vertical hydraulic conductivity (K_z)	1-5	0.002-8	3×10^{-5}-12	m/d	Mikita et al. 2011; Wu et al. 2010
Specific storage (S_s)	2-5	5×10^{-5}-8×10^{-4}	7×10^{-6}-1.4×10^{-3}	1/m	Kelly, 2004; Mikita et al. 2011
Specific yield (S_y)	1-5	0.005-0.2	0-0.27		Johnson, 1967; Elhassan et al. 2001
Streambed K_z	1	0.8		m/d	
Drain conductance (Simulating springs)	1	0.4		1/d	
Effective porosity	1-5	0.25-0.4			
Precipitation infiltration rate		0.5			
Paddy field water infiltration rate		0.3 (non-planting period) ≥ 1.5 mm/d (planting period)			

Table 7.3 Pumping rate of municipal wells in the Ashikaga area.

Municipal well groups	Pumping rate (m^3/d)	Mean screen depth (m)	Well depth (m)	Well number and Type
AT1	3,400	-	11	1 Shallow well
AT2	1,300	-	11	1 Shallow well
AT3	34,500	-	7	1 Shallow well
AT4	22,000	10.9 (deep wells)	6.5 (shallow well)	1 Shallow well + 4 Deep wells
AT5	32,000	-	6.3	1 Shallow well
AT6	76,00	49.9	-	5 Deep wells
AT7	1,900	29.7	-	3 Deep wells

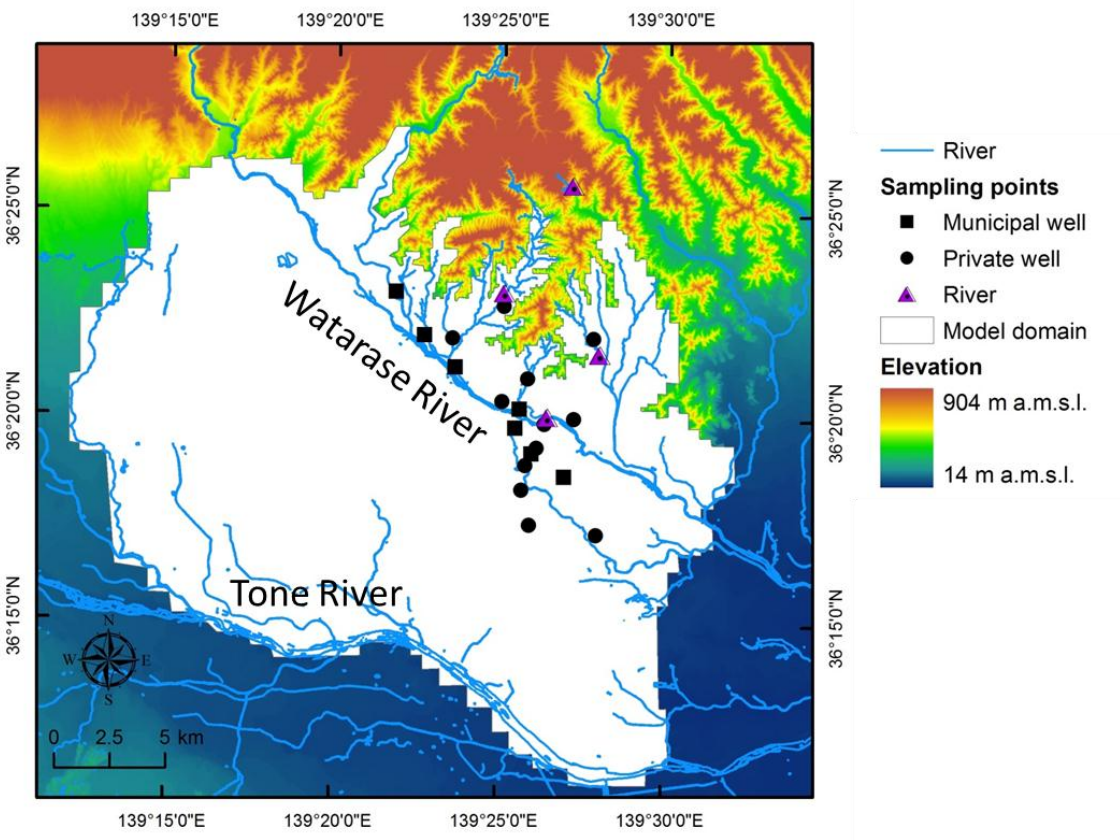

Figure 7.1 Location of the model domain for the Ashikaga area.

(a)

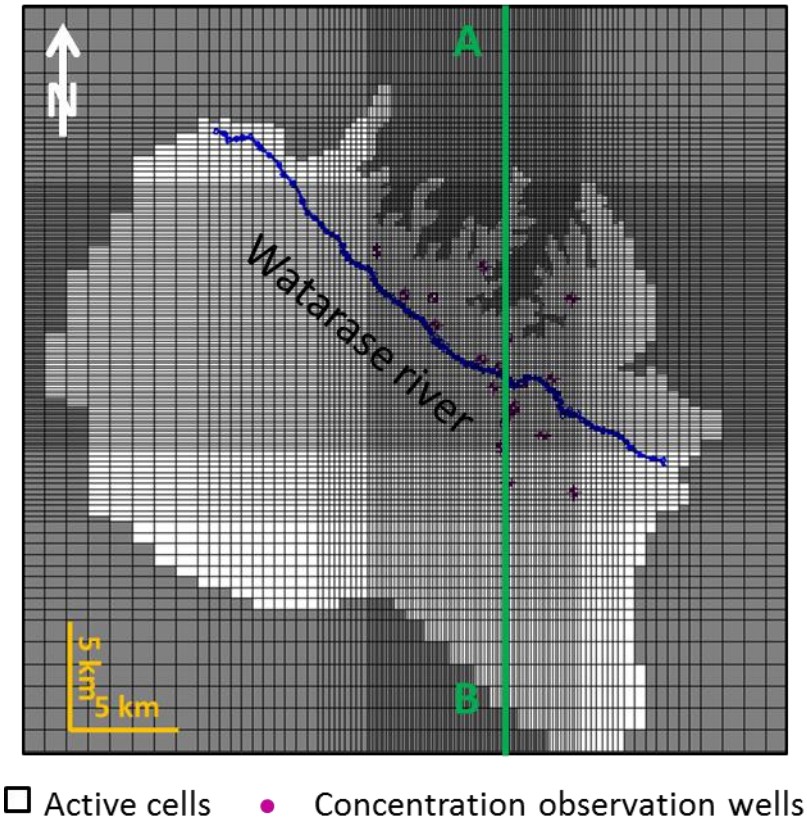

(b)

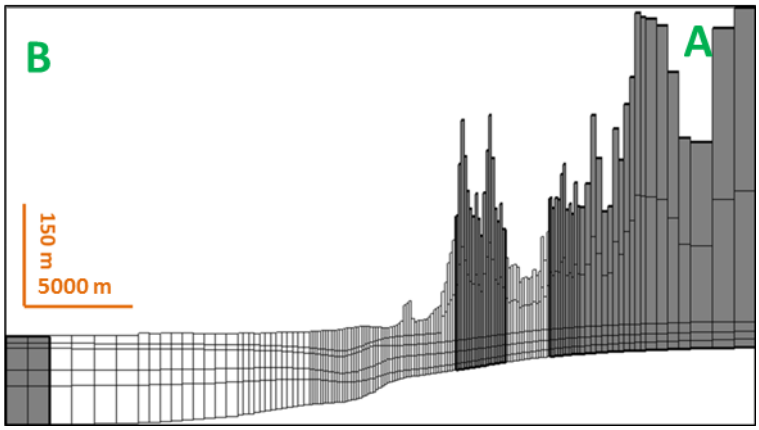

Figure 7.2 (a) The model domain with grid design, and (b) cross section A-B showing layer settings for the Ashikaga area.

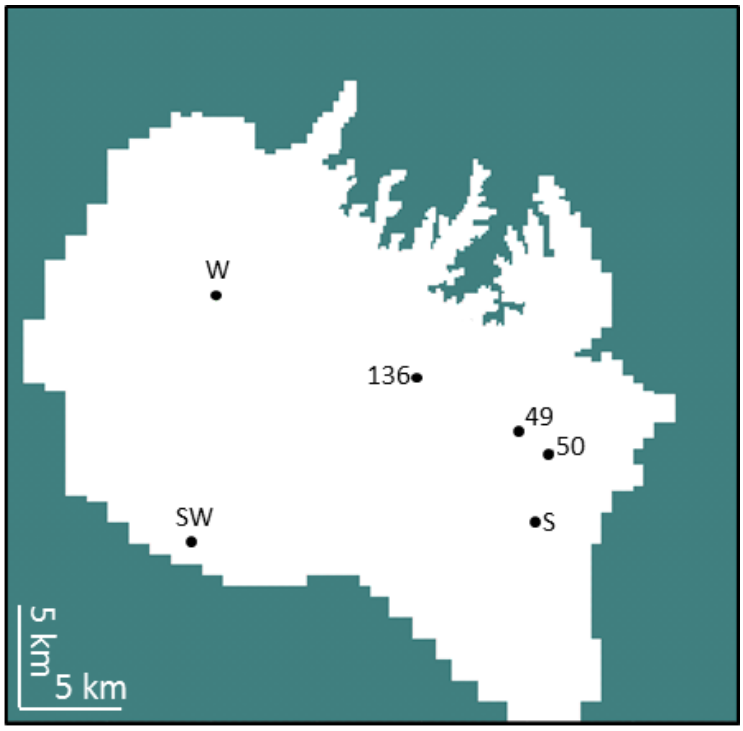

Figure 7.3 Location of head observation wells for numerical simulation for the Ashikaga area.

(a)

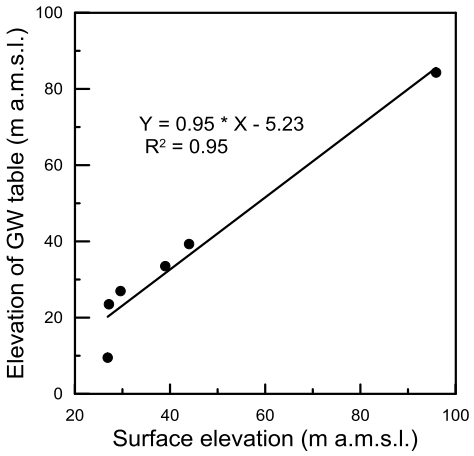

(b)

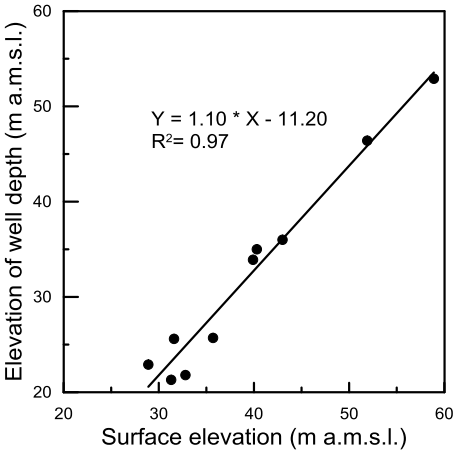

(c)

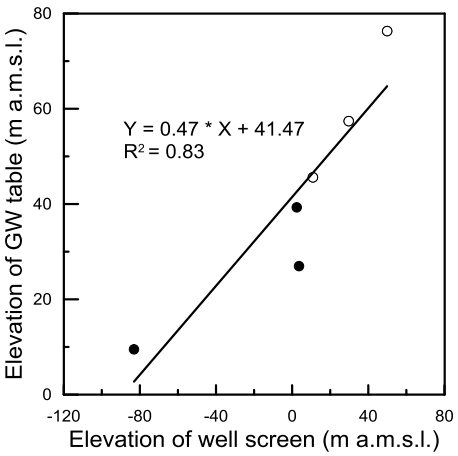

Figure 7.4 The relationship of (a) elevations of ground surface and groundwater table at head observation wells, (b) surface elevation and inquired elevation of well depth at 10 concentration observation wells, and (c) elevation of well screen and elevation of groundwater table at wells 49, 50, and 136 (closed circle) and at wells AT4, AT6, and AT7 (open circle) in the Ashikaga area. The groundwater tables at wells AT4, AT6 and AT7 are those described in the borehole data (before pumping).

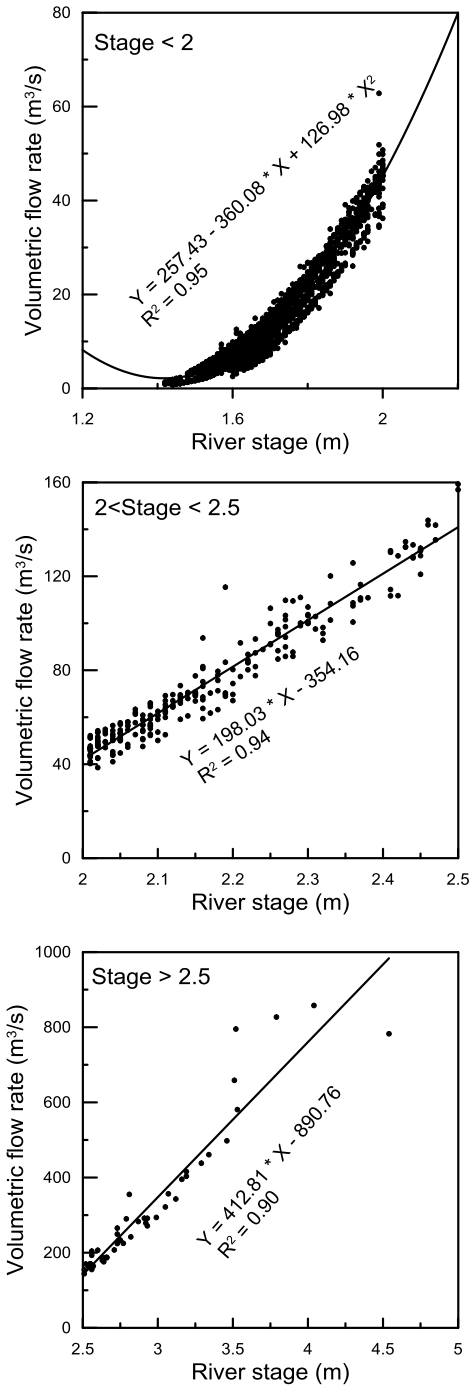

Figure 7.5 The statistical analysis of the relationship between river stage and volumetric flow rate in a period from 1992 to 2001 for the Ashikaga area.

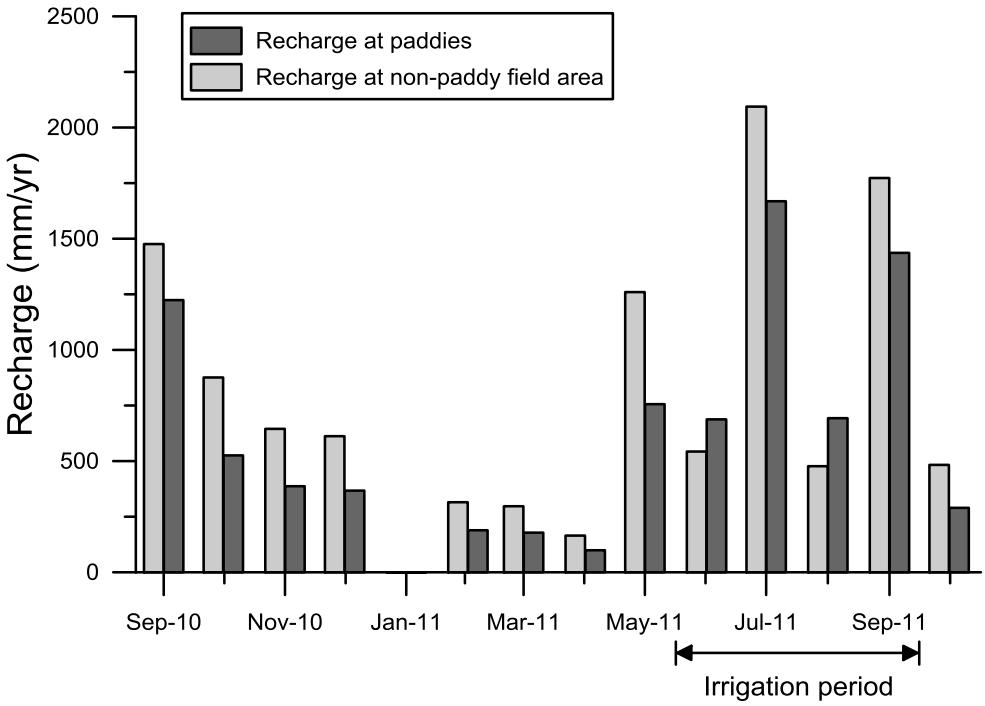

Figure 7.6 Estimated recharge at paddies and at non-paddy field area for numerical simuaiton for the Ashikaga area.

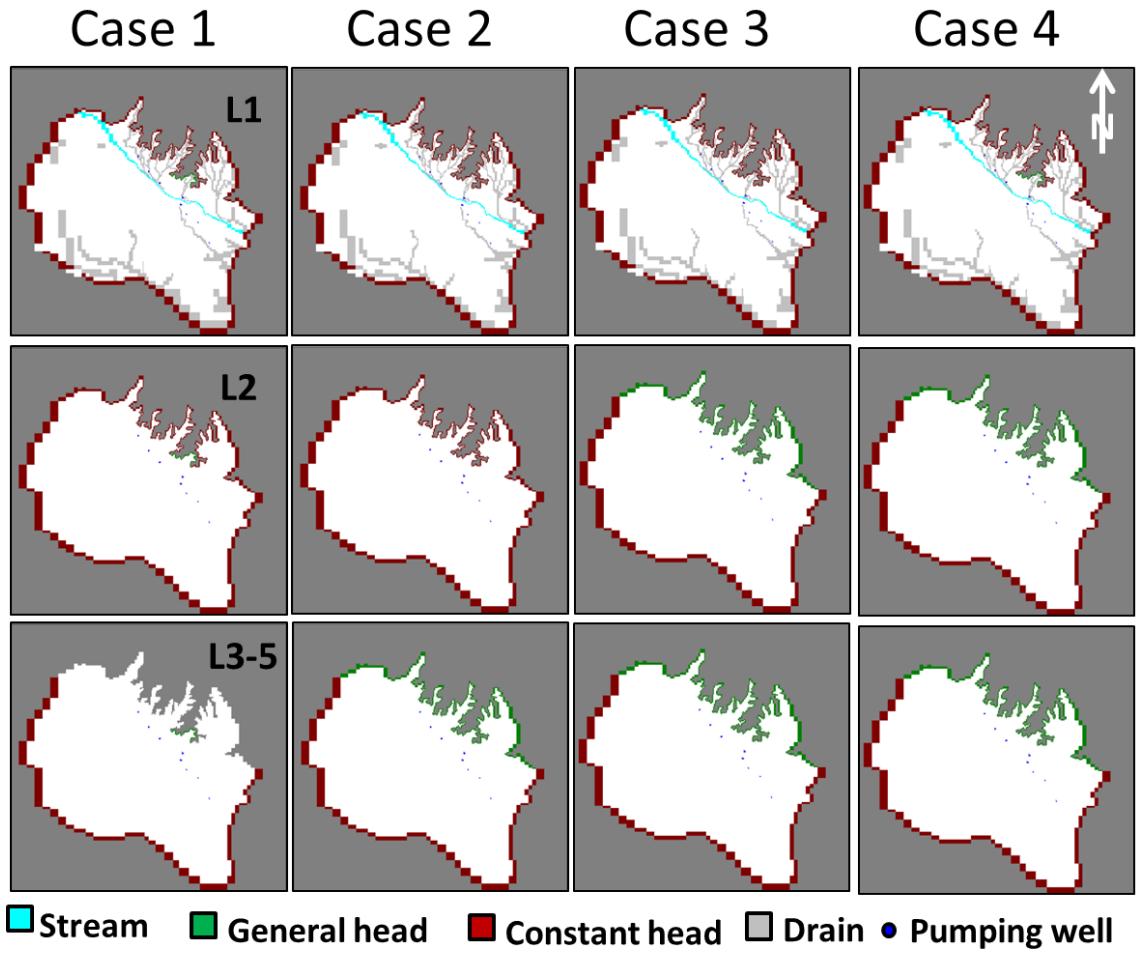

Figure 7.7 The northern boundary setting for Case 1 to Case 4 of simulation for the Ashikaga area.

(a)

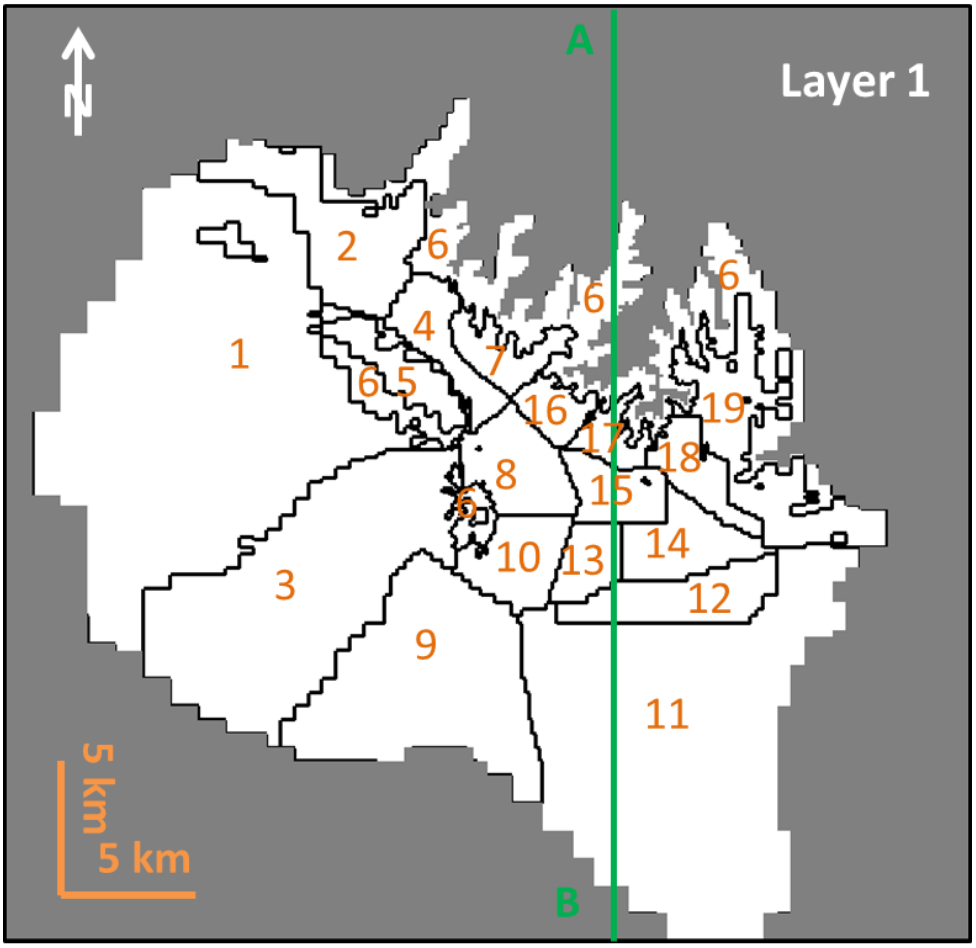

(b)

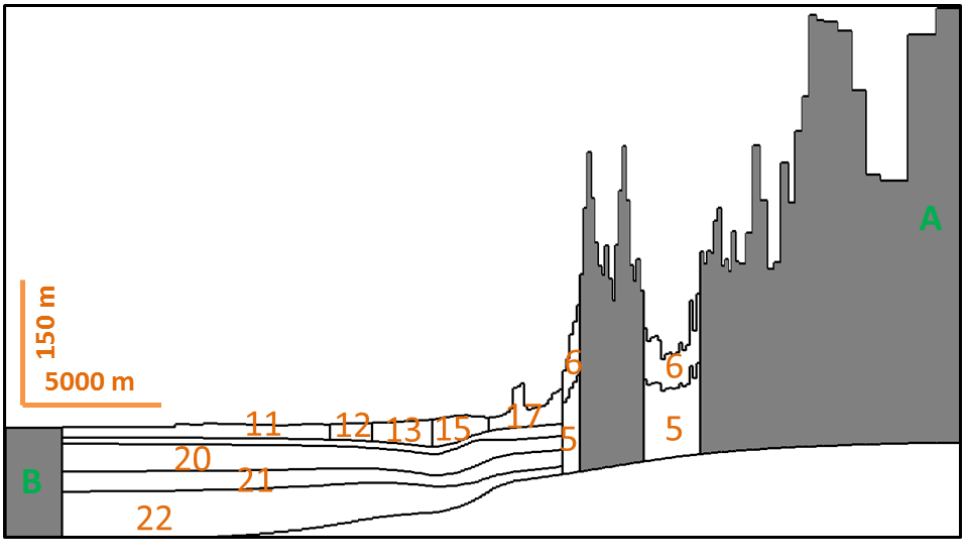

Figure 7.8 Parameter setting zones (a) in Layer 1 of numerical model for the Ashikaga area with (b) cross section A-B showing parameter setting zones for deep aquifers.

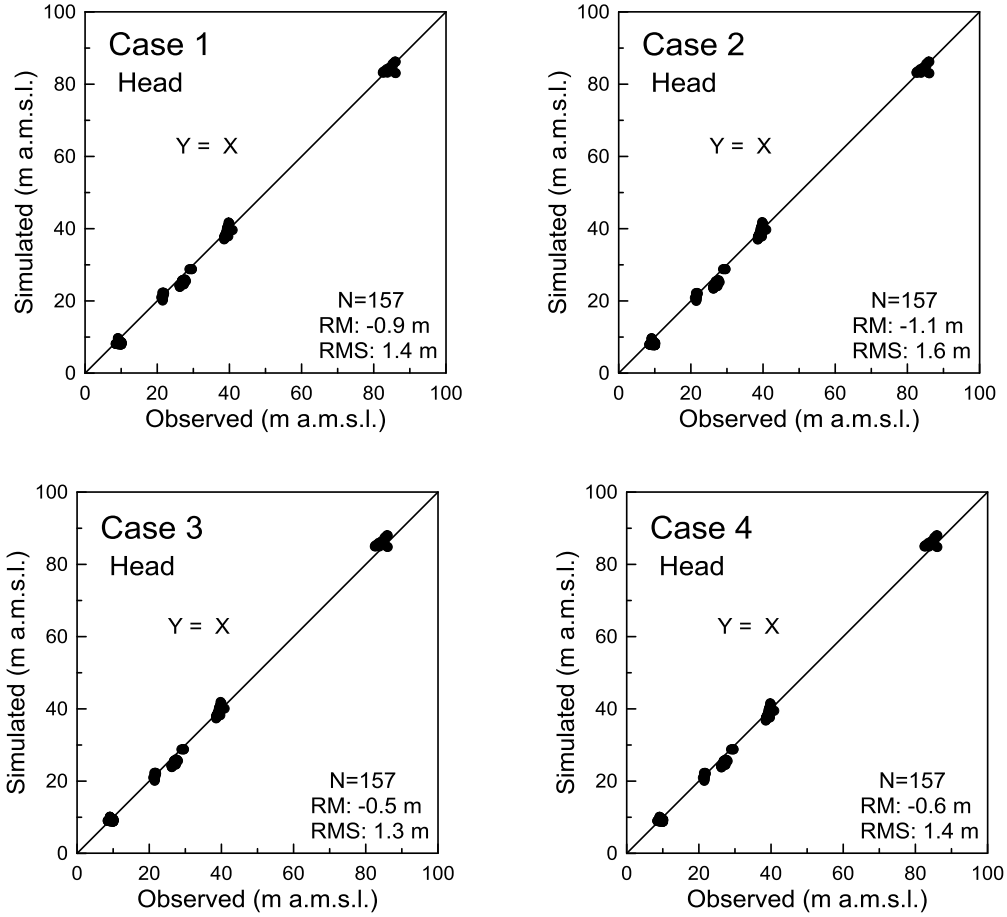

Figure 7. 9 Observed and estimated head for 4 simulation cases for the Ashikaga area.

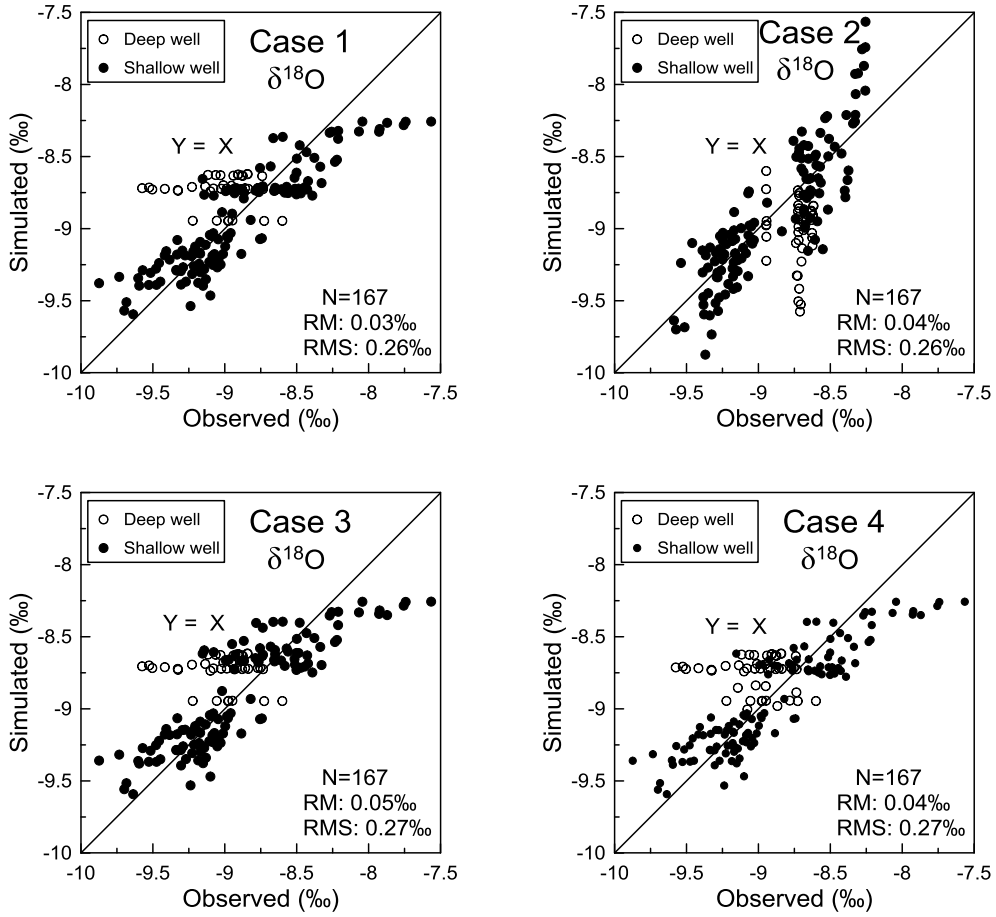

Figure 7.10 Same as Fig. 7.9, but for $\delta^{18}O$.

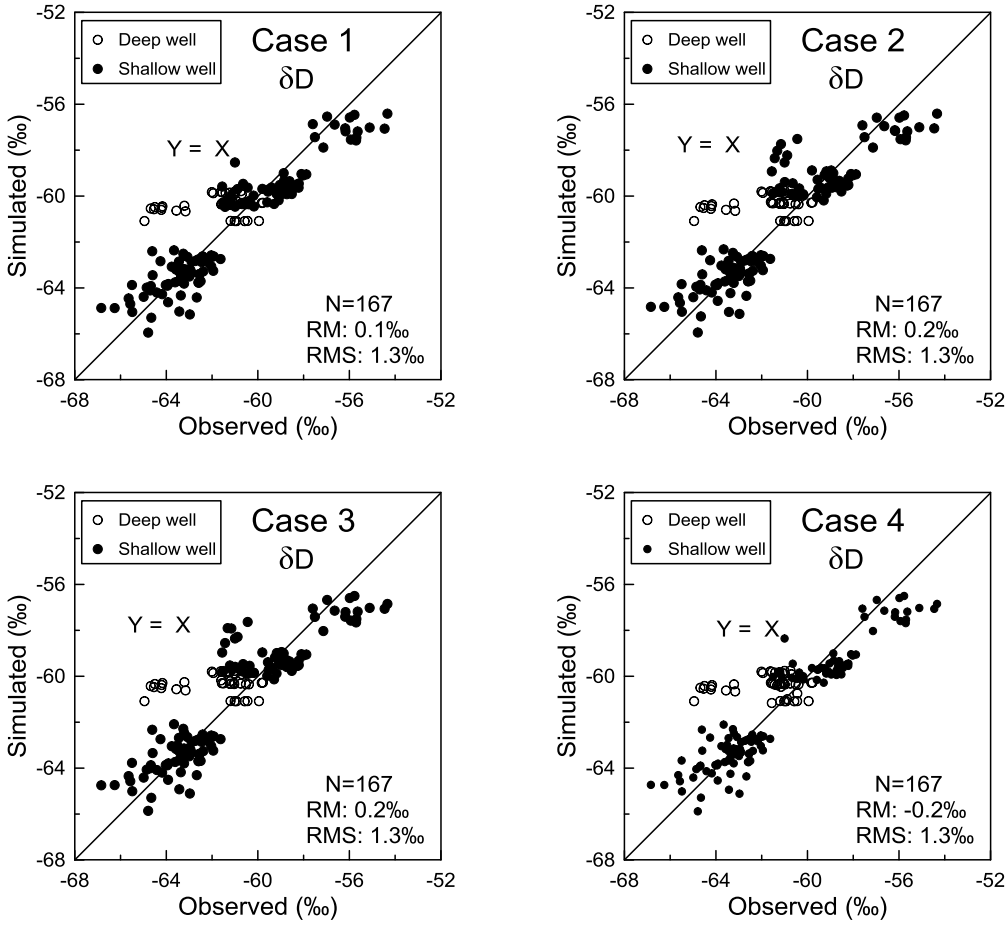

Figure 7.11 Same as Fig. 7.9 and Fig. 7.10, but for δD.

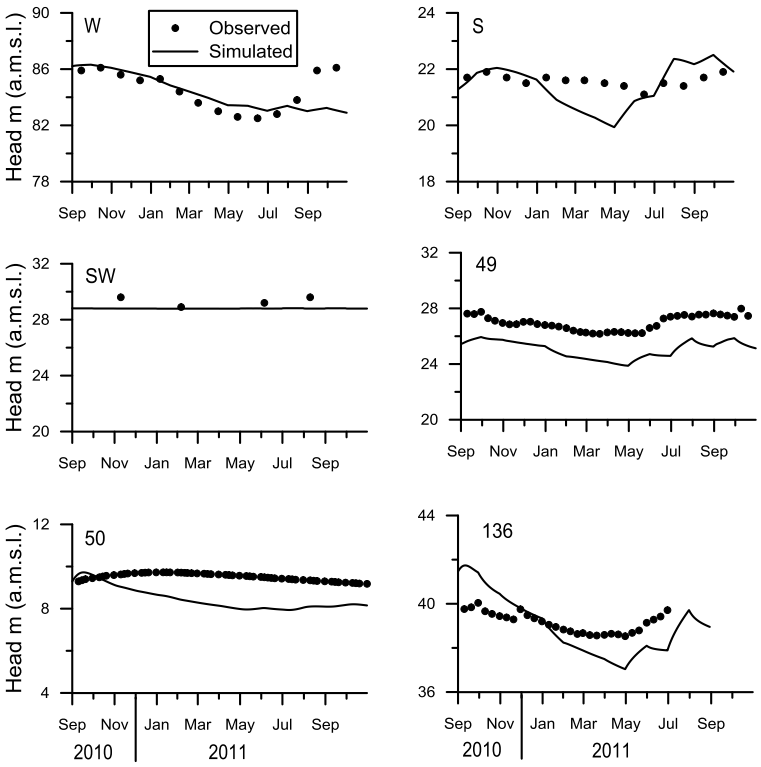

Figure 7.12 Temporal variation of observed and simulated groundwater head in Case 1 for the Ashikaga area.

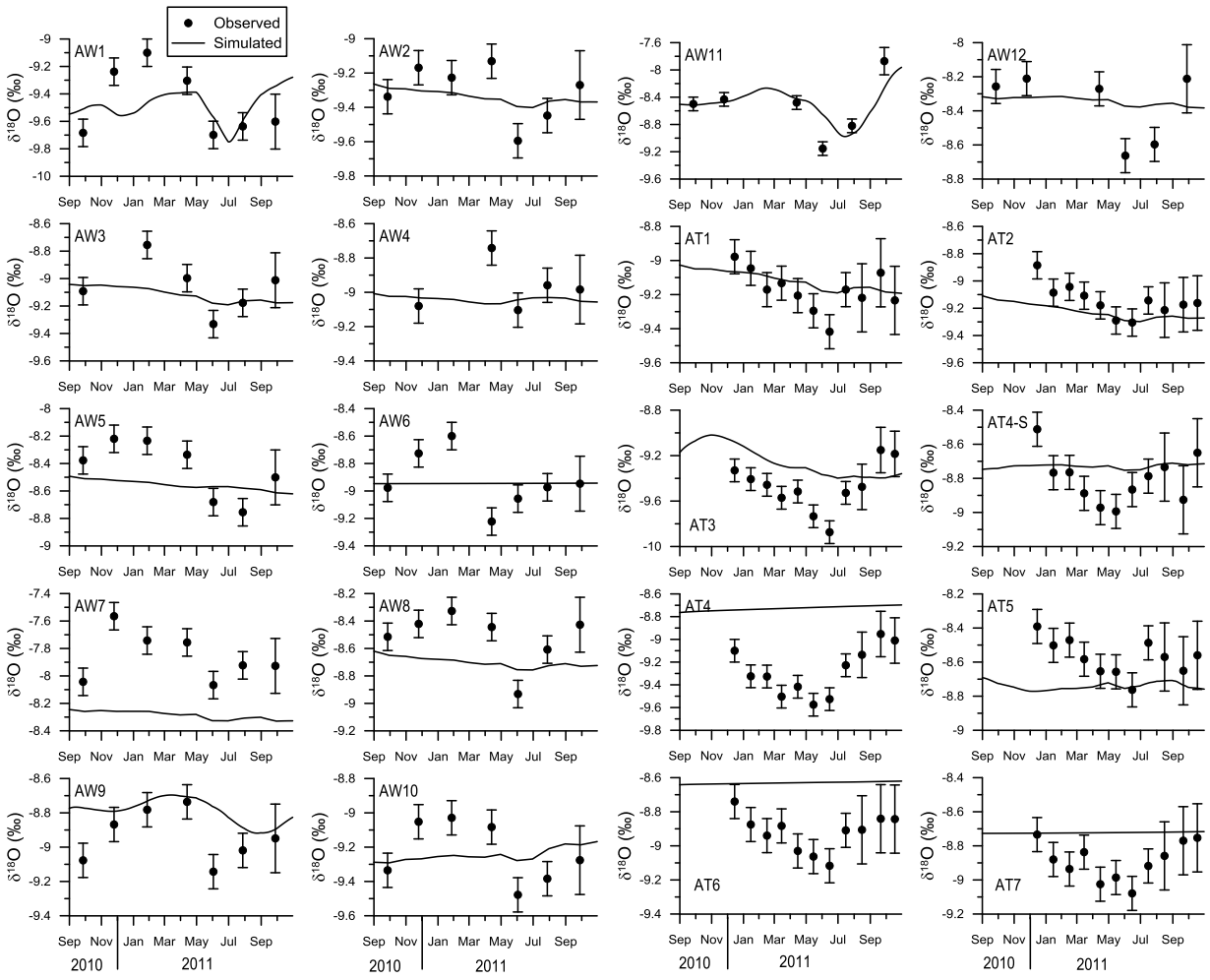

Figure 7.13 Same as Fig. 7.12, but for $\delta^{18}O$. The AT4_S represents the shallow well at municipal well-group of AT4.

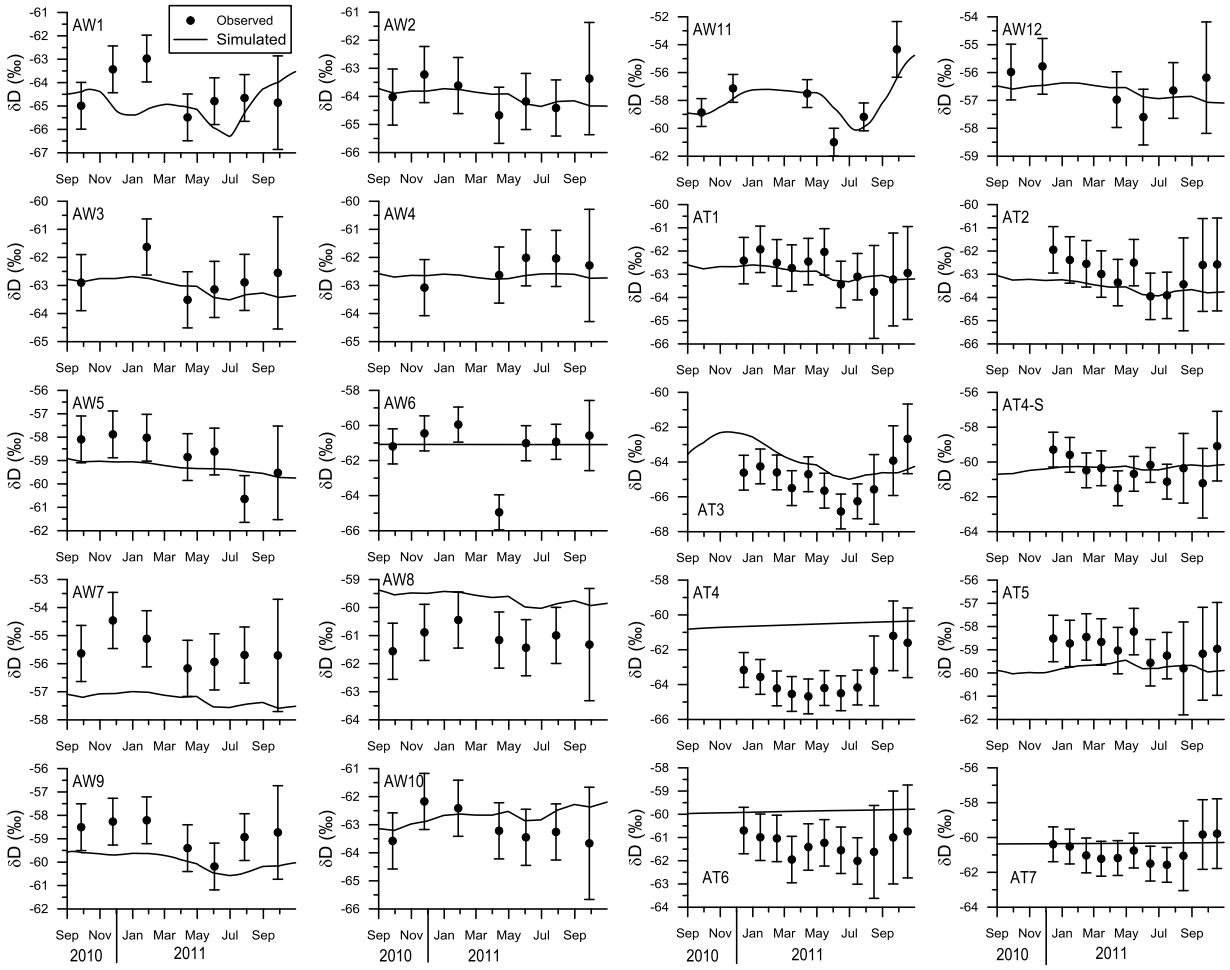

Figure 7.14 Same as Fig. 7.12 and Fig. 7. 13, but for δD.

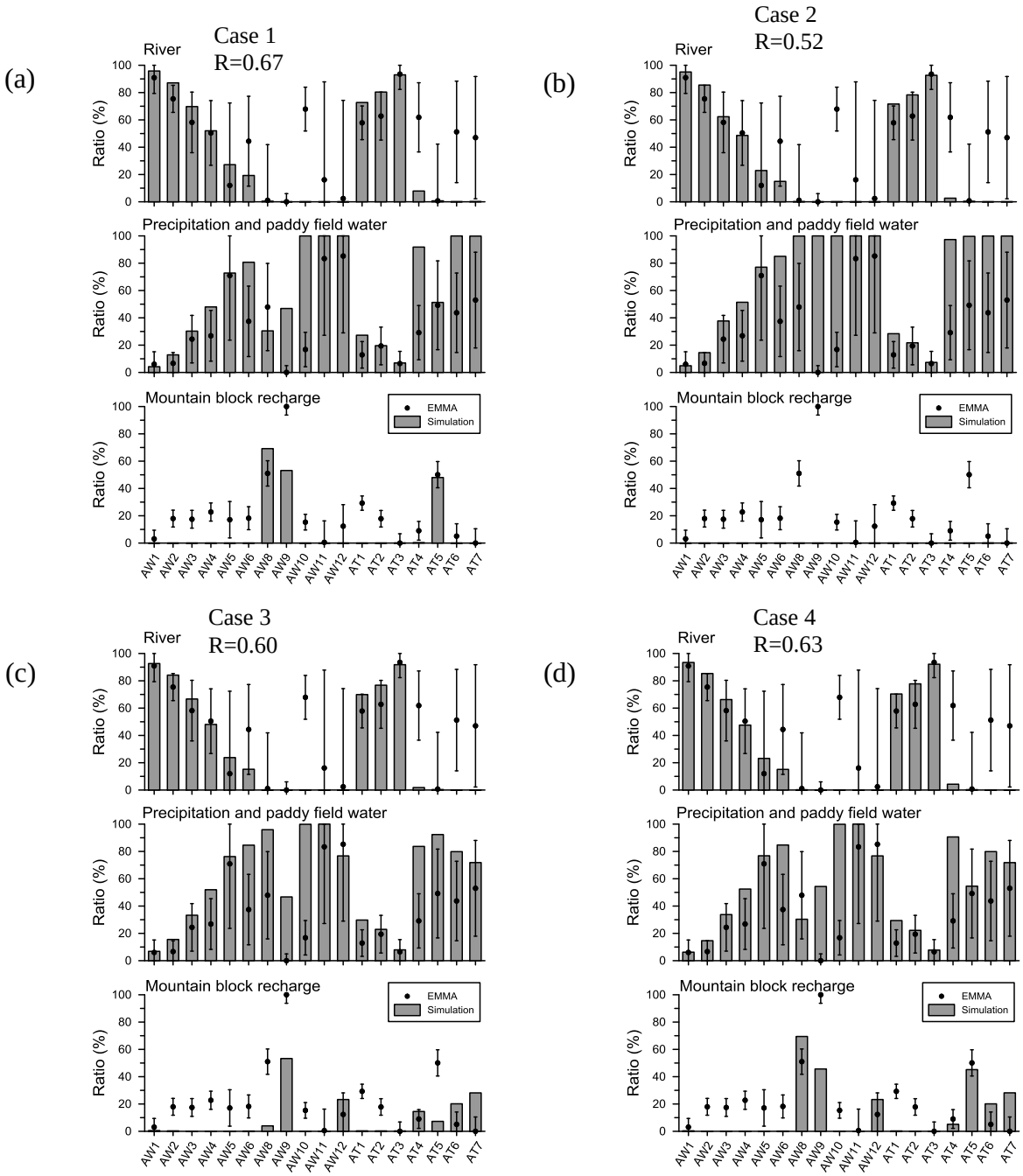

Figure 7.15 Comparison of the estimated contribution ratios of recharge sources of groundwater by numerical simulation and by EMMA for the Ashikaga area. The *R* is correlation coefficient between the ratios estimated by numerical simulation and EMMA.

(a)

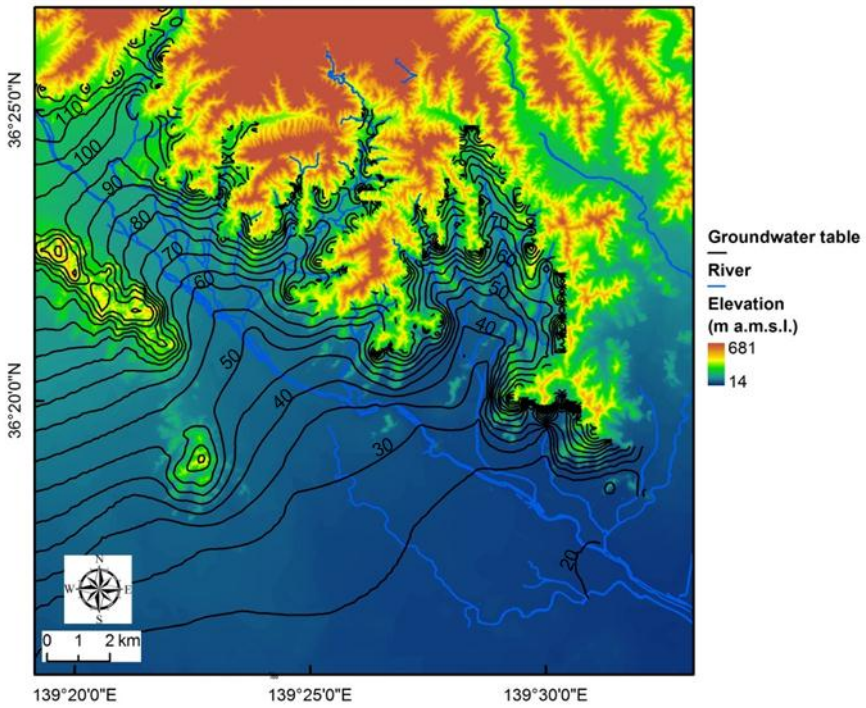

(b)

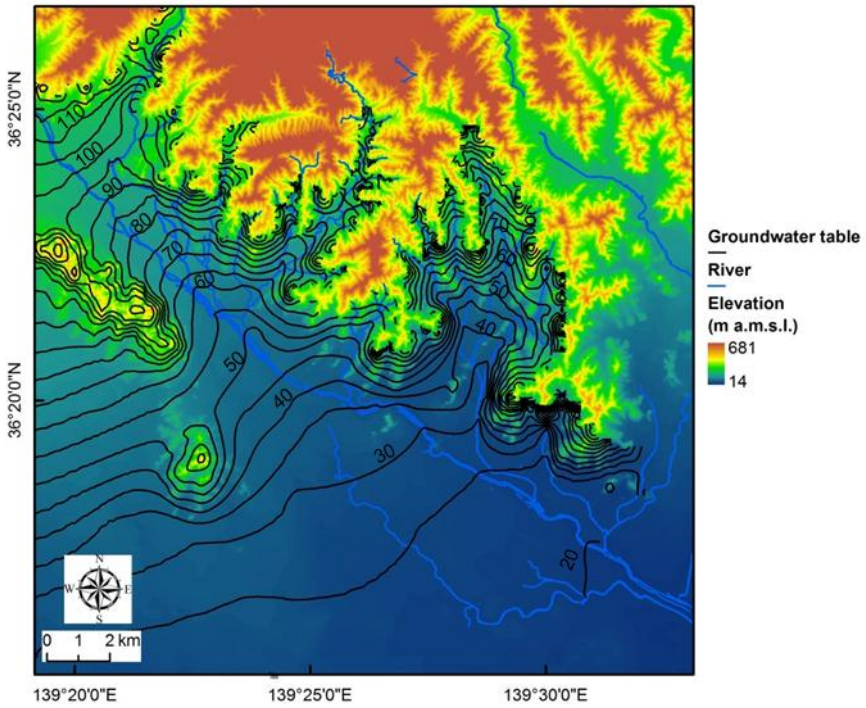

Figure 7.16 Spatial distribution of groundwater table in unconfined aquifer on (a) 15th January, 2011 (dry season) and (b) 15th July 2011 (wet season) for the Ashikaga area.

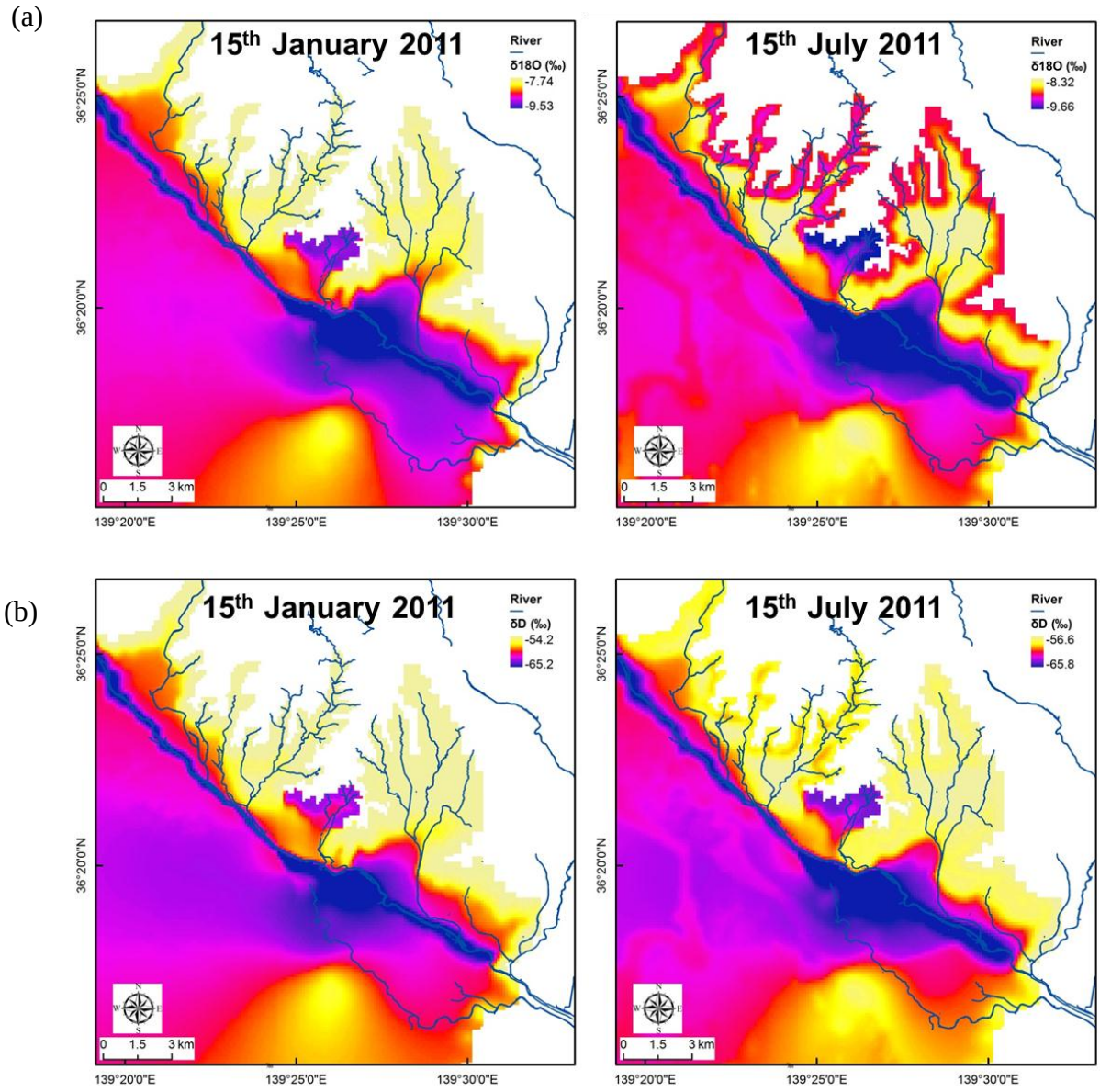

Figure 7.17 Spatial distribution of (a) $\delta^{18}O$ and (b) δD on (left)15th January (dry season) and (right) 15th July 2011 (wet season) for the Ashikaga area.

(a)

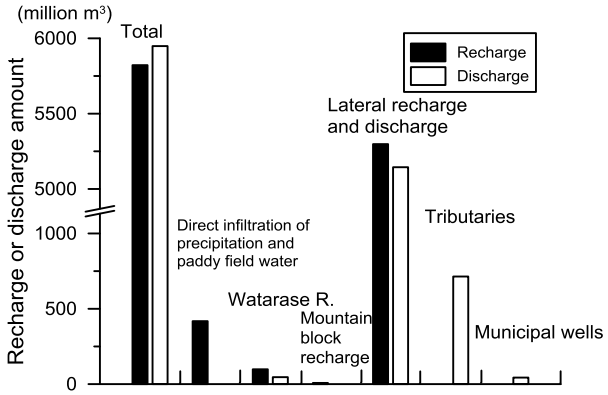

(b)

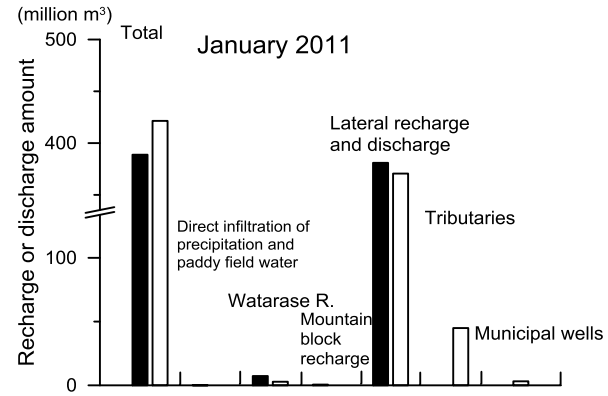

(c)

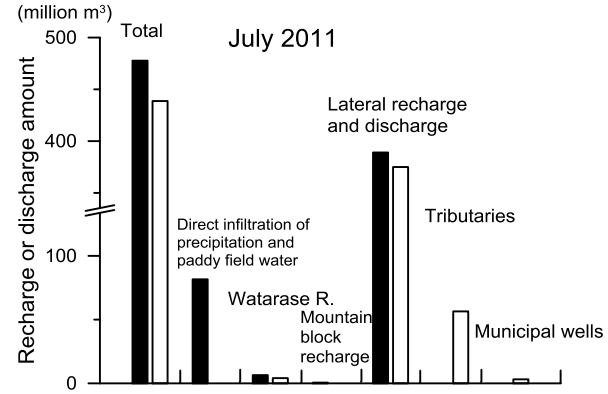

Figure 7.18 Amounts of recharge and discharge of groundwater for the whole model domain for the Ashikaga area (a) during simulation period (September 2010 to October 2011), (b) on January 2011 (dry season) and (c) on July 2011 (wet season).

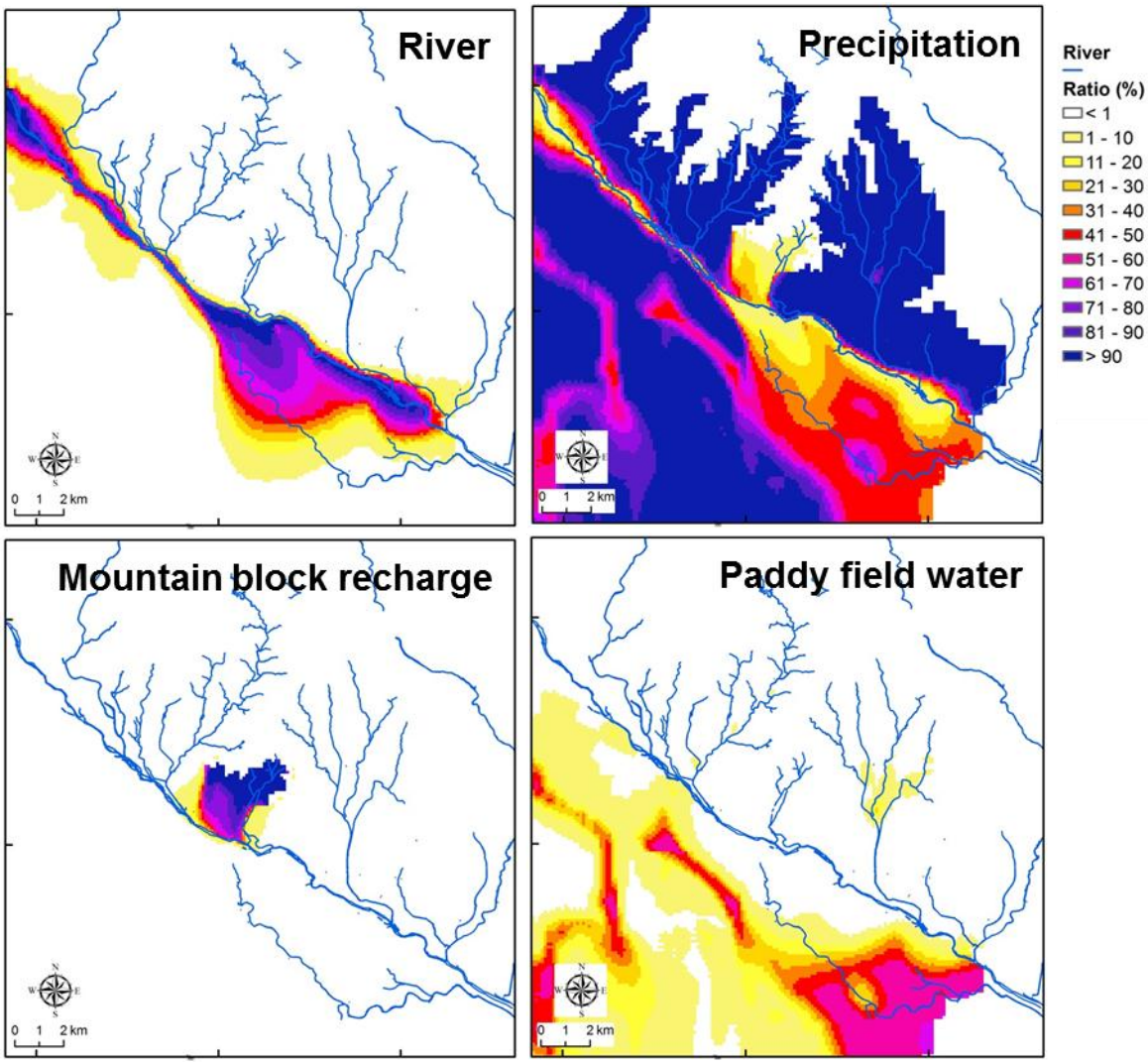

Figure 7.19 Spatial distribution of contribution ratios of recharge sources in the Ashikaga area on 15th January, 2011 (dry season).

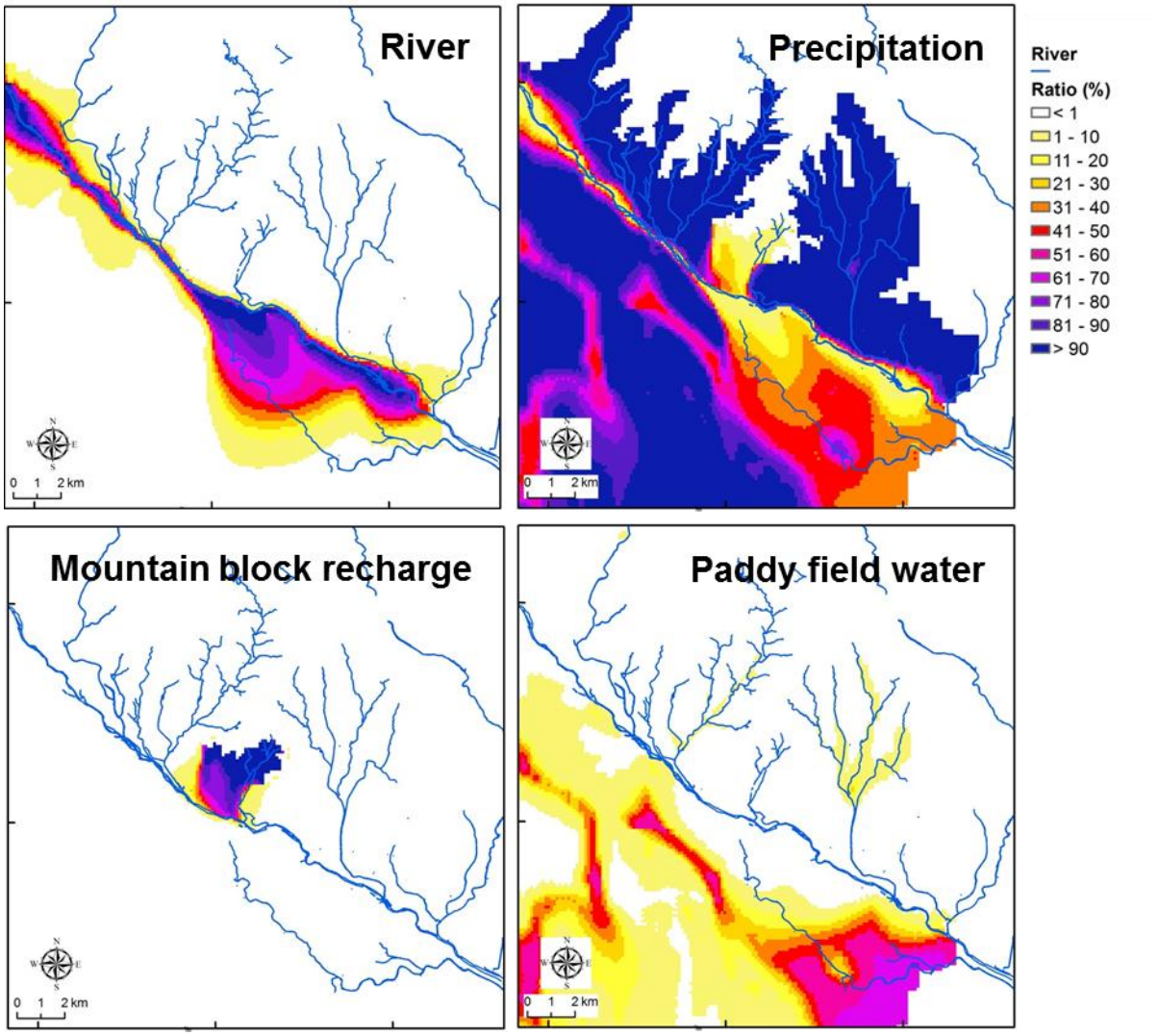

Figure 7.20 Same as Fig. 7.19, but on 15th July, 2011 (wet season).

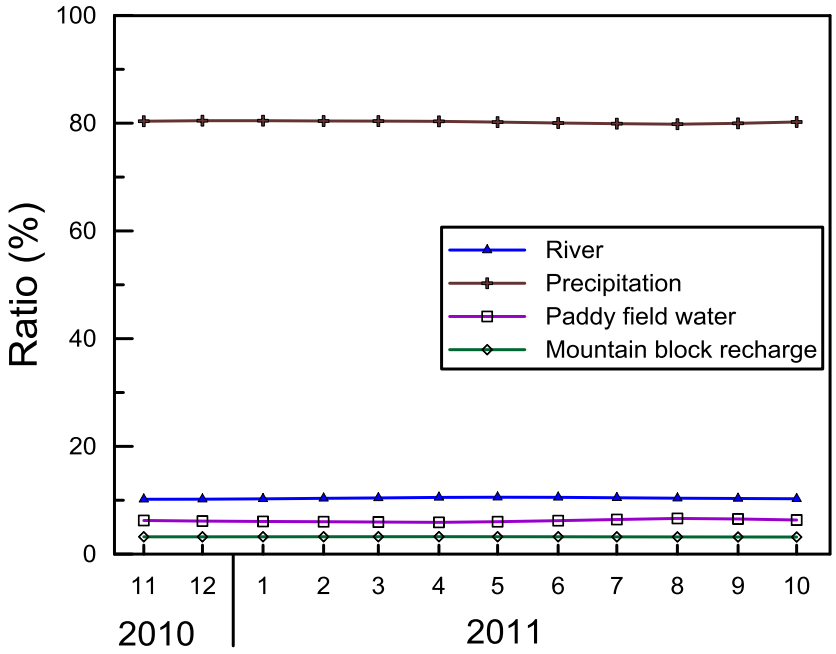

Figure 7.21 Monthly variation of mean contribution ratios of recharge sources in the whole model domain for the Ashikaga area during the period between November 2010 and October 2011.

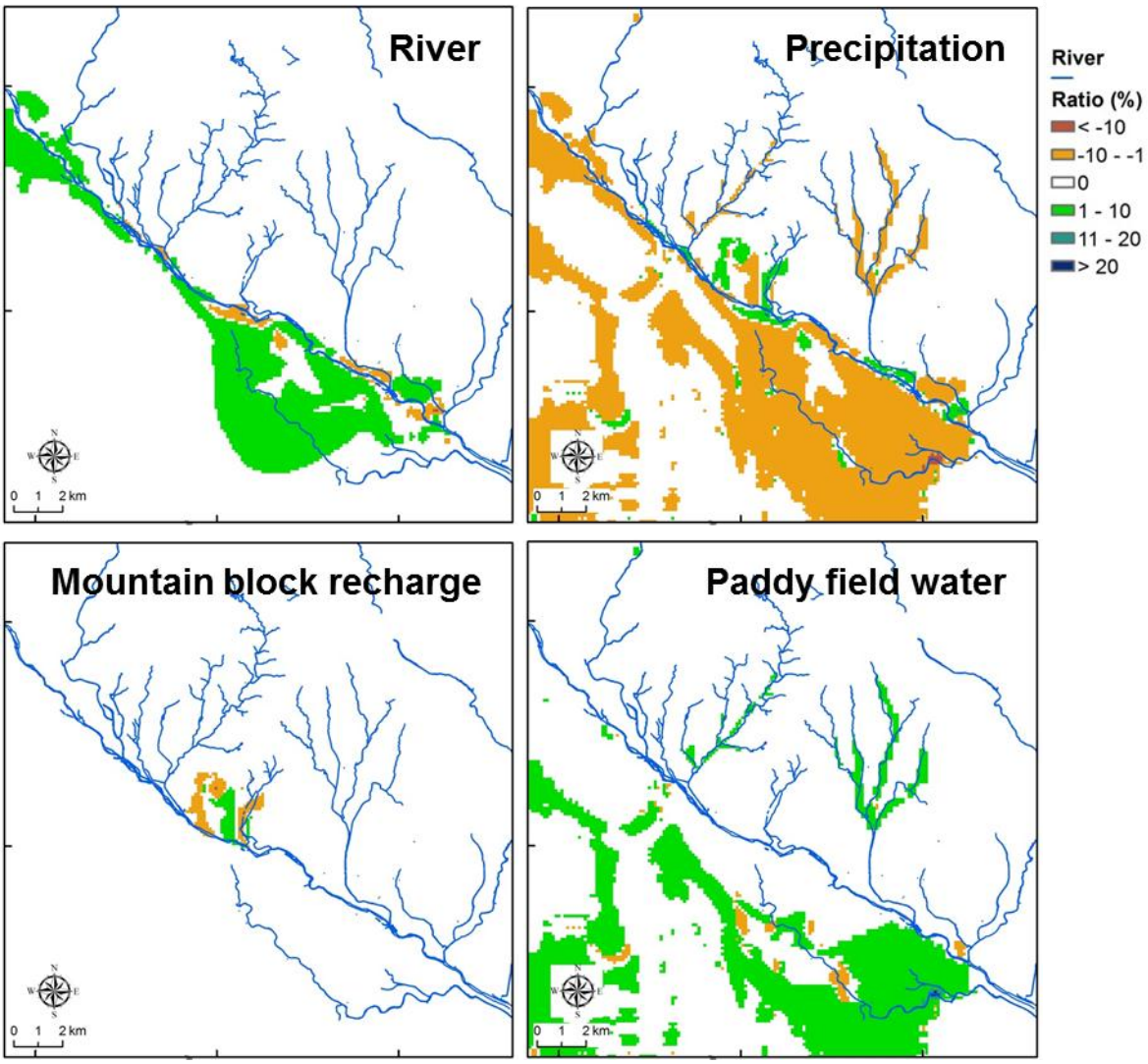

Figure 7.22 The changes of contribution ratio of river, precipitation, mountain block recharge and paddy field water from January, 2011 (dry season) to July, 2011 (wet season) in the Ashikaga area. Positive values represent the contribution ratios increased from dry season to wet season and vice versa.

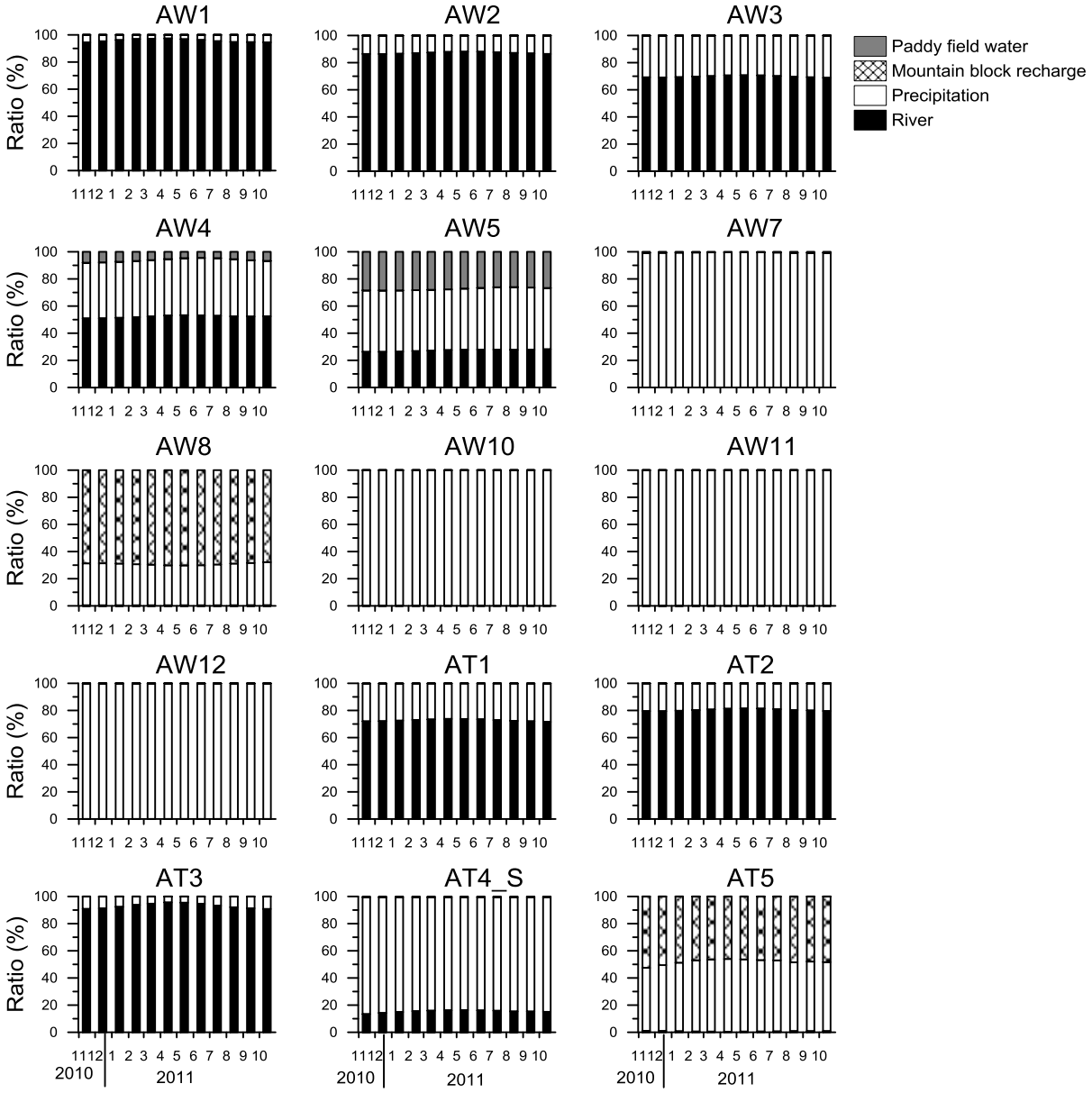

Figure 7.23 Month to month variations of contribution ratios of recharge sources at the shallow wells in the Ashikaga area.

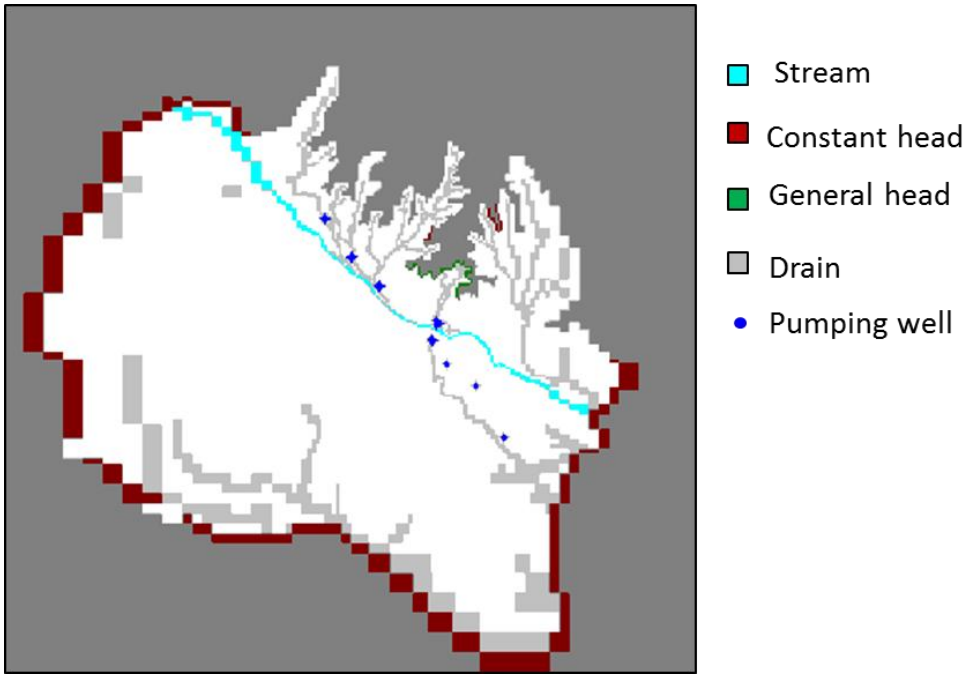

Figure 7.24 Boundary setting of Layer 1 in Case 5 for the Ashikaga area.

(a)

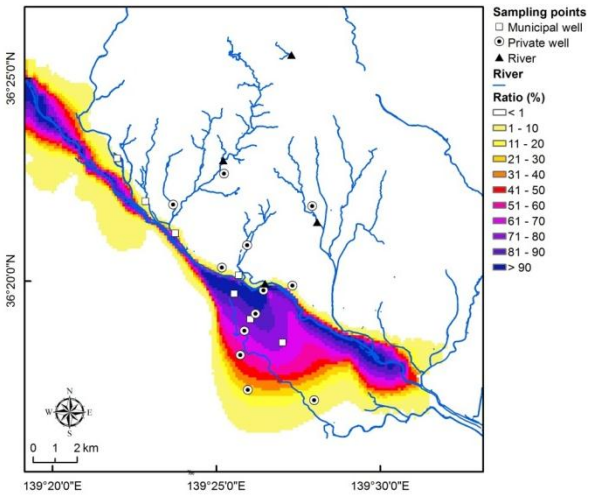

(b)

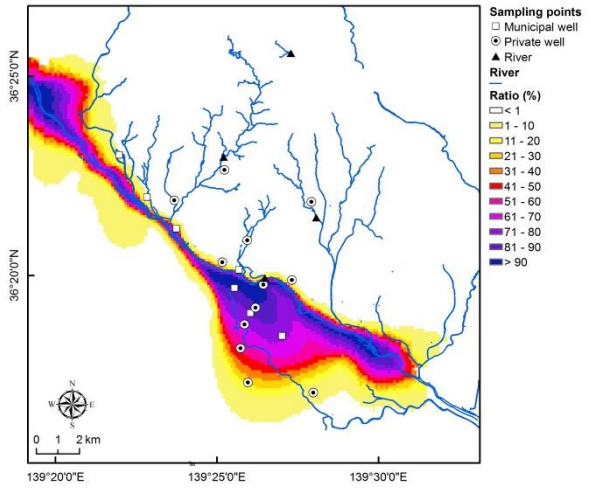

Figure 7.25 Comparison of the spatial distribution of contribution ratio of the Watarase River between (a) Case 1 and (b) Case 5.

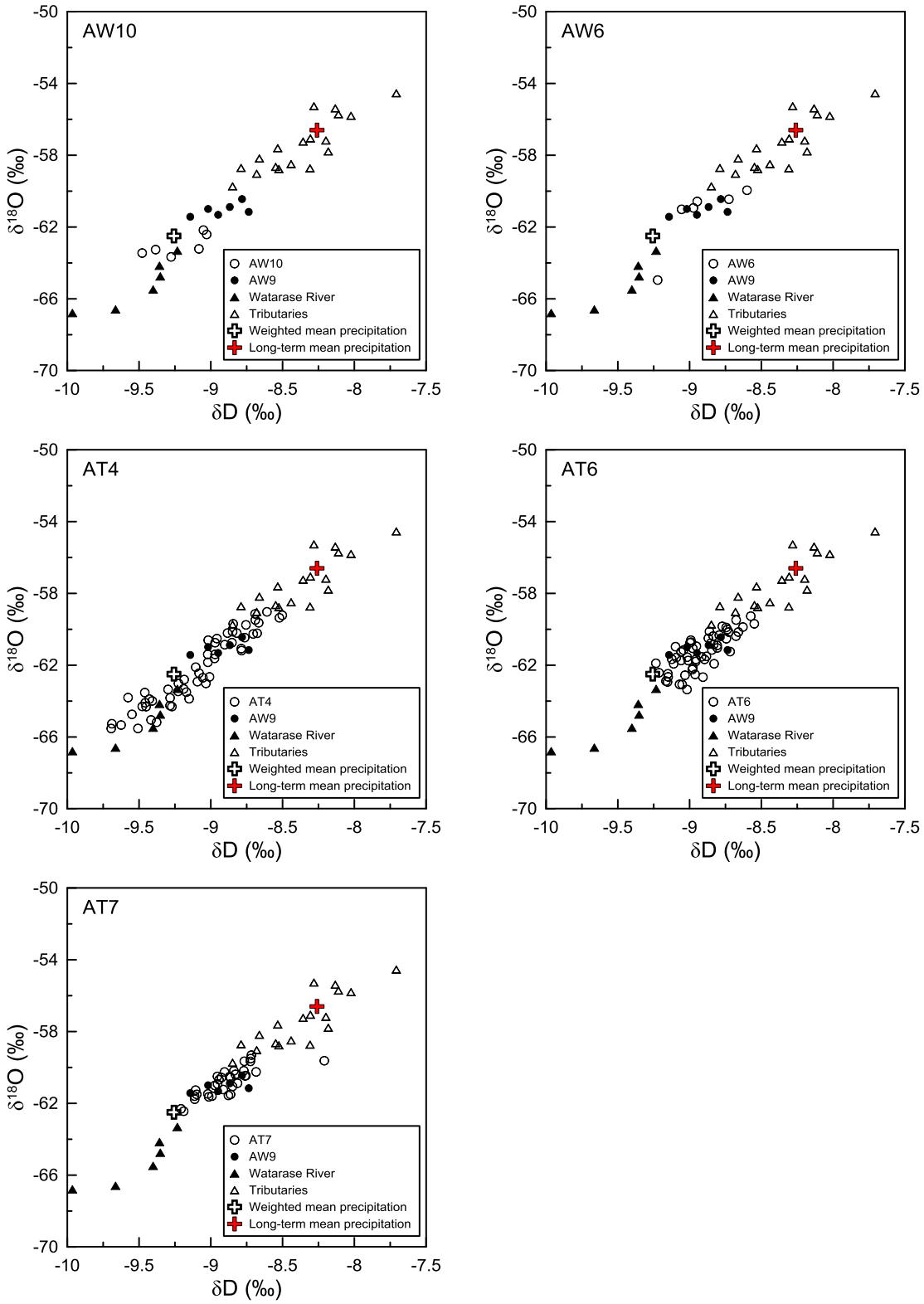

Figure 7.26 Plot of $\delta^{18}O$ vs. δD for groundwater at selected wells, river water and precipitation in the Ashikaga area.

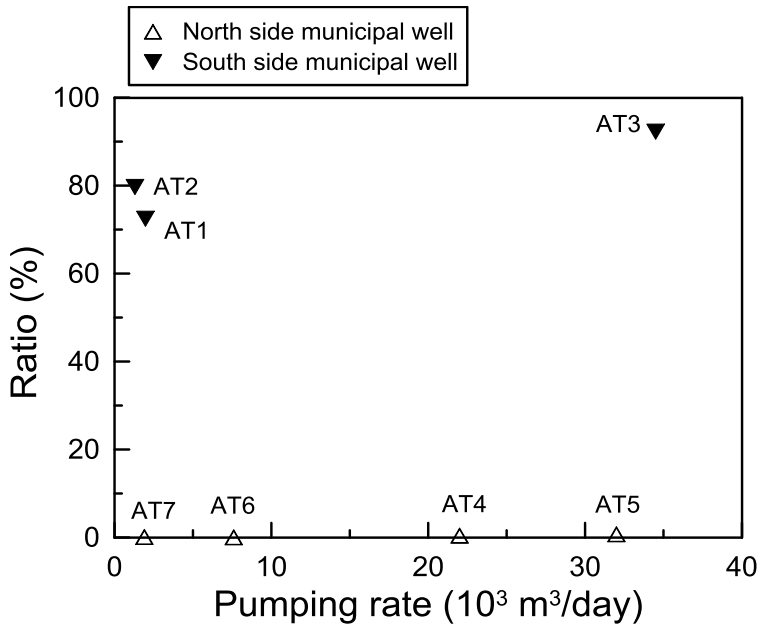

Figure 7.27 Relationship of river water contribution ratio estimated by numerical simulation with pumping rate for the Ashikaga area.

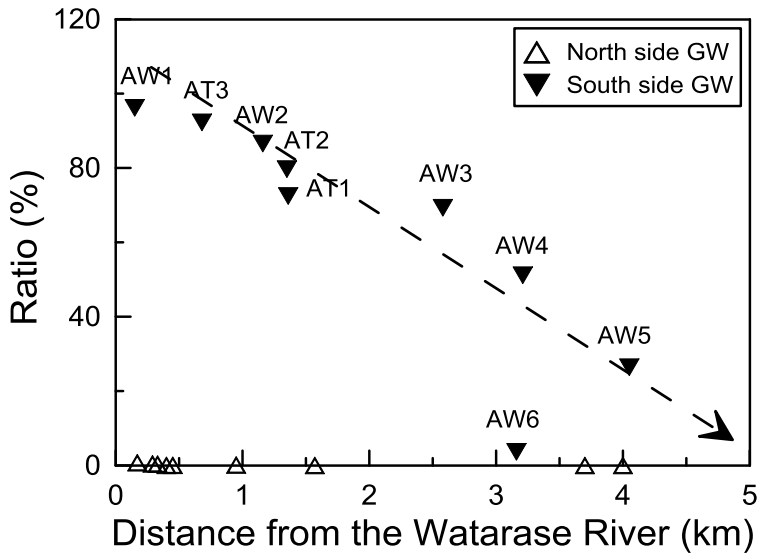

Figure 7.28 Relationship of river water contribution ratio estimated by numerical simulation with distance from the Watarase River.

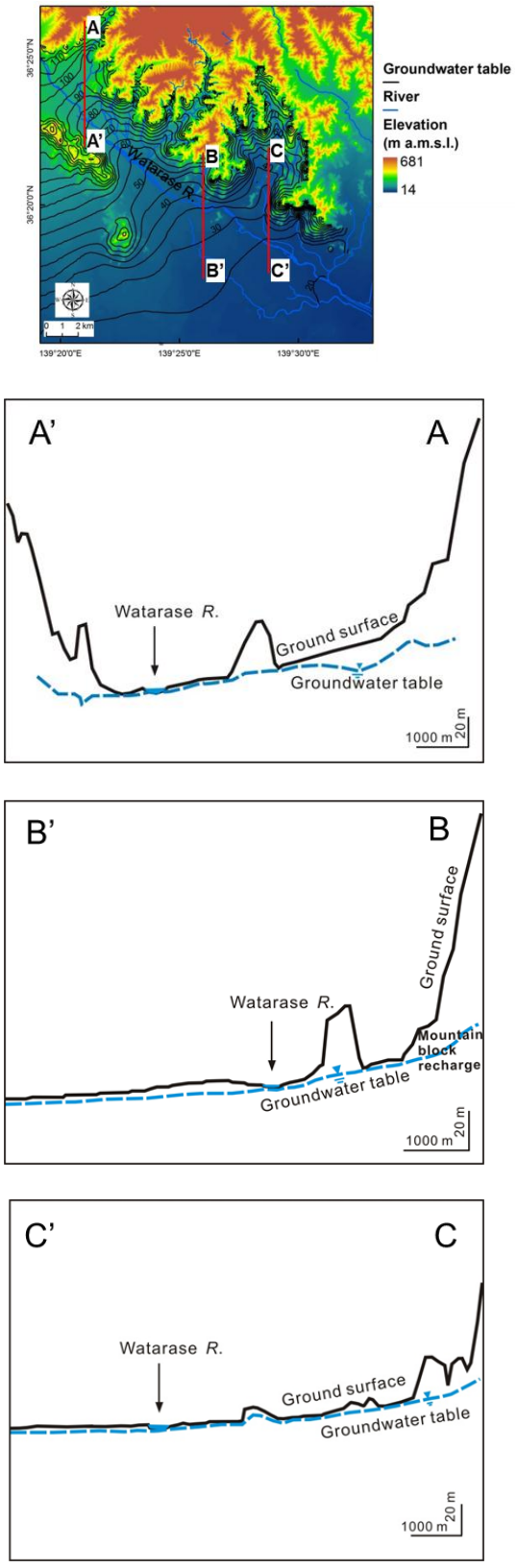

Figure 7.29 Cross sections showing the relationship among ground surface, groundwater table, and locations of mountains and the Watarase River in the Ashikaga area.

Chapter 8
General discussion

8.1 Comparison between two study areas

The spatial distribution of contribution ratio of river water in the Nasunogahara area is almost symmetric with respect to the Sabi River, while in the Ashikaga area it is asymmetric with respect to the Watarase River (Fig. 8.1). However, the river contribution ratio at the upstream and downstream of the Watarase River is almost symmetric. The flow direction of the main river (i.e., Sabi River) is nearly perpendicular to the mountain-plain boundary in the Nasunogahara area, while the flow direction of the main river (i.e., the Watarase River) is nearly parallel to the mountain-plain boundary in the Ashikaga area (Fig. 8.2). The different large scale topographic settings are the major factors control the different spatial distribution characteristics of river-recharged groundwater. The flow directions of the other rivers in the Nasunogahara area are also nearly perpendicular to the mountain-plain boundary in the Nasunogahara area. However, the tributaries of the Watarase River run perpendicular to the Watarase River in the Ashikaga area. Under control of the large scale topographic settings, the river sediments is symmetric with respective to the Sabi River in the Nasunogahara area (Fig. 3.4). Due to the restriction of mountains, the river sediments mainly occurred at valleys in the north side, while large area in the south side for the Ashikaga area (Fig. 3.8). The distribution characteristics of river-recharge dominated area are similar as the distribution characteristics of river sediments in two study areas, further indicating the controlling effect of large scale topographic settings on the groundwater-river interaction. This finding agrees with O'Driscoll et al. (2010), which proved that the asymmetrical distribution of topography and sediments can result in measurable differences in river-groundwater interactions.

The extent of river-recharge dominated area is up to 2.5 km away from the channel of the Sabi River in the upstream of the Nasunogahara area, while the extent reaches 1.5 km away from the channel in the downstream. In the Ashikaga area, the extent of river recharged groundwater with more than 50% of contribution ratio on the south side of midstream of the Watarase River reaches to 4 km at maximum, but the extent is less than 1 km on the north side of corresponding reach. At the upstream of the Watarase River, the extent of river-recharge dominated area reaches to 1.5 km. As we mentioned in above chapters, the contribution ratio of river water decreased with distance from the river channel. However, with the same distance from the river channel, the contribution ratios of river water at points N1 and N2 in Fig. 8.2a are different. Also the contribution ratios of river water at points A1, A2 and A3 in Fig. 8.2b are varied. Points of N1 and A3 are located in the river-recharge-dominated area, that is, the contribution ratio of river water at N1 and A3 are larger than 50%. However, the contribution ratio of river water at N2, A1 and A2 are less than 50%. It was to say that the location is an important factor for the groundwater-river interaction.

In the Nasunogahara area, the aquifer lateral recharge and mountain block recharge was restricted by the impermeable fault. The restriction probably results in large amount of river seepage in the upstream part of the Nasunogahara area. On the other hand, the fold structure in the Ashikaga area transmits mountain block recharge to the study domain. The mountain block suppresses the river seepage in the north side (mountain side) of the Watarase River.

Precipitation infiltration is the main recharge source in both Nasunogahara area and Ashikaga area. In the Nasunogahara area, the mean contribution ratio of precipitation for the unconfined aquifer in the model domain during 1-yr simulation was 59%. For the Ashikaga area, the mean contribution ratio of precipitation for the unconfined aquifer in the model domain during 14-months simulation was 81%. The infiltration of paddy field water is relatively small in two study areas. The mean contribution ratio of paddy field water was 16% for the Nasunogahara area and 6% for the Ashikaga area. The contribution of paddy field water was highly related to

the distribution of paddy field and the contribution ratio becomes higher in the irrigation period. However, the contribution ratio of paddy field water is no more than 50% at maximum in paddy fields in the Nasunogahara area and at sampled wells in the Ashikaga area. The limited distribution of paddy field and the short irrigation period are the main reasons restricting the recharge from paddy field.

Land use is an important factor influencing the groundwater recharge. As shown in Fig. 5.16 and Fig. 7.20, the contribution ratio of precipitation is relatively low at zones where the contribution ratio of paddy field water is high. The contribution ratio of precipitation is also decreased at zones where the contribution ratio of paddy field water increased from dry season to wet season (Fig. 5.19 and Fig. 7.22). However, the contribution ratio of river water was not found to have relationship with the contribution ratio of paddy field water. Although the land use has significant influence on precipitation infiltration, it does not affect the groundwater-river interaction.

Generally, the contribution ratio of river water and paddy field water increased at the highly influenced area (i.e., contribution ratio $\geq$ 50%) from dry season to wet season (Fig. 5.19 and Fig. 7.22). The relative contribution of precipitation decreased at the highly influenced area. The contribution ratio mountain block recharge increased at the highly influence area, while decreased at mountain block recharge boundary.

8.2 Comparison between different approaches

As mentioned in Chapter 5, the estimated contribution ratios of river waters by numerical simulation at concentration wells are almost the same as the estimated results by the EMMA in the Nasunogahara area, while the contribution ratio of the Sabi River is overestimated by the EMMA at G6. With the difference at G6, the spatial distribution of river water contribution ratio estimated by the EMMA and the simulation for the Nasunogahara area are still similar (Fig. 8.3). However, the computed contribution ratios of paddy field water by the simulation have 10%

difference from the estimated contribution ratios by the EMMA. The error at point scale may induced by the uncertain inputs of distribution and hydraulic properties of paddy field to the numerical model. Therefore, combined use of the simulation and the EMMA could improve the reliability of results and mitigate the limitations in each approach.

In the Ashikaga area, the estimated mean contribution ratio of paddy field water (6%) is larger than the mountain block recharge (3%) in the unconfined aquifer of the model domain by the simulation approach. However, the contribution ratio of paddy field water at the concentration observation well except AW5, where the contribution ratio is 27%, does not exceed 10%. The result satisfies the assumption that paddy field water is not the main recharge source at the sampling wells in Chapter 6. Therefore, the precipitation, river and mountain block recharge were used as three main recharge sources at observation wells for the EMMA in Chapter 6 is valid.

The estimated river water contribution ratios from the simulation have similar values from the EMMA at wells in the south side of the Watarase River for the Ashikaga area (Fig. 8.4). However, the estimated river contribution ratios from the EMMA are obviously lager than the results from the simulation at wells on the north side of the Watarase and a deep well (AW6) on the south side (Fig. 7.15a). The difference of estimated contribution ratios by two approaches are even more than 50%. As mentioned in section 7.4, the large difference is probably caused by the mixture of waters precipitated in the study period and before the study period, that is, the uncertain concentration/composition of end member of precipitation results in the estimation errors by the EMMA. Although the EMMA accompanies with some uncertainties, it is still capable of providing very useful information for preparing the numerical simulation. For some specific sites such as AW7 in the Ashikaga area, the EMMA could give more reliable results due to the numerical model failing to reflect the sub-grid scale heterogeneity. Comparing the results from the EMMA with the numerical simulation could validate the reliability of both results and enlighten modeler for seeking physical mechanics causing the difference between two methods.

Generally, the improved numerical simulation with stable isotopes supplies more detailed and more reliable results than the tracer approach (i.e., EMMA) does. The numerical simulation is especially useful for areas with sparse hydrometric data. However, errors could be induced by the uncertain inputs and the sub-grid-scale heterogeneity for the numerical simulation. Typically for the contribution ratio of paddy field water at the point scale, the computing results from the EMMA is better than the numerical simulation. Therefore, combined use of two methods is capable of improving reliability of the results and mitigating limitations in each approach.

(a)

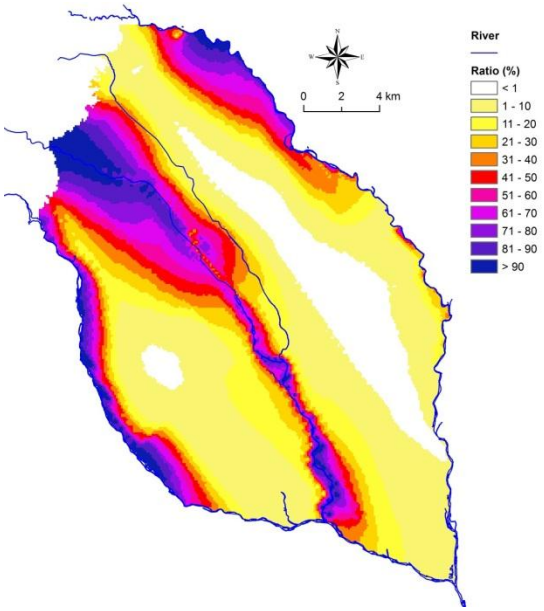

(b)

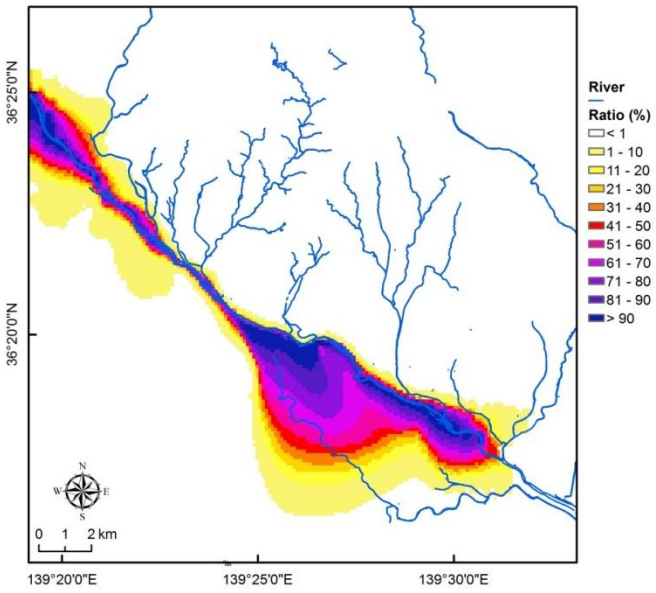

Figure 8.1 The spatial distribution of river water contribution ratio in (a) the Nasunogahara area and (b) the Ashikaga area.

(a)

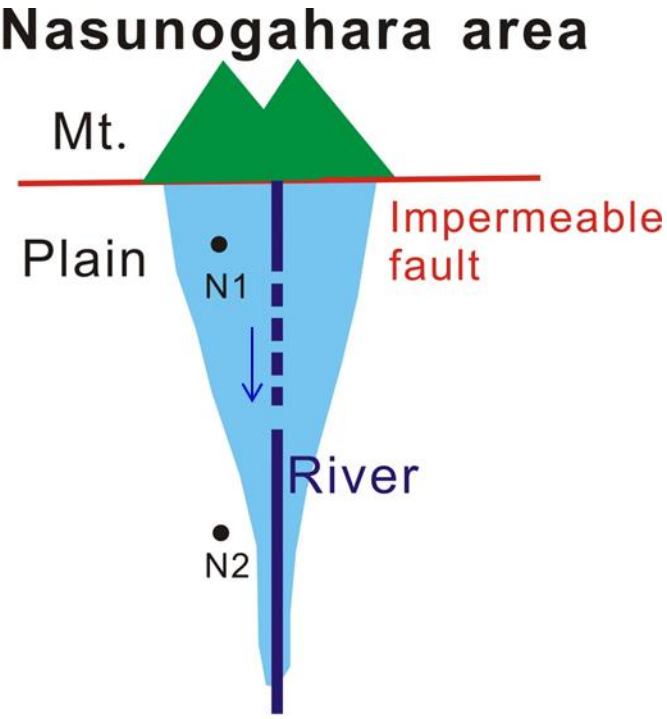

(b)

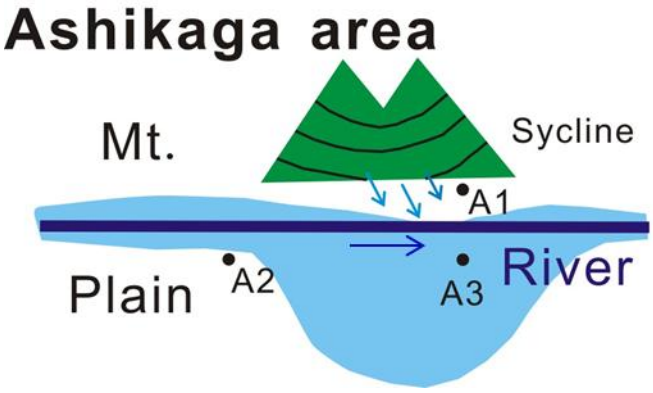

Figure 8.2 Schematic diagram showing the characteristics of areas of river-recharge dominated areas (shallow blue) and their influencing factors for (a) the Nasunogahara area and (b) the Ashikaga area.

(a)

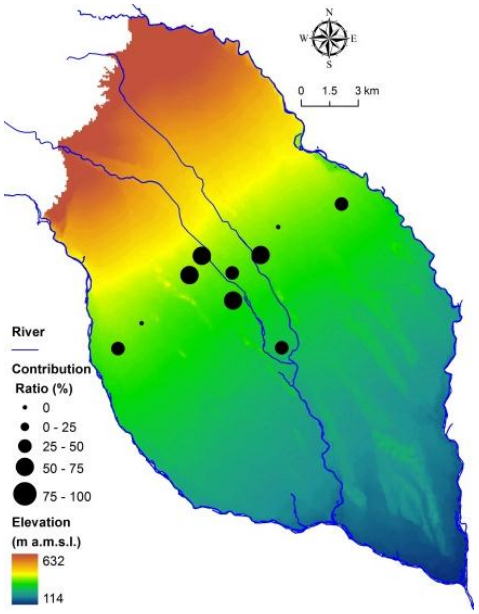

(b)

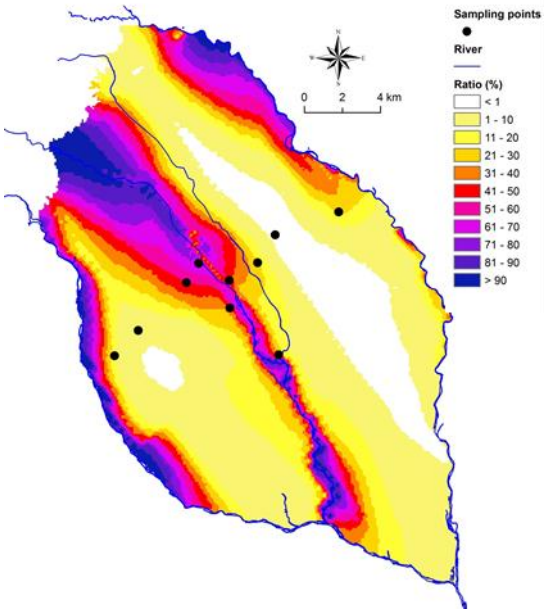

Figure 8.3 Comparison of estimated river water contribution ratio by (a) EMMA and (b) numerical simulation in the Nasunogahara area.

(a)

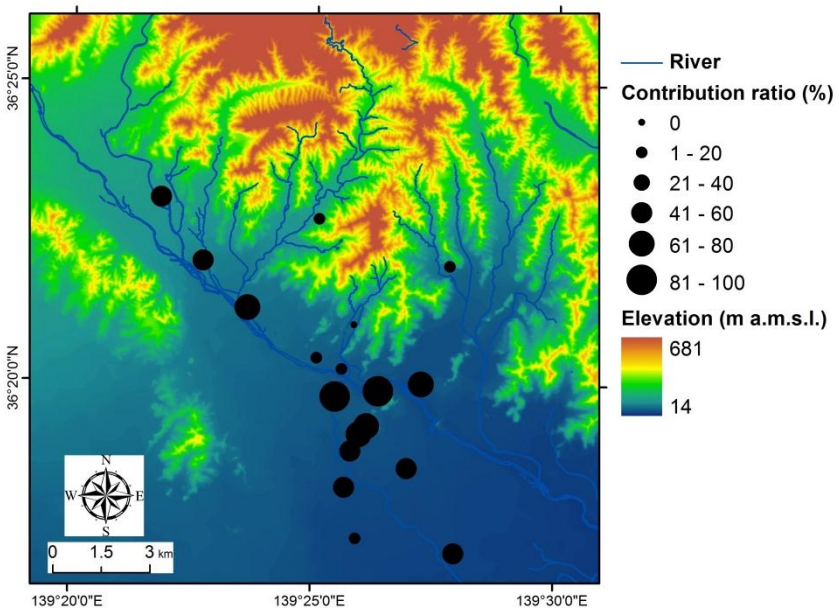

(b)

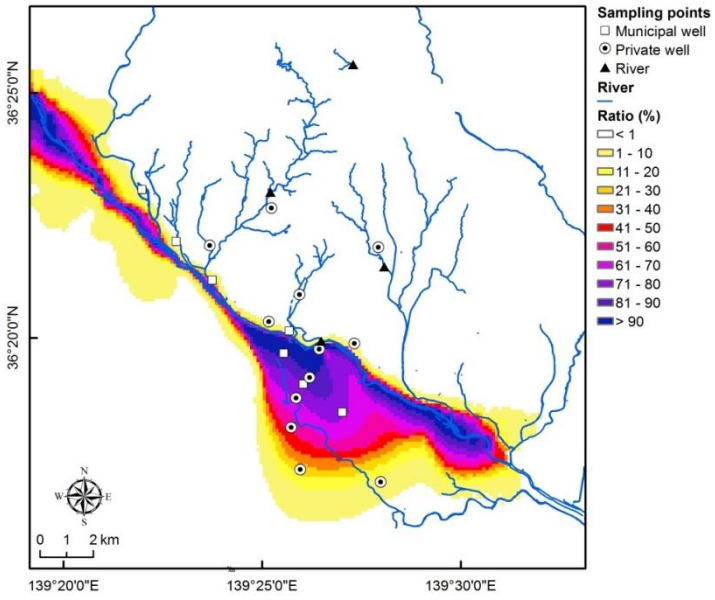

Figure 8.4 Comparison of estimated river water contribution ratio by (a) EMMA and (b) numerical simulation in the Ashikaga area.

Chapter 9
Conclusions

To elucidate the spatiotemporal behavior of groundwater-river interaction in the mountain-plain transitional area, two different approaches were employed. A tracer approach (i.e., end-member mixing analysis with isotopic and hydrochemical tracers) was first used to identify the main recharging sources and their corresponding contribution ratios in the Nasunogahara area and the Ashikaga area. Based on the results from the tracer approach, numerical simulation was done to understand the recharge and discharge mechanisms in the study areas, with special focuses on the dynamics of river seepage and its controlling factors. “Stable isotopic tracers” were added to the numerical model as simulation terms additional to hydraulic head data to improve the calibration. The numerical simulation was further validated through comparison of the results from the tracer approach and the simulation approach at the two study areas.

The main conclusions of the present study are summarized as follows:

1. The main recharge sources to plain aquifers are precipitation, river water, paddy field water and mountain block recharged groundwater. Precipitation is the most dominant one and further subdivided into direct infiltration at the plain surface and lateral recharge through adjacent mountain shallow aquifers. River seepage is also an important recharge mechanism especially at areas close to river channel, while its contribution ratio is variable depending on the distance from the channel and geographical/geological settings (e.g., fan apex/middle/rim zones, large topographic slope direction versus river flow direction, and fault or syncline/anticline structures). River acts not only as a recharge source but also as discharge paths in lower elevation zones as well as springs and pumping wells. Such groundwater-river interaction moderately changes seasonally although it is relatively more intensive in wet season.

2. In the Nasunogahara area, the river seepage accounts for 29% of total recharge. The seepage of the Sabi River, an intermittent river, is larger than two permanent rivers (i.e., Naka River and Houki River). The Sabi River works as a losing river as a whole in the area, while it changes to a gaining river in dry season. On the other hand, two permanent rivers are gaining rivers as a whole. However, they also act as groundwater recharge sources at upstream area. Spatial and temporal variation of seepage from the Sabi River is especially large; 80% of Sabi River seepage is occurred in the upstream area and the monthly amount of the seepage in wet season is 4 times greater than in dry season. The spatial structure of the river seepage is symmetric with respect to the channel. The extent of river recharged groundwater with more than 50% of contribution ratio reaches to 2.5 km from the channel in the upstream and 1.5 km in the downstream. Mountain block recharge is not found in the Nasunogahara area.
3. In the Ashikaga area, the Watarase River acts as a losing river as a whole and the tributaries are the main discharge paths of groundwater. The spatial characteristic of river seepage is symmetric with respect to the Watarase River channel at the upstream and downstream reach, while it is asymmetric at the midstream reach. At the upstream and downstream reach, river-recharge-dominated area with more than 50% contribution ratio is found with an extent of 1.5 km from the channel to the both side. However, the reach extended up to 4 km from the channel in the south side at the midstream reach, while it is less than 1 km in the north side. However, even near the river channel, mountain block recharge tends to suppress the river seepage toward the mountain side. The river contribution ratio increases from dry season to wet season for river-recharged groundwater.
4. Factors affecting the groundwater-river interaction in the mountain-plain transitional landscapes are large-scale topographic settings, location and geology. Difference of spatial structure of river-recharge-dominated areas between the Nasunogahara and the Ashikaga areas attributes mainly to topographic settings. The flow direction of main rivers in the

Nasunogahara area is almost perpendicular to the mountain-plain boundary, while the main river in the Ashikaga area runs nearly parallel to the boundary. This is the reason why the river recharge dominated area is symmetric in the former and is asymmetric in the latter. In the former case, spatial extent of river-recharge-dominated areas is wider in the upstream than in downstream. Faults can prevent mountain block recharge and syncline structures are likely to promote mountain block recharge, reducing groundwater-river interaction. In addition, the groundwater-river interaction varies in different locations (e.g., fan apex/middle/rim zones). The induced recharge from rivers by groundwater pumping was not obvious in the two study areas.

5. The contribution of paddy field water to groundwater recharge is remarkable at relatively low lands, where the paddy field occupy as a dominant land use, during the irrigation period. However, the contribution ratio of paddy field water does not exceed 50% at maximum and its mean ratio over the whole area is relatively small in comparison to that of precipitation and river water. Limited distribution of paddy field and the short irrigation period are main reasons restricting the recharge from paddy field.
6. The tracer approach is a very simple and effective method to estimate the recharge sources and their contribution ratios to groundwater, and the results from tracer approach also helps in constructing the conceptual model for numerical simulations. However, the tracer approach always accompanies with errors due to the uncertainty in concentration/composition for the end members. The errors are estimated to be more than 50% in some cases. The numerical simulation approach with stable isotopes supplies more reliable results than the tracer approach does. This approach is especially useful for areas with sparse hydrometric data. Although the uncertain inputs and the sub-grid-scale heterogeneity may induce errors for computing the contribution ratio of paddy field water at point scale, combined use of the tracer and the numerical simulation is capable of improving reliability of the results and mitigating limitations of the numerical simulation.

Acknowledgments

I would like to express my deep and sincere gratitude to my advisor Dr. Tsutomu Yamanaka for the continuous support of my Ph.D study and research. His wide knowledge and his logical way of thinking have been of great value for me. His understanding, encouraging and personal guidance have provide a good basis for the present thesis.

I am also deeply grateful to my former advisor Prof. Tadashi Tanaka, for his constructive advice and encouragement during the early period of this work.

I wish to express my gratitude to all the advisors in Laboratory of Hydrological Science, University of Tsukuba: Prof. Norio Tase, Prof. Michiaki Sugita, Prof. Jun Asanuma and Prof. Maki Tsujimura for their fruitful comments during the period of achievement of this work.

I would like to give my sincere thanks to Mr. Masayoshi Yamaguchi, Mr. Tadao Matsuzaki and Mr. Takashi Arai of the Municipal Water Department, Ashikaga City, for their help in collecting water samples and borehole logs of municipal wells.

I thank my colleagues of Laboratory of Hydrological Science, University of Tsukuba, especially Ms. Henda Jelassi and Mr. Makoto Mikita for their technical suggestions while learning numerical simulation. I also thank Mr. Pei Wang and Ms. Wenchao Ma for their cooperative fieldwork and encouragements. I am grateful to Mr. Zhongwang Wei, Mr. Atsushi Hayashi and all the members of Yamanaka laboratory for their support and discussion.

I wish to express my special thanks to my master’s advisor Prof. Xun Zhou in China University of Geosciences for his help and moral support.

I also wish to thank to all my friends for their moral support.

I am grateful to the Chinese government and University of Tsukuba for their financial support.

Finally, I would like to express my heartiest thanks to my parents, sister and brother for their continuous encouragements and moral support.

References

Aishlin, P., McNamara, J.P., 2011. Bedrock infiltration and mountain block recharge accounting using chloride mass balance. Hydrological Processes, 25(12): 1934-1948.

Banks, E.W., Simmons, C.T., Love, A.J., Shand, P., 2011. Assessing spatial and temporal connectivity between surface water and groundwater in a regional catchment: Implications for regional scale water quantity and quality. Journal of Hydrology, 404(1-2): 30-49.

Barthold, F.K., Tyralla, C., Schneider, K., Vaché, K.B., Frede, H., Breuer, L., 2011. How many tracers do we need for end member mixing analysis (EMMA)? A sensitivity analysis. Water Resources Research, 47, W08519, doi:10.1029/2011WR010604.

Ben-Itzhak, L.L., Gvirtzman, H., 2005. Groundwater flow along and across structural folding: an example from the Judean Desert, Israel. Journal of Hydrology, 312(1-4): 51-69.

Bowen, G.J., 2008. Spatial analysis of the intra-annual variation of precipitation isotope ratios and its climatological corollaries. Journal of Geophysical Research, 113(D5), D05113, doi:10.1029/2007JD009295.

Burns, D.A., McDonnell, J.J., Hooper R.P., Peters N.E., Freer, J.E., Kendall, C., Beven K., 2001. Quantifying contributions to storm runoff through end-member mixing analysis and hydrologic measurements at the Panola Mountain Research Watershed (Georgia, USA). Hydrological Processes, 15(10): 1903-1924.

Clark, I., Fritz, P., 1997. Environmental Isotopes in Hydrogeology. CRC Press, New York, 328pp.

Cox, M.H., Su, G.W., Constantz, J., 2007. Heat, chloride, and specific conductance as ground water tracers near streams. Ground Water, 45(2): 187-95.

Dansgaard, W., 1964. Stable Isotopes in Precipitation. Tellus, 16(4): 436-468.

Diersch, H.J.G., 1979. Finite Element subsurface FLOW system. WASY GmbH Institute for Water Resources Planning and Systems Research.

Doctor, D.H., Alexander Jr, E.C., Petrič, M., Kogovšek, J., Urbanc, J., Lojen, S., Stichler, W., 2006. Quantification of karst aquifer discharge components during storm events through end-member mixing analysis using natural chemistry and stable isotopes as tracers. Hydrogeology Journal, 14(7): 1171-1191.

Doherty, J., 1998. Visual PEST: Graphical Model Independent Parameter Estimation. Watermark Computing and Waterloo Hydrogeologic Inc.Carroll, R., Pohll, G., Earman, S., Hershey, R., 2008. A comparison of groundwater fluxes computed with MODFLOW and a mixing model using deuterium: Application to the eastern Nevada Test Site and vicinity. Journal of Hydrology, 361(3-4): 371-385.

Cho, J., Mostaghimi, S., Kang, M.S., 2010. Development and application of a modeling approach for surface water and groundwater interaction. Agricultural Water Management, 97(1): 123-130.

Constantz, J., 2008. Heat as a tracer to determine streambed water exchanges. Water Resources Research, 44, W00D10, doi:10.1029/2008WR006996.

Covino, T.P., McGlynn, B.L., 2007. Stream gains and losses across a mountain-to-valley transition: Impacts on watershed hydrology and stream water chemistry. Water Resources Research, 43, W10431, doi:10.1029/2006WR005544.

Dahan, O., McGraw, D., Adar, E., Pohll, G., Bohm, B., Thomas, J., 2004. Multi-variable mixing cell model as a calibration and validation tool for hydrogeologic groundwater modeling. Journal of Hydrology, 293(1-4): 115-136.

Derx, J., Blaschke, A.P., Blöschl, G., 2010. Three-dimensional flow patterns at the river–aquifer interface — a case study at the Danube. Advances in Water Resources, 33(11): 1375-1387.

Eastoe, C.J., Hutchison, W.R., Hibbs, B.J., Hawley, J., Hogan, J.F., 2010. Interaction of a river with an alluvial basin aquifer: Stable isotopes, salinity and water budgets. Journal of Hydrology, 395(1-2): 67-78.

Elhassan, A.M., Goto, A., Mizutani, M., 2001. Combining a tank model with a groundwater model for simulating regional groundwater flow in an alluvial fan. Irrigation, Drainage and Rural Engineering Journal, 215: 21-29.

Elhassan, A.M., Goto, A., Mizutani, M., 2003. Effect of conjunctive use of water for paddy field irrigation on groundwater budget in an alluvial fan. Agricultural Engineering International: the CIGR Journal of Scientific Research and Development, V, LW 03002.

Elhassan, A.M., Goto, A., Mizutani, M., 2006. Simulated effects of changing land use on shallow aquifer of Nasunogahara basin, Japan. An American Society of Agricultural and Biological Engineers meeting presentation, paper No. 062285.

Facchi, A., Ortuani, B., Maggi, D., Gandolfi, C., 2004. Coupled SVAT-groundwater model for water resources simulation in irrigated alluvial plains. Environmental Modelling & Software, 19(11): 1053-1063.

Fleckenstein, J.H., Krause, S., Hannah, D.M., Boano, F., 2010. Groundwater-surface water interactions: New methods and models to improve understanding of processes and dynamics. Advances in Water Resources, 33(11): 1291-1295.

Fleckenstein, J.H., Niswonger, R.G., Fogg, G.E., 2006. River-aquifer interactions, geologic heterogeneity, and low-flow management. Ground Water, 44(6): 837-52.

Fujinawa, K., 1981. The role of water for agricultural use as the source of groundwater recharge; analysis of groundwater in Nasuno-ga-hara Basin by a mathematical model. Bulletin of the national research institute of agricultural engineering, 21: 127-141 (*in Japanese with English abstract*).

Gauthier, M.J., Camporese, M., Rivard, C., Paniconi, C., Larocque, M., 2009. A modeling study of heterogeneity and surface water-groundwater interactions in the Thomas Brook catchment, Annapolis Valley (Nova Scotia, Canada). Hydrol Earth Syst Sc, 13: 1583-1596.

Girard, P., da Silva, C.J., Abdo, M., 2003. River-groundwater interactions in the Brazilian Pantanal. The case of the Cuiabá River. Journal of Hydrology, 283(1-4): 57-66.

Gupta, P., Noone, D., Galewsky, J., Sweeney, C., Vaughn, B.H., 2009. Demonstration of high-precision continuous measurements of water vapor isotopologues in laboratory and remote field deployments using wavelength-scanned cavity ring-down spectroscopy (WS-CRDS) technology. Rapid Communications in Mass Spectrometry, 23(16): 2534-2542.

Hancock, P.J., 2002. Human impacts on the stream-groundwater exchange zone. Environmental management, 29(6): 763-781.

Harbaugh, A.W., Banta, E.R., Hill, M.C., McDonald, M.G., 2000. MODFLOW-2000, the U.S. Geological Survey modular ground-water model — User guide to modularization concepts and the Ground-Water flow process. U.S. Geological Survey Open-File Report 00-92, 121p.

Harbaugh, A.W., McDonald, M.G., 1996a. User's documentation for MODFLOW-96, an update to the U.S. Geological Survey modular finite-difference ground-water flow model. U.S. Geological Survey Open-File Report 96-485, 56p.

Harbaugh, A.W., McDonald, M.G., 1996b. Programmer's documentation for MODFLOW-96, an update to the U.S. Geological Survey modular finite-difference ground-water flow model. U.S. Geological Survey Open-File Report 96-486, 220p.

Harvey, F.E., Sibray, S.S., 2001. Delineating ground water recharge form leaking irrigation canals using water chemistry and isotopes. Ground Water, 39(3): 408-421.

Harvey, J.W., Bencala, K.E., 1993. The effect of streambed topography on surface-subsurface water exchange in mountain catchments. Water Resources Research, 29(1): 89-98.

Harvey, J.W., Wagner, B.J., Bencala, K.E., 1996. Evaluating the reliability of the stream tracer approach to characterize stream-subsurface water exchange. Water Resources Research, 32(8): 2441-2451.

Henriksen, H.J., Troldborg, L., Højberg, A.L., Refsgaard, J.C., 2008. Assessment of exploitable groundwater resources of Denmark by use of ensemble resource indicators and a numerical groundwater–surface water model. Journal of Hydrology, 348(1-2): 224-240.

Hiyama, T., Suzuki, Y., 1991. Groundwater in the Nasuno basin — spatial and seasonal changes in water quality. Hydrology (Journal of Japanese Association of Hydrological Sciences), 21: 143-154 (*in Japanese with English abstract*).

Hunt, R.J., Coplen, T.B., Haas, N.L., Saad, D.A., Borchardt, M.A., 2005. Investigating surface water–well interaction using stable isotope ratios of water. Journal of Hydrology, 302(1-4): 154-172.

Izbicki, J.A., Stamos, C.L., Nishikawa, T., Martin, P., 2004. Comparison of ground-water flow model particle-tracking results and isotopic data in the Mojave River ground-water basin, southern California, USA. Journal of Hydrology, 292(1-4): 30-47.

Johnson, A.I. 1967. Specific yield — compilation of specific yields for various materials. U.S. Geological Survey Water Supply Paper 1662-D. 74p.

Jones, J.P., Sudicky, E.A., Brookfield, A.E., Park, Y.J., 2006. An assessment of the tracer-based approach to quantifying groundwater contributions to streamflow. Water Resources Research, 42(2), W02407, doi:10.1029/2005WR004130.

Jones, J.P., Sudicky, E.A., McLaren, R.G., 2008. Application of a fully-integrated surface-subsurface flow model at the watershed-scale: A case study. Water Resources Research, 44(3), W03407, doi:10.1029/2006WR005603.

Kelly, B.P., 2002. Ground-water flow simulation and chemical and isotopic mixing equation analysis to determine source contributions to the Missouri River alluvial aquifer in the vicinity of the independence, Missouri, well field. U.S. Geological Survey Water-Resources Investigations Report, 2002-4208, 31p.

Kelly, B.P., 2004, Simulation of ground-water flow, contributing recharge areas, and ground-water travel time in the Missouri River alluvial aquifer near Ft. Leavenworth, Kansas: U.S. Geological Survey Scientific Investigations Report 2004-5215, 69p.

Kim, N.W., Chung, I.M., Won, Y.S., Arnold, J.G., 2008. Development and application of the integrated SWAT–MODFLOW model. Journal of Hydrology, 356(1-2): 1-16.

Krause, S., Bronstert, A., 2005. An advanced approach for catchment delineation and water balance modelling within wetlands and floodplains. Advances in Geosciencs, (5): 1-5.

Krause, S., Bronstert, A., Zehe, E., 2007. Groundwater-surface water interactions in a North German lowland floodplain — Implications for the river discharge dynamics and riparian water balance. Journal of Hydrology, 347(3-4): 404-417.

Kumar, M., Ramanathan, A., Keshari, A.K., 2009. Understanding the extent of interactions between groundwater and surface water through major ion chemistry and multivariate statistical techniques. Hydrological Processes, 23(2): 297-310.

LaBolle, E.M., Ahmed, A.A., Fogg, G.E., 2003. Review of the Integrated Groundwater and Surface-Water Model (IGSM). Ground Water, 41(2): 238-246.

Lambs, L., 2004. Interactions between groundwater and surface water at river banks and the confluence of rivers. Journal of Hydrology, 288(3-4): 312-326.

Lautz, L.K., Siegel, D., 2006. Modeling surface and ground water mixing in the hyporheic zone using MODFLOW and MT3D. Advances in Water Resources, 29(11): 1618-1633.

Leake, S.A., and Prudic, D.E., 1991, Documentation of a computer program to simulate aquifer-system compaction using the modular finite-difference ground-water flow model: U.S. Geological Survey Techniques of Water-Resources Investigations, book 6, chap. A2, 68p.

Liu, F.J., Williams, M.W., Caine, N., 2004. Source waters and flow paths in an alpine catchment, Colorado Front Range, United States. Water Resources Research, 40(9), W09401, doi:10.1029/2004WR003076.

Mikita, M., Yamanaka, T., Lorphensri, O., 2011. Anthropogenic changes in a confined groundwater flow system in the Bangkok basin, Thailand, part I: was groundwater-recharge enhanced?. Hydrological Processes: 25 (17): 2726-2733.

Miyazaki, N., Namewada, K., Iwasaki, S., 2005. Quality changes of agricultural water passing through paddy fields. Bulletin of the Tochigi Prefectural Agricultural Experiment Station, 55: 45-55 (*in Japanese with English abstract*).

Momikura, K., 1986. Groundwater in Kanto Plain-Nasu Plain, in: Study group of agricultural groundwater (Eds.), Groundwater in Japan. Chikyu-sha, Tokyo, 270-286 (*in Japanese*).

Nakaya, S., Uesugi, K., Motodate, Y., Ohmiya, I., Komiya, H., Masuda, H., Kusakabe, M., 2007. Spatial separation of groundwater flow paths from a multi-flow system by a simple mixing model using stable isotopes of oxygen and hydrogen as natural tracers. Water Resources Research, 43(9), W09404, doi:10.1029/2006WR005059.

Niswonger, R.G., Prudic, D.E., Pohll, G., Constantz, J., 2005. Incorporating seepage losses into the unsteady streamflow equations for simulating intermittent flow along mountain front streams. Water Resources Research, 41(6), W06006, doi:10.1029/2004WR003677.

O'Driscoll, M., Johnson, P., Mallinson, D., 2010. Geological controls and effects of floodplain asymmetry on river-groundwater interactions in the southeastern Coastal Plain, USA. Hydrogeology Journal, 18(5): 1265-1279.

Phillips, D.L., Gregg, J.W., 2001. Uncertainty in source partitioning using stable isotopes. Oecologia, 127(2): 171-179.

Poage, M.A., Chamberlain, C.P., 2001. Empirical relationships between elevation and the stable isotope composition of precipitation and surface waters: Considerations for studies of paleoelevation change. American Journal of Science, 301: 1-15.

Ponce, V.M., Pandey, R.P., Kumar, S., 1999. Groundwater recharge by channel infiltration in El Barbon basin, Baja California, Mexico. Journal of Hydrology, 214: 1-7.

Prudic, D.E., 1989, Documentation of a computer program to simulate stream-aquifer relations using a modular, finite-difference, ground-water flow model: U.S. Geological Survey Open-File Report 88-729, 113p.

Qin, D., Qian, Y., Han, L., Wang, Z., Li, C., Zhao, Z., 2011. Assessing impact of irrigation water on groundwater recharge and quality in arid environment using CFCs, tritium and stable isotopes, in the Zhangye Basin, Northwest China. Journal of Hydrology, 405(1-2): 194-208.

Ravazzani, G., Rametta, D., Mancini, M., 2011. Macroscopic cellular automata for groundwater modelling: A first approach. Environmental Modelling & Software, 26(5): 634-643.

Refsgaard, J.C., Storm, B., 1995. MIKE SHE, In: Singh, V.P. (Eds), Computer models of watershed hydrology. Water Resources Publication, pp. 809-846.

Reynolds, D.A., Marimuthu, S., 2006. Deuterium composition and flow path analysis as additional calibration targets to calibrate groundwater flow simulation in a coastal wetlands system. Hydrogeology Journal, 15(3): 515-535.

Rodriguez, L., Cello, P., Vionnet, C., Goodrich, D., 2008. Fully conservative coupling of HEC-RAS with MODFLOW to simulate stream-aquifer interactions in a drainage basin. Journal of Hydrology, 353:129-142.

Rushton, K.R., Tomlinson, L.M., 1979. Possible Mechanisms for Leakage between Aquifers and Rivers. Journal of Hydrology, 40(1-2): 49-65.

Sai, S., Oba, T., 1978. Groundwater flow in Nasu fan as revealed by tritium tracer, in: Ichikawa, M., Kayane, I., (Eds.), Water balance in Japan. Kokon-shoin, Tokyo, pp. 156-165 (*in Japanese*).

Sanford, W., Plummer, L.N., McAda, D., Bexfield, L., Anderholm, S., 2004. Hydrochemical tracers in the middle Rio Grande Basin, USA: 2. Calibration of a groundwater-flow model. Hydrogeology Journal, 12: 389-407.

Sanz, D., Gómez-Alday, J.J., Castaño, S., Moratalla, A., De las Heras, J., Martínez-Alfaro, P. E., 2009. Hydrostratigraphic framework and hydrogeological behaviour of the Mancha Oriental System (SE Spain). Hydrogeology Journal, 17(6): 1375-1391.

Sanz, D., Castaño, S., Cassiraga, E., Sahuquillo, A., Gómez-Alday, J.J., Peña, S., Calera, A., 2011. Modeling aquifer-river interactions under the influence of groundwater abstraction in the Mancha Oriental System (SE Spain). Hydrogeology Journal, 19(2): 475-487.

Sarwar, A., Eggers, H., 2006. Development of a conjunctive use model to evaluate alternative management options for surface and groundwater resources. Hydrogeology Journal, 14(8): 1676-1687.

Sasaki, M., Ajisaka, T., Okamoto, A., 1958. Hydrogeology of the Nasu Plain, Tochigi Prefecture. Journal of Geography, 67: 59-73 (*in Japanese with English abstract*).

Scibek, J., Allen, D.M., Cannon, A.J., Whitfield, P.H., 2007. Groundwater-surface water interaction under scenarios of climate change using a high-resolution transient groundwater model. Journal of Hydrology, 333(2-4): 165-181.

Smerdon, B.D., Allen, D.M., Grasby, S.E., Berg, M.A., 2009. An approach for predicting groundwater recharge in mountainous watersheds. Journal of Hydrology, 365(3-4): 156-172.

Somura, H., Goto, A., Matsui, H., Ali Musa, E., 2008. Impacts of nutrient management and decrease in paddy field area on groundwater nitrate concentration: a case study at the Nasunogahara alluvial fan, Tochigi Prefecture, Japan. Hydrological Processes, 22(24): 4752-4766.

Song, X., Liu, X., Xia, J., Yu, J., Tang, C., 2006. A study of interaction between surface water and groundwater using environmental isotope in Huaisha River basin. Science in China Series D: Earth Sciences, 49(12): 1299-1310.

Sophocleous, M., 2002. Interactions between groundwater and surface water: the state of the science. Hydrogeology Journal, 10(1): 52-67.

Sophocleous, M., Perkins, S.P., 2000. Methodology and application of combined watershed and ground-water models in Kansas. Journal of Hydrology, 236(3-4): 185-201.

Stichler, W., Maloszewski, P., Bertleff, B., Watzel, R., 2008. Use of environmental isotopes to define the capture zone of a drinking water supply situated near a dredge lake. Journal of Hydrology, 362(3-4): 220-233.

Storey, R.G., Howard, K.W.F., Williams, D.D., 2003. Factors controlling riffle-scale hyporheic exchange flows and their seasonal changes in a gaining stream: A three-dimensional groundwater flow model. Water Resources Research, 39(2), 1034, doi:10.1029/2002WR001367.

Subyani, A.M., 2004. Use of chloride-mass balance and environmental isotopes for evaluation of groundwater recharge in the alluvial aquifer, Wadi Tharad, western Saudi Arabia. Environmental Geology, 46(6-7): 741-749.

Swain, E.D., Wexler, E.J., 1992. A coupled surface-water and ground-water flow model for simulation of stream-aquifer interaction, U.S. Geological Survey open-file report 92-138, 162pp.

VanderKwaak, J.E., 1999. Numerical simulation of flow and chemical transport in integrated surface-subsurface systems. Ph.D thesis, University of Waterloo, Waterloo, Ontario., Canada, 242 p.

VanderKwaak, J.E., Loague, K., 2001. Hydrologic-response simulations for the R-5 catchment with a comprehensive physics-based model. Water Resources Research, 37(4): 999-1013.

Vogt, T., Hoehn, E., Schneider, P., Freund, A., Schirmer, M., Cirpka, O.A., 2010. Fluctuations of electrical conductivity as a natural tracer for bank filtration in a losing stream. Advances in Water Resources, 33(11): 1296-1308.

Wakui, H., 2007. Numerical simulation on isotopic changes in groundwater in the Nasu Fan, Tochigi Prefecture. Master thesis, University of Tsukuba, Tsukuba, Japan, 73pp.

Wakui, H., Yamanaka, T., 2006. Sources of groundwater recharge and their local differences in the central part of Nasu fan as revealed by stable isotope. Groundwater Hydrology (Journal of Japanese Association of Hydrological Sciences), 48(2): 263-277 (*in Japanese with English abstract*).

Ward, A.S., Gooseff, M.N., Singha, K., 2010. Characterizing hyporheic transport processes — Interpretation of electrical geophysical data in coupled stream–hyporheic zone systems during solute tracer studies. Advances in Water Resources, 33(11): 1320-1330.

Waseda, A., Nakai, N., 1983. Isotopic compositions of meteoric and surface waters in central and northeast Japan. Chikyukagaku, 17: 83-91 (*in Japanese*).

Weingartner, R., Viviroli, D., Schädler, B., 2007. Water resources in mountain regions: a methodological approach to assess the water balance in a highland-lowland-system. Hydrological Processes, 21(5): 578-585.

Westbrook, C.J., Cooper, D.J., Baker, B.W., 2006. Beaver dams and overbank floods influence groundwater-surface water interactions of a Rocky Mountain riparian area. Water Resources Research, 42, W06404, doi:10.1029/2005WR004560.

Westhoff, M.C., Bogaard, T.A., Savenije, H.H.G., 2010. Quantifying the effect of in-stream rock clasts on the retardation of heat along a stream. Advances in Water Resources, 33(11): 1417-1425.

Wilson, J.L., Guan, H., 2004. Mountain-Block Hydrology and Mountain-Front Recharge, in: Phillips, F.M., Hogan, J., Scanlon, B. (Eds), Groundwater recharge in a desert environment: The southwestern United States. AGU, Washington, DC, 23p.

Winter, T.C., Buso, D.C., Shattuck, P.C., Harte, P.T., Vroblesky, D.A., Goode, D.J., 2008. The effect of terrace geology on ground-water movement and on the interaction of ground water and surface water on a mountainside near Mirror Lake, New Hampshire, USA. Hydrological Processes, 22(1): 21-32.

Winter, T.C., Harvey, J.W., Franke, O.L., Alley, W.M., 1998. Groundwater and surface water, a single resource. US Geological Survey Circular 1139, 79p.

Woessner, W.W., 2000. Stream and fluvial plain ground water interactions: Rescaling hydrogeologic thought. Ground Water, 38(3): 423-429.

Wroblicky, G.J., Campana, M.E., Valett, H.M., Dahm, C.N., 1998. Seasonal variation in surface-subsurface water exchange and lateral hyporheic area of two stream-aquifer systems. Water Resources Research, 34(3): 317-328.

Wu, Y., Zhang, Y., Wen, X., Su, j., 2010. Hydrologic cycle and water resource modeling for the Heihe River basin in Northwestern China. Science Press, Beijing, China, 199p (*in Chinese*).

Xi, H.Y., Feng, Q., Si, J.H., Chang, Z.Q., Cao, S.K., 2010. Impacts of river recharge on groundwater level and hydrochemistry in the lower reaches of Heihe River Watershed, northwestern China. Hydrogeology Journal, 18(3): 791-801.

Yamamoto, S., Terada, M., 1980. Groundwater in the Nasu alluvial fan. Bulletin of Rissho University, 67: 17-36 (*in Japanese*)

Yamanaka, T., Onda, Y., 2010. On measurement accuracy of liquid water isotope analyzer based on wavelength-scanned cavity ring-down spectroscopy (WS-CRDS). Bulletin of Terrestrial Environmental Research Center, University of Tsukuba, No. 12, in press (*in Japanese*).

Yamanaka, T., Mikita, M., Lorphensri, O., Shimada, J., Kagabu, M., Ikawa, R., Toshio, N., Tsujimura, M., 2011a. Anthropogenic changes in a confined groundwater flow system in the Bangkok Basin, Thailand, part II: how much water has been renewed? Hydrological Processes, 25(17): 2734-2741.

Yamanaka, T., Shimada, J., Tsujimura, M., Lorphensri, O., Mikita, M., Hagihara, A., Onodera, S., 2011b. Tracing a confined groundwater flow system under the pressure of excessive groundwater use in the lower central plain, Thailand. Hydrological Processes, 25(17): 2654-2664.

Yamanaka, T., Wakui, H., 2009. Intensive groundwater-surface water interaction in an alluvial fan: Assessment using a numerical model and isotopic tracer. From Headwaters to the Ocean: Hydrological Changes and Watershed Management, 321-327.

Yuan, R., Song, X., Zhang, Y., Han, D., Wang, S., Tang, C., 2011. Using major ions and stable isotopes to characterize recharge regime of a fault-influenced aquifer in Beiyishui River Watershed, North China Plain. Journal of Hydrology, 405(3-4): 512-521.

Zheng, C., 1990. MT3D: A modular three-dimensional transport model for simulation of advection, dispersion and chemical reactions of contaminants in groundwater systems. Report to the U. S. Environmental Protection Agency, 170 p.

Zheng, C., Wang, P.P., 1999. MT3DMS: a modular three-dimensional multispecies transport model for simulation of advection, dispersion, and chemical reactions of contaminants in groundwater systems; documentation and user's guide. Contract Report SERDP-99-1, U.S. Army Engineer Research and Development Center, Vicksburg, MS.